ENERGY EFFICIENCY CONTROL OF DIRECT EXPANSION AIR CONDITIONING SYSTEMS

by

Jun Mei

Submitted in partial fulfillment of the requirements for the degree

Philosophiae Doctor (Electronic Engineering)

in the

Department of Electrical, Electronic and Computer Engineering

Faculty of Engineering, Built Environment and Information Technology

UNIVERSITY OF PRETORIA

May 2018

SUMMARY

ENERGY EFFICIENCY CONTROL OF DIRECT EXPANSION AIR CONDITIONING
SYSTEMS

by

Jun Mei

The dynamic mathematical models for direct expansion air conditioning (DX A/C) systems with respect to indoor carbon dioxide (CO_2) concentration, relative humidity and air temperature and the coupling effects among them have been built in this thesis. To reduce the energy cost and improve the energy efficiency for DX A/C systems while maintaining both indoor air quality (IAQ) and thermal comfort at acceptable levels, a hierarchical control structure is proposed in this thesis. This control structure includes two levels. The upper level is an open loop optimal controller to generate the optimal setpoints of indoor CO_2 concentration, relative humidity and air temperature for the lower level controller. The lower level designs a closed-loop model predictive control (MPC) controller to optimize the transient processes reaching the setpoints where the energy efficiency improvement and energy cost savings are achieved.

In Chapter 2, the control objective is to improve both IAQ and thermal comfort as well as energy efficiency for a DX A/C system. The details of a hierarchical control structure in this chapter are

as follows: In the upper layer, an energy-optimised open loop controller is proposed based on an optimization of energy consumption of the DX A/C system and given reference points of indoor CO_2 concentration, relative humidity and air temperature to generate a unique and optimised steady state for the lower layer controller. In the lower layer, the closed-loop MPC controller is proposed such that the indoor CO_2 concentration, relative humidity and air temperature follow the steady state computed by the upper layer, whereas the energy efficiency is improved. To facilitate the MPC design, the nonlinear DX A/C control system is linearized around the optimised steady state.

In Chapter 3, the control objective is to lower the energy cost and consumption of a DX A/C system while maintaining both IAQ and thermal comfort at comfort levels. To achieve this purpose, an autonomous hierarchical control (AHC) structure is designed and described below. The upper level is an open loop nonlinear optimal controller, which optimizes the predicted mean vote (PMV) index and the energy cost for the DX A/C system under a time-of-use (TOU) price structure of electricity according to the changing environment over a 24-hour period, to generate the tradeoff setpoints of indoor CO_2 concentration, relative humidity and air temperature for the lower level controller. The lower layer is formed as a closed-loop MPC to track the trajectory reference points calculated by the optimization layer. This AHC strategy means the upper controller can adaptively and automatically set the setpoints and the lower layer adaptively and optimally tracks them, minimizing energy consumption and costs. In addition, in this chapter, the volumes of outside air allowed to enter the DX A/C system are regarded as varying with the changing circumstance over a day and are optimized by the AHC. Moreover, a supply fan to steer the pressure swing absorption with a built-in proportional-integral (PI) controller is proposed to lower the indoor CO_2 concentration such that it would reduce the complexity of computation for the AHC and the cost of hardware.

In Chapter 4, the control objective is to reduce energy cost, improve energy efficiency, and reduce communication resources, computational complexity and conservativeness, as well as peak demand for a multi-zone building multi-evaporator air conditioning (ME A/C) system while maintaining multi-zones' thermal comfort and IAQ at comfort levels. To realize this objective and to consider the interaction effects between rooms, we present an autonomous hierarchical distributed control (AHDC) method. The upper level is an open loop nonlinear optimizer, which only collects measurement information and solves a distributed steady state optimization problem to adaptively and automatically generate time-varying and optimised reference points of indoor CO_2 concentration, relative humidity and air temperature for the lower-layer controllers, by minimizing the demand and energy costs of

a multi-zone building ME A/C system under the TOU price structure of electricity according to the changing circumstance during the day. The lower level also uses local information to track the trajectory references calculated by the upper-layer distributed controller, via distributed MPC controllers. The proposed hierarchical control strategy is distributed in two layers since they use only local information from the working zone and its neighbours.

To validate the performance of these hierarchical control strategies for DX A/C systems, simulation tests are performed in this thesis. In Chapter 2, simulations are provided to show that the closed-loop regulation of the MPC controller and the energy-optimised open loop controller can maintain indoor CO_2 concentration, relative humidity and air temperature at their desired setpoints with small deviations and reduce the effect of indoor cooling and pollutant loads. The simulations also demonstrate that the controllers are superior to conventional controllers in terms of energy efficiency. In Chapter 3, the simulation tests show that the AHC strategy can reduce more energy consumption and cost than the baseline strategy. In addition, the tests demonstrate that the AHC scheme is not sensitive to the physical parameters of the DX A/C system. In Chapter 4, to show the performance of the two-layer distributed control strategies, a case study is given. The simulation tests demonstrate that the AHDC strategy is capable of shifting demand from peak hours to off-peak hours and reducing the energy cost for a multi-zone building ME A/C system while maintaining multi-zones' IAQ and thermal comfort at comfort levels.

Lastly, Chapter 5 concludes all the findings of this thesis and provides some ideas for possible work in future research.

ACKNOWLEDGMENT

PUBLICATIONS

JOURNAL PAPERS

[J1] J. Mei and X. Xia, "Energy-efficient predictive control of indoor thermal comfort and air quality in a direct expansion air conditioning system," *Applied Energy*, vol. 195, pp. 439–452, 2017.

[J2] J. Mei, X. Xia and M. Song, "An autonomous hierarchical control for improving indoor comfort and energy efficiency of a direct expansion air conditioning system," *Applied Energy*, vol. 221, pp. 450–463, 2018.

[J3] J. Mei and X. Xia, "Distributed control for a multi-evaporator air conditioning system," *Control Engineering Practice, revised*, 2018.

CONFERENCE CONTRIBUTIONS

[C1] J. Mei, B. Zhu, and X. Xia, "Model predictive control for optimizing indoor air temperature and humidity in a direct expansion air conditioning system," in *The 27th Chinese Control and Decision Conference (2015 CCDC)*, Qingdao, China, 23-25 May, 2015.

[C2] J. Mei, B. Zhu and X. Xia, "Predictive control for thermal comfort and energy efficiency in a direct expansion air conditioning system," *2015 Chinese Automation Congress (CAC)*, Wuhan, China, 27-29 November, 2015.

[C3] J. Mei and X. Xia, "Nonlinear model reduction for direct expansion air conditioning and MPC control of indoor climate and energy efficiency," in *2017 29th Chinese Control And Decision Conference (CCDC)*, Chongqing, China, 28-30 May, 2017.

[C4] J. Mei and X. Xia, "A reduced model for direct expansion air conditioning system and energy efficiency MPC control of indoor climate," in *2017 13th IEEE International Conference on Control Automation (ICCA)*, Ohrid, Macedonia, 3-6 July, 2017.

[C5] J. Mei and X. Xia, "Hierarchical Control Method to Improve Comfort and Energy Efficiency and Reduce Demand in DX A/C System," in *2017 Control Conference Africa (CCA)*, vol. 50, no. 2, pp. 243-244, 7-8 December 2017.

[C6] J. Mei and X. Xia, "Multi-zone building temperature control and energy efficiency using autonomous hierarchical control strategy," in *2018 14th IEEE International Conference on Control Automation (ICCA)*, Alaska, USA, 12-15 June, 2018.

[C7] J. Mei and X. Xia, "Distributed resource allocation for multi-zone commercial buildings," in *2018 10th International Conference on Applied Energy (ICAE2018)*, Hongkong, China, 22-25 August 2018.

LIST OF ABBREVIATIONS

A/C	Air conditioning
ANN	Artificial neural network
ASHRAE	American Society of Heating, Refrigerating and Air-Conditioning Engineers
BESTEST	Building energy simulation test
DDC	Direct digital control
DS	Degree of superheat
DX A/C	Direct expansion air conditioning
EEV	Electronic expansion valve
HVAC	Heating, ventilation and air conditioning
ME A/C	Multi-evaporator air conditioning
MIMO	Multi-input-multi-output
MPC	Model predictive control
NCCA	Novel capacity control algorithm
IAQ	Indoor air quality
PD	Proportional-Derivative
PMV	Predicted mean vote
PI	Proportional-Integral
PPD	Predicted percentage dissatisfied
PSA	Pressure swing adsorption
QP	Quadratic programming
TOU	Time-of-use
VAV	Variable air volume

LIST OF SYMBOLS

A_1 — Heat transfer area of the DX evaporator in the dry-cooling region, m^2

A_2 — Heat transfer area of the DX evaporator in the wet-cooling region, m^2

A_0 — Total heat transfer area of the DX evaporator, m^2

A_{win} — Total window area, m^2

C_a — Specific heat of air, kJ kg^{-1} °C^{-1}

C_c — CO$_2$ concentration of conditioning space, ppm

C_s — CO$_2$ concentration of supply air, ppm

d — Cross-sectional area of the conditioned space, m^2

G — Amount of CO$_2$ emission rate of people, m^3/s

h_{fg} — Latent heat of vaporization of water, kJ/kg

h_{r1} — Enthalpy of refrigerant at evaporator inlet, kJ/kg

h_{r2} — Enthalpy of refrigerant at evaporator outlet, kJ/kg

i — Room number

k_{fan} — Coefficient of supply fan speed, m^3/r

k_{spl} — Coefficient of supply fan heat gain, kJ/m^3

k_P, k_I — Proportional and integral gains of PI controller

m_r — Mass flow rate of refrigerant, kg/s

M_{air} — Moisture load of fresh air ventilation, kg/s

M_{load} — Moisture load of conditioned space, kg/s

$Occp$ — Number of occupants

P_{comp} — Power consumption of the condenser fan, kW/h

P_{con} — Power consumption of the compressor, kW/h

P_{eva} — Power consumption of the evaporator, kW/h

Q_{air} — Fresh air ventilation load, kW

Q_{load} — Sensible heat load of conditioned space, kW

Q_{rad} — Solar radiative heat flux density, W/m^2

Q_{spl} — Heat gain of supply fan, kW

S_{fan} — Supply fan speed, rpm

T_d — Air temperature leaving the dry-cooling region on air side, °C

T_s — Temperature of supply air from the DX evaporator, °C

T_w	Temperature of the DX evaporator wall, °C
T_z	Air temperature of conditioned space, °C
T_0	Temperature of outside air, °C
v_a	Air face velocity for the DX cooling coil, m/s
v_f	Air volumetric flow rate, m^3/s
v_s	Volume flow rate of air supply, m^3/s
V	Volume of conditioned space, m^3
V_{h1}	Air side volume of the DX evaporator in the dry-cooling region on air side, m^3
V_{h2}	Air side volume of the DX evaporator in the wet-cooling region on air side, m^3
W_s	Moisture content of supply air from the DX evaporator, kg/kg dry air
W_z	Air moisture content of conditioned space, kg/kg dry air
W_0	Air moisture content of outside, kg/kg dry air
α_1	Heat transfer coefficient between air and the DX evaporator wall in the dry-cooling region, $kW\,m^{-2}\,°C^{-1}$
α_2	Heat transfer coefficient between air and the DX evaporator wall in the wet-cooling region, $kW\,m^{-2}\,°C^{-1}$
ε_{win}	Transmissivity of glass of window
ρ	Density of moist air, kg/m^3

TABLE OF CONTENTS

LIST OF FIGURES

LIST OF TABLES

CHAPTER 1   INTRODUCTION

1.1   BACKGROUND

The total energy consumption of the world market will increase by 36% between 2008 and 2035 [1]. This energy consumption can be divided into four main sectors: residential, commercial, transportation and industrial. The rise in energy consumption by buildings has been significant in most part of the world. The building sector accounted for 21% of energy consumption in the world in 2008[1]. In the USA, the building sector accounted for 41% of primary energy consumption among all sectors in 2010[2]. In South Africa, the residential, commercial and public services sectors share 40% of electricity consumption, and based on National Electrification Statistics, electricity consumption is expected to increase constantly[3].

Because of the increase in the population, enhancement of comfort, global climate change and more time spent indoors, energy consumption in the building sector displays an upward trend. Therefore, most countries are focusing on the building sector as having the greatest potential for energy savings necessitated by increasing energy demands, energy price and environmental issues.

Building's energy demand is the main reason of electricity consumption owing to rapidly escalating space environmental quality requirements (such as thermal comfort, indoor air quality (IAQ), ventilation, refrigeration and so on), which leads to significant greenhouse gas emissions. Energy consumption demands in buildings are directly related to air conditioning (A/C) systems. A/C systems account for half of a building's energy usage. At the same time, owing to greenhouse effects the global

---

[1] https://www.eia.gov/outlooks/ieo/

[2] https://openei.org/doe-opendata/dataset/buildings-energy-data-book/resource/4516b230-4234-4778-b87f-64bc6ab0b529.

[3] file:///C:/Users/user/Downloads/essa3361.pdf.

temperature is increasing steadily, which in turn has caused an increase in the use of A/C systems. Accordingly, lowering the energy consumption in A/C systems of buildings is an important factor in lowering greenhouse gas emissions.

The study reported in this dissertation is motivated by the considerable energy efficiency and energy cost potential in the building sectors. Energy management of building A/C systems has become important and hence the need to lower the energy cost and improve the energy efficiency of buildings. In addition to improving the energy efficiency of buildings, interventions can be made in other ways [2, 3], such as appliances operation scheduling [4, 5, 6], hybrid energy system supplies [7, 8, 9], generator maintenance scheduling [10], lighting retrofitting and metering schemes [11, 12, 13, 14], envelope and whole building retrofitting schemes [15, 16], facility retrofitting and maintenance schemes [17, 18, 19] and an energy-water nexus [20, 21]. Therefore, building energy efficiency is a very broad field involving multiple layers and focuses. Energy efficiency improvement can also be effected in other sectors such as transportation scheduling including, overhead cranes [22] and belt conveyor [23] and industry application aspects [24, 25]. The main topic of the thesis is the scope of the energy management strategies of building A/C systems, which will be introduced in the following sections.

1.2 A/C CONTROL SYSTEM FRAMEWORK

1.2.1 Indoor comfort control

Lowering building energy usage should not sacrifice user benefits [26]. User-health is related to energy efficiency in some aspects. Nowadays, more and more people are working indoors much of the time, therefore providing high thermal comfort and IAQ levels for users would contribute to increased work efficiency and productivity. Effective energy management of building A/C systems can ensure IAQ, thermal comfort and energy efficiency.

In [27], the authors designed two controllers for a heating, ventilation and air conditioning (HVAC) system, including feedback and feed-forward controllers, to improve the control performance (smaller temperature variations) as well as energy efficiency. The use of optimization algorithms in various applications related to energy management in building A/C systems has been increasing significantly

over recent years. A multi-objective genetic algorithm was used [28] to obtain predictive control of air conditioned systems. The simulation results demonstrated that this method would achieve good temperature regulation with important energy savings.

Ensuring indoor air humidity at an acceptable level is an important factor since it has a direct impact on indoor thermal comfort level and the operational efficiency of buildings' A/C installations [29]. In fact, in cities with highly humid climates, such as Cape Town or Hongkong, high humidity may still adversely affect indoor thermal comfort level and the energy efficiency of building A/C systems, even when indoor air temperature has been maintained at a desired value. Various humidity control approaches have been applied in large-scale central and chilled water A/C systems, such as pre-conditioning outdoor air and heat pipe technologies [30, 31], or chemical and mechanical dehumidification desiccant mechanisms [32, 33, 26, 34]. A wavelet-based artificial neural network (ANN) with a proportional-derivative (PD) controller was proposed [35] for an A/C system to control indoor relative humidity and air temperature, where thermal comfort and energy efficiency of the system was improved. For controlling indoor humidity, a chiller/boiler was added to this A/C system. For controlling indoor relative humidity and air temperature, an evaporation pressure control method was addressed [36] based on the evaporator pressure and the relative humidity readings.

Nowadays, IAQ has become increasingly important and is regulated by A/C system design and control. The indoor relative humidity, air temperature and carbon dioxide (CO_2) concentration have been regarded as the three major factors of indoor thermal comfort and air quality. In recent years, more and more researchers have focused on how to improve thermal comfort and IAQ as well as energy efficiency. In [37], a genetic algorithm was used to find the optimal settings of the multiple variable process (i.e. air handling unit supply air temperature, outdoor ventilation rate and chilled water temperature setpoints) by optimising the cost function including thermal comfort, energy consumption, IAQ, maximum allowed relative humidity and minimum allowed ventilation flow to reduce energy usage while keeping multi-zones' thermal comfort and IAQ at acceptable levels. A multi-objective optimization was proposed in [38] to optimize indoor air condition for HVAC system in order to achieve high thermal comfort and acceptable air quality for occupants with efficient energy consumption all the time. However, they did not consider the coupling effects between indoor CO_2 concentration, relative humidity and air temperature. In many cases, these coupling effects cannot be ignored. In fact, the experimental results [39] illustrated that the indoor CO_2 concentration correlated with indoor air temperature. Furthermore, the indoor CO_2 concentration is affected by air humidity as discovered

through measurement investigation and data analysis [40]. As far as the researcher knows, there are few studies in the literature that discuss how to control indoor air temperature, relative humidity and CO_2 concentration simultaneously, taking into account the coupling effects between them and the energy efficiency of A/C systems.

1.2.2 Peak demand control

In addition to reducing overall energy consumption by building A/C systems, another significant need for building controls is to reduce peak power demands. Because buildings, especially commercial and office buildings, mainly consume energy during peak hours, the peak-average ratio (PAR) can be high in the electricity grid [41]. Both electricity suppliers and customers are extremely focused on peak demand because of economic and environmental challenges. New power plants are constantly being built every year; however, this still merely serves to remit the rapidly increasing peak demand, which reduces efficiency in non-peak hours and leads to higher energy costs for buildings. Therefore, it is of great importance to use advanced strategies to reduce or shift the peak demand.

Demand response (DR) as a concept has paid more attention to buildings as an effective way to reduce the peak demand. DR encourages end-users to adjust their electric usage in good time based on electricity price. Advanced electricity rate structures including real-time pricing (RTP), time-of-use (TOU) and critical-peak-pricing (CPP), are usually applied by utilities. It is illustrated that with these time-varying rate structures users have opted to reduce their energy cost by taking DR action [42, 43, 44]. In [45], a cost-effective control scheme was proposed for building HVAC system to shift the energy usage away from the peak hours while thermal comfort and IAQ levels are maintained.

For reducing peak demand, most buildings are operated according to a simple on-off strategy: the A/C systems are turned on during the occupied period and turned off otherwise. The setpoints of thermostats are usually fixed during the entire occupied period. This strategy is simple but not optimal for energy efficiency or cost-effectiveness [46]. Some alternative strategies are proposed to reduce significant peak demand by adopting pre-cooling (or pre-heating) during a non-occupied period and changing setpoints during peak hours. These strategies use the building's thermal mass to shift the power demand. However, the setpoint schedule is pre-determined, which does not consider the time-varying outdoor and indoor conditions and the states of HVAC systems. A number of researchers have focused on

reducing the peak demand by adjusting the operational scheduling of HVAC systems [47, 48]. However, these methods are not able to deal with the impact of disturbances such as buildings' internal loads and weather conditions. Therefore, it is of great interest and potential to develop advanced approaches to energy and cost savings for building A/C systems as well as handling disturbances.

1.2.3   Model predictive control

Model predictive control (MPC) has become one of the most successful advanced control strategies, which is capable of maintaining a comfortable temperature and achieving energy efficiency in buildings [49, 50, 51]. Other advantages of an MPC algorithm for building HVAC systems include robustness, tunability and flexibility [52]. The MPC strategy has also been applied in intervention strategies for other sectors, such as human immunodeficiency virus (HIV) infection [53], the dense medium coal washing process [54], power dispatch problems [55] and transportation systems [56]. Therefore, it has inspired many researchers employing MPC algorithms for HVAC systems to enhance both indoor thermal comfort and energy efficiency [57, 58, 59]. An MPC strategy is capable of improving potential building energy efficiency and thermal comfort and the performance is better than conventional PI controllers reported in [49]. In [60], an economic MPC method was presented for optimizing the building demand and energy cost under a TOU price policy to improve temperature comfort and reduce demand, as in [61, 62]. In [60], the simulation results showed that the MPC strategy is able to shift the peak demand to off-peak hours and reduce energy costs more in comparison with a baseline case. However, the goodness-of-fit for temperature and power models is 76.22% and 80.3%, respectively, which mean that the non-accuracy is approximately 24% and 20%, respectively, due to modelling a linear system. The authors have also tested on particular days to show the advantage of MPC over its baseline strategy, but it can be seen from the tests that load shifting on particular days is no more than 24%, which implies that the performance of the MPC strategy was unsatisfactory.

In [63], the authors proposed a hybrid model predictive control (HMPC) scheme, including a classical MPC and a neural network feedback linearization, to minimise the energy and cost of running HVAC systems in commercial buildings. Though the study modelled a nonlinear HVAC system, it was to be controlled based on a linearized system by feedback linearization, which added control variables and in turn increased computational complexity. This control method was also used in [64]. In [65], an MPC strategy was presented to reduce energy cost and demand while keeping indoor temperature at a

comfort level. To facilitate the MPC controller, the nonlinear HVAC system is linearized around an equilibrium point. This equilibrium point is obtained by fixing the supply fan and solving a state point. In [66], the authors proposed a practical cost and energy-efficient MPC strategy for HVAC load control under dynamic real-time electricity pricing. The simulation results displayed that the MPC strategy can lead to significant reductions in energy consumption and cost for occupancies. However, the building's nonlinear thermal model is linearized and used as the plant to be controlled by the presented MPC strategy. A model-based predictive controller combined with a building energy management system was purposed to improve indoor environmental quality, including CO_2 concentration, air temperature, relative humidity and illuminance, and minimize energy costs in [67]. However, the study did not consider the coupling effects between them.

1.2.4   Hierarchical control

To enhance energy efficiency while maintaining both indoor IAQ and thermal comfort at comfort ranges, another MPC strategies based on energy scheduling were proposed in [68, 59, 69]. In [69], a hierarchical control method was proposed for enhancing energy efficiency while maintaining the predicted mean vote (PMV) index at zero, i.e., PMV=0. The simulation results suggested that the strategy can save more energy in comparison with the authors' previous work [68]. However, a practical nonlinear MPC optimizer is designed in the upper layer to provide an impulse air temperature reference for the lower layer PI controller, which inevitably increases the computational burden. Moreover, the weather conditions and cooling loads are based on predicted data, which means the lower PI controller may not effectively follow the reference calculated by the upper layer. In [70], the authors considered two levels of the controller hierarchy to minimize energy usage and maintain temperature comfort. However, this control strategy is scheduled based on a linearized system which causes loss of accuracies in the model.

1.2.5   Large-scale A/C system control

Advanced building structures are extremely complicated because they are equipped with multiple A/C systems. Effective energy management of multi-zone building A/C systems has potentially improved energy efficiency and indoor comfort levels. In recent years, this interesting topic has inspired many researchers to study how to advance the strategies for controlling building A/C systems.

In [71], the authors proposed a combined genetic algorithm and feed-forward control for HVAC systems to improve energy efficiency and indoor air quality. Compared with the optimal control strategy in [37], the control strategy in [71] considered the optimal outdoor air ratio entering the system. In [72], the authors presented a model-based optimal ventilation control approach for multi-zone VAV A/C systems aimed at minimizing the total fresh air flow rate by compromising thermal comfort, IAQ and total energy usage. In [73, 74], the authors proposed an optimal control algorithm based on adaptive predictive model and the recursive least squares estimation technique to control indoor CO_2 concentration, relative humidity and air temperature, simultaneously. This was achieved by optimising the energy consumption of variable refrigerant flow and VAV combined A/C systems, as in [75, 39]. A data-mining approach for the optimization of HVAC systems was presented in [76], as in [77]. However, these approaches are rarely able to handle the impact of disturbances such as building multi-zones' internal heat loads and time-varying weather conditions.

Though MPC yields better performance to handle the above issues over other control approaches, the size of the optimization problem increases rapidly when the dimension of the building HVAC systems is large. A centralized MPC technique was proposed for multi-zone building HVAC systems to improve energy efficiency and temperature comfort [78, 79, 80]. In the centralized control structure case, all the subsystems are controlled by one MPC law. The model used for prediction consists of the coupling elements. When this algorithm is used to control building HVAC systems in a large number of rooms, especially connected zones and rooms, this algorithm is impractical, since the optimization problems may be difficult to solve in a reasonable time and the control systems are not easy to maintain. To improve computational efficiency, one of the effective control strategies is a decentralized control approach. Large-scale control problems are decomposed into several independent controllers, which can consider each local control parameter [81, 82]. In [81], the results demonstrated that the predicted performance loss was 28.58%. In [82], the simulation results demonstrated that the performance of comfort level is not better than that of the centralized MPC strategy, though the energy efficiency level is close to the centralized method, due to rarely considering the coupling between neighbouring zones. To improve comfort level and reduce computational demand for buildings, a superior choice is to use a distributed control algorithm. The structure of the distributed control strategy is similar to a decentralized law but is essentially a different approach [83]. The distributed control decomposes the centralized control to a group of local agents that communicate with their neighbors, making it possible to use them for large-scale dynamically coupled systems. A communication network that allows collaboration among the local control laws allows improvement of global system performance

compared to a decentralized structure. Moreover, the computational demand of this control strategy should be significantly reduced compared to the centralized structure [84].

Because of the advantages of distributed model predictive control (DMPC), this approach has recently been widely employed to reduce computational demand and handle the coupling among subsystems [85, 86, 87, 88]. Despite DMPC having a superior performance to other control strategies, the purely DMPC algorithms are very conservative for application [88] when the systems are nonlinear. In [86], a DMPC was proposed to improve energy efficiency while maintaining each zone's air temperature within a comfort level. In [85], the DMPC algorithm employed, only required the predicted output to exchange information with its neighbors for every sampling period. However, this algorithm could only obtain Nash equilibrium, which may not be the optimal solution. In [87], the authors presented a DMPC algorithm to control the building multi-source multi-zone temperature regulation problem. In order to attenuate the online computational burden, the DMPC algorithm was implemented based on a Bender' decomposition. The results demonstrated that the computational and convergence time of this algorithm was superior to that of the centralized MPC. However, the energy efficiency of this DMPC algorithm was not particularly good compared to the centralized MPC algorithm, as in [88].

In [89], a centralized MPC supervisor calculated evaporator cooling and pressure setpoints for multiple rooms and balanced temperature regulation with energy efficiency; these reference points were tracked by local level decentralized MPC controllers. More recently, in [90], the authors proposed a method that combined the closed-loop distributed and centralized structures to design a hierarchical control scheme to balance computational complexity and conservativeness. In the study, the upper layer controller collects temperature and predictive information from all rooms and zones, which means that the centralized scheduling (CS) needs to communicate with all rooms. Moreover, the trajectory reference in the optimization objectives is given and fixed over a 24-hour period, as in [85, 86, 88]. Centralized control and distributed MPC schemes following a fixed trajectory reference were also reported in other fields [91]. In [92], the results demonstrated that the MIMO MPC strategy following preprogrammed time-varying reference points can reduce energy consumption and cost more when compared with a fixed trajectory reference. In [93], the authors proposed centralized control and distributed control schemes together to improve energy efficiency and thermal comfort. Although the optimal references are preprogrammed and time-varying, the upper layer optimization problem is nonlinear, and solving it for a large building using centralized approaches is computationally cumbersome, leading to scalability issues. Furthermore, for implementation, centralized approaches require transmission of zone-level

models and sensor information to the CS, leading to engineering difficulties and increasing information exchange.

1.3   DX A/C CONTROL SYSTEM FRAMEWORK

1.3.1   DX A/C system

A direct expansion air conditioning (DX) system, as one of A/C systems, uses a refrigerant vapour expansion/compression (RVEC) cycle to directly cool the supply air to a building because the evaporator is in direct contact with the supply air. The main components of a DX A/C system include an EEV, the outdoor compressor, a condenser coil and the evaporator placed indoor as shown in Fig. 1.1. Compared to common centrally chilled water-based A/C systems, the advantages of the DX A/C systems are simpler system configuration, better energy efficiency [94], and generally less cost of ownership and ease of maintenance. Consequently, DX A/C systems have been commonly employed in buildings over recent decades, particularly in small to medium scaled buildings. However, most current DX A/C systems use single-speed supply fans and compressors, which operate by on-off cycling as a low-cost method to maintain indoor air temperature only. This causes either indoor air overcooling or irretentive indoor air humidity. ON/OFF cycling thus results in a lower level of indoor thermal comfort for users. When advanced variable speed inverters technology is widely applied in DX A/C systems, the indoor relative humidity and air temperature can simultaneously be controlled by DX A/C systems by employing the varying speeds of the supply fans and compressors [95, 96].

However, since the complex dynamic features of heat and mass transfer happen at variable speed DX A/C system and there is strong cross-coupling between dry-bulb temperature and wet-bulb temperature inside the evaporator, it is extremely hard to design a simple control method to keep indoor relative humidity and air temperature at the appropriate comfort levels simultaneously. For example, the transient performance of two feedback control loops (i.e. the control loop for relative humidity by the varying speed of the supply fan and the control loop for air temperature by the varying speed of the compressor) when using a conventional proportional-integral-derivative (PID) feedback controller would be inherently poor because of the strong coupling effect between the two feedback loops, to control indoor relative humidity and air temperature [95]. To overcome and decouple the difficulties

of the strong coupling effect, many advanced control algorithms have been developed. The control strategies are mainly based on an empirical-based model and physical-based model.
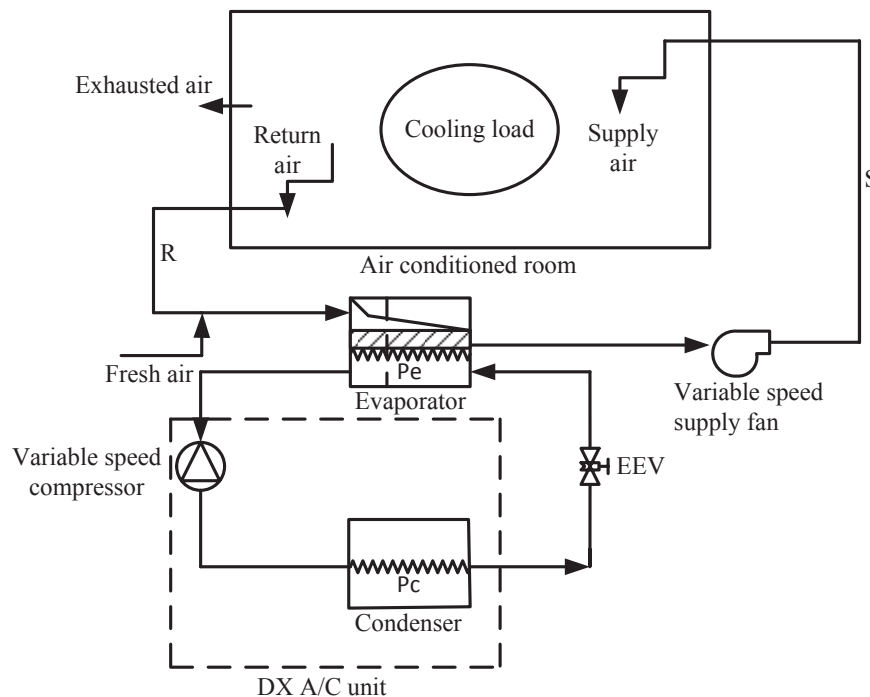
Figure 1.1. Schematics of a simplified DX A/C system.

1.3.2 DX A/C system control based on empirical-based models

There are many empirical-based methods to control the variable speed of DX A/C systems. Among various empirical-based methods, artificial neural network (ANN) has been widely used as an empirical-based modelling training technique, which has recently drawn many researchers' attention owing to its advantages of simplicity and good behavior on time response and accuracy of the modelled physical processes. An ANN-based control strategy was presented for a DX A/C system to control indoor relative humidity and air temperature simultaneously [97, 98]. The developed ANN-based dynamic model was trained off-line by using the operational data involving either a training point or a specific point. It would be incorrect to validate the performance of the proposed method when the operating conditions of the system are beyond the training point. Therefore, the performance of this designed ANN-based control approach can only be guaranteed when the training data are near the system operating point based on the off-line.

To ensure that the ANN-based controller is applied in the entire operating range of a DX A/C system, an ANN-based dynamic model with an on-line adaptive controller was proposed to control indoor relative humidity and air temperature simultaneously through the varying speeds of the compressor and the supply fan reported in [99]. The controllability test results showed that this strategy achieved high control accuracy and the operational data was within entire expected operating range. However, in this study, the ANN-based training method with an on-line adaptive controller was only tested at a fixed inlet relative humidity and air temperature. The inlet relative humidity and air temperature directly affected the output cooling capacity of the DX A/C system reported in [100]. Therefore, training data for adopting an empirical-based model controller for a variable speed DX A/C system to simultaneous control indoor relative humidity and air temperature should be within the entire possible operating ranges of the system, which include not only data for varying the speeds of the supply fan and the compressor, but also for varying the inlet relative humidity and air temperature from the DX evaporator. That implies that different indoor air setpoint settings in the conditioning space are governed by the DX A/C system. Nonetheless, the strong coupling between heat and mass transfer, such as sensible heat and latent heat loads that occur mainly in the wet-cooling region at the air side of the DX evaporator, may further affect accuracy when using an ANN-based model for controlling indoor relative humidity and air temperature simultaneously if the model is used beyond the range of training data.

Motivated by the above issues, a novel ANN-aided fuzzy logic controller for a variable speed DX A/C system was proposed to control indoor relative humidity and air temperature simultaneously by combining the complementary merits of fuzzy logic controllers and ANN modelling reported in [101]. The simulation results showed the satisfactory control performance in terms of control accuracy and sensitivity with different inlet relative humidity and air temperature. There is still an obstacle of heat and mass transfer for sensible heat and latent heat loads taking place at the wet-cooling region and dry-cooling region on the air side of the DX evaporator that is extremely complex and strongly coupled, it may be necessary to propose a novel ANN-based model and control method to solve this issue.

1.3.3   DX A/C system control based on physical-based models

The development of physical-based models for depicting the operational process of DX A/C systems can provide a direct description of the natural phenomena and reflect their detailed operational charac-

teristics since these are derived from physical laws. For example, with the model, the transient and steady state behavior of the system can be predicted, and the influence of input variables, such as air volumetric flow rate and mass flow rate of refrigerant, as well as the air side states can be identified [102, 103, 104, 105]. The steady state and transient response processes for components of a DX variable air volume (VAV) A/C system were illustrated in [102]. In [103], dynamic mathematical models for a DX A/C system were built based on the principle of energy and mass conservation balance and validated through experimental tests. In the study, the coupling loop between relative humidity and air temperature is considered, which is beneficial for decoupling the two strongly coupled loops of a DX A/C system to control the indoor relative humidity and air temperature simultaneously. The validated models are expected to be very useful for future work in designing an effective controller for a DX A/C system to control indoor relative humidity and air temperature simultaneously. The extremely complicated process of heat and mass transfer occurring on the DX cooling coil was developed under a steady-state equipment sensible heat ratio reported in [105].

In [106], a feedback controller for a DX A/C system was designed to avoid the use of a problematic measurement of A/C system immediately downstream of a cooling coil by controlling action. In [107, 108], a direct digital control (DDC) based capacity controller was designed for a DX A/C system to achieve indoor relative humidity and air temperature at a comfortable level by varying the speeds of the compressor and supply fan. The simulation results showed that the designed controller could achieve reasonable control sensitivity and accuracy. However, the measured indoor cooling load is taken as a controlled parameter, which cannot be obtained constantly owing to the thermal inertia of the indoor air. Therefore, it is difficult to achieve good performance in controlling sensitivity and accuracy. In [109], an H-L control algorithm, which is a DX A/C system operating at high speeds of the supply fan and the compressor when the indoor air temperature cannot reach its setpoint and at low speeds otherwise, was proposed. The experimental results suggested that the H-L control algorithm could achieve higher control performances of indoor relative humidity and energy efficiency in comparison with conventional on-off control. However, the development of H-L control could not achieve accurate control of indoor relative humidity and air temperature. The stability of command following and disturbance rejection could not be guaranteed.

A multi-input-multi-output (MIMO) linear quadratic Gaussian (LQG) controller was presented based on a DX A/C system to control indoor relative humidity and air temperature simultaneously and maintain these at their setpoints through the varying speeds of the supply fan and the compressor in

[110]. The command-following and disturbance rejection capability tests showed that the proposed MIMO LQG controller can effectively control indoor relative humidity and air temperature with high control performance of accuracy and sensitivity. However, the LQG controller is designed based on a linearization dynamic model. Furthermore, the system is linearized around a particular operating point of a DX A/C system. For a real DX A/C system, the controller should be operated over a wider working range. In [111], the authors proposed another control strategy by employing a PID controller with a degree of superheat (DS) to improve the stability and operating efficiency of a DX A/C system. However, in this study, the DX A/C system was still linearized around a particular operating point. In [112], the authors proposed a novel DDC-based capacity controller including a numerical calculation algorithm and a conventional proportional-integral (PI) feedback controller for a DX A/C system to control an electronic expansion valve (EEV). The experimental results showed that the control performance on the supply air temperature with this capacity controller is well maintained at the desired value and desired space air temperature is achieved. However, the controller performance can only be achieved based on fixing the air temperature entering the air-cooled condenser, the condenser air flow rate, the supply air static pressure and the degree of refrigerant superheat at the exit of the evaporator. In reality, the controller for a real DX A/C system should be applied to a wider working range.

To control multi-zone buildings' relative humidity and air temperature simultaneously, an energy-efficient multi-evaporator (ME) A/C system was proposed in [113]. Experimental results demonstrated that the control performance of the proposed capacity control algorithm was further improved in comparison with its previous work. However, under certain operating conditions, controlling indoor air temperature by using the novel capacity control algorithm could still cause significant fluctuations owing to using a temperature of dead-band and time-delay for compressor start-up. Nonetheless, interaction with other indoor units may be an important impact factor but was rarely considered. To improve energy efficiency with superior thermal comfort and IAQ levels for multi-zone building ME A/C system, a suitable optimization method is required for making each room's CO_2 concentration, humidity and air temperature consistent with their desired references. To realize this, one should consider a case when each DX unit can exchange information with its neighbors. A generalized control heuristic and simplified model predictive control strategy were proposed for DX A/C systems to provide comfort temperature and energy savings [114].

1.4   RESEARCH GAP

Firstly, based on findings from the literature, no study to discuss how to control indoor CO_2 concentration, relative humidity and air temperature simultaneously, taking into account of three coupling effects among them and in terms of the energy efficiency of DX A/C systems, has been reported in the literature so far. Therefore, controlling both IAQ and thermal comfort and taking into account energy efficiency for DX A/C systems will bring new control issues and increase the difficulty of control owing to the complex physical phenomenon inside a DX A/C system. In addition, although the findings in literature considered both IAQ and thermal comfort control issues in other A/C systems, they did not consider the coupling effects among them. These problems have been considered in this thesis. Nonlinear DX A/C control systems with respect to CO_2 concentration, relative humidity, air temperature and the coupling effects among them have been built in this thesis.

Secondly, [110] proposed a MIMO LQG controller for a DX A/C system to control indoor relative humidity and air temperature simultaneously with little consideration towards energy efficiency. In the study, the work point is near a specific operational point. For a real DX air conditioner, the controller should be operated over a wider working range. For controlling other nonlinear A/C systems, most of the researchers employed MPC controllers to optimize the plant attaining equilibrium operational points or specific operational points. These strategies may not be optimised in terms of cost-effectiveness or energy efficiency. These issues have been solved in this thesis. In this thesis, the proposed controller is designed based on a wider range of work point. In Chapter 2, an open loop optimal controller is first proposed to minimize the energy consumption of a nonlinear DX A/C system to generate an optimised and unique steady state. The MIMO MPC controller is designed to optimize the transient reaching this steady state while energy efficiency improvements are achieved. More details of this method are presented in Chapter 2.

Thirdly, MPC based on setpoint in terms of energy scheduling strategies and TOU policy for A/C systems were reported in the literature to reduce peak demand. None of them uses MPC based on setpoint adaptively preprogrammed and TOU policy in terms of energy and comfort scheduling to lower peak demand for A/C systems. In addition, the allowed outdoor air entering the system is fixed over a 24-hour period [73, 74, 115]. The outside weather circumstances are time-varying. In chapter 2, a VAV ventilation fan was added to a DX A/C system and have been used to reduce indoor air CO_2 concentration, which would increase the cost of hardware and the complexity of building DX A/C

systems. This hardware can also be commonly used in the HVAC systems to improve IAQ. Moreover, the PMV index can be conventionally used as an indicator of thermal comfort. As reported in findings in the literature, indoor thermal comfort affected by IAQ. It is, therefore, necessary to extend the PMV index such that it can represent both IAQ and thermal comfort. What's more, the heat and mass transfer on the air side of the evaporator has not been handled effectively in literature including empirical-based model and physical-based model methods. These issues have been solved in Chapter 3 of this thesis. In Chapter 3, the MIMO MPC controller and an open loop optimal controller, which adaptively and autonomously generates optimal and time-varying reference signals for the closed-loop controller, are designed. Details of this scheme and the control performance are presented.

Finally, according to the current practice of multi-zone building ME A/C system or HVAC systems and research reported in the above literature, no effective control strategy can handle interaction between rooms for the ME A/C system. Although studies on multi-zone building HVAC systems taking into account the interaction between rooms were recently reported in the literature. However, these strategies require more communication resources and were rarely solved in terms of energy efficiency, demand shifting and energy cost, computational complexity and conservativeness simultaneously. Therefore, there is a need to propose a new hierarchical distributed control strategy to improve the performance of energy efficiency, demand shifting and energy cost, and reduce the communication resources, computational complexity and conservativeness for the multi-zone building ME A/C system while keeping multi-zones' IAQ and thermal comfort at comfort levels. Therefore, two controllers, including an open loop distributed controller taking into account DR action to shift peak demand and a closed-loop distributed controller, are designed in this thesis to study energy efficiency and cost savings improvement of the multi-zone building ME A/C system. Details of the two distributed controllers are described in Chapter 4 of this thesis.

1.5 SCOPE AND OBJECTIVES

Motivated by the above issues, there is great potential for energy and cost savings with advanced control of A/C systems while maintaining both indoor IAQ and thermal comfort at comfort levels. The focus of this thesis is the design of new control strategies for DX A/C systems that improve comfort levels for occupants and at the same time reduce energy consumption and cost of buildings. The methodology to be described in the thesis can also be applied to other types of A/C systems.

The main purposes of this thesis are the following:

- To develop dynamical mathematical equations for DX A/C systems with consideration of the coupling effects of CO_2 concentration, relative humidity and air temperature.

- To develop a hierarchical control strategy for a DX A/C system that can adaptively and autonomously generate the optimised and time-varying setpoints scheduling of indoor CO_2 concentration, relative humidity and air temperature which can be used to operate the DX A/C systems with higher energy efficiency and more cost saving.

- To develop a hierarchical control method to improve the energy efficiency, reduce the energy cost, shift peak demand and maintain multi-zones' IAQ and thermal comfort at comfort levels for building ME A/C system.

1.6   RESEARCH CONTRIBUTION AND LAYOUT OF THE DISSERTATION

The main contributions of this thesis have been published in two international journal papers and a third one has been submitted. Moreover, several conference contributions have been published or accepted. These contributions are listed in the section on publication.

The main topic of this thesis is to develop a hierarchical control scheme to lower energy consumption and cost for building DX A/C systems while maintaining both IAQ and thermal comfort at comfort ranges. The contributions are briefly highlighted below in a representation of the layout of this dissertation.

- Building dynamical models for DX A/C control systems with respect to indoor CO_2 concentration, air temperature and relative humidity with consideration for the coupling effects between them.

- Design of two controllers for a DX A/C system, consisting of an energy-optimised open loop nonlinear controller and a regulation MIMO MPC controller, to improve both indoor IAQ and thermal comfort and maintain them at comfortable levels while minimizing energy consumption.

- Design of two controllers for a DX A/C system, including an energy and comfort open loop optimal controller and the tracking MPC controller, to lower energy consumption and cost while keeping both IAQ and thermal comfort at comfort levels.

- Design of a two-layer distributed control scheme to reduce energy consumption and cost, communication resources, computational complexity and conservativeness simultaneously, while maintaining multi-zones' IAQ and thermal comfort at comfort levels.

- The designed autonomous hierarchical distributed control strategy (AHDC) is capable of shifting the peak demand to off-peak hours for buildings.

The layout of this dissertation follows the order of improving both indoor IAQ and thermal comfort, minimizing energy consumption, and reducing cost while maintaining both IAQ and thermal comfort in acceptable ranges and shifting demand for the DX A/C systems.

Specifically, Chapter 2 describes a DX A/C system and its main components, and models dynamic mathematical equations of a DX A/C system with respect to indoor CO_2 concentration, relative humidity and air temperature taking account of three coupling effects between them based on principles of mass and energy balance. This is used to facilitate the research work for this dissertation. A hierarchical control strategy is designed first, followed by the performance of this control strategy through energy efficiency, setpoint regulation, reference following and disturbance rejection.

In Chapter 3, an autonomous hierarchical control (AHC) is designed to reduce energy consumption and cost for a DX A/C system in a changing environment over a 24-hour period in this chapter. The use of the nonlinear DX A/C control system given in chapter 2 is also used in this chapter, but the correlation of the moisture content and air temperature at the evaporator outlet has been released. After that, an open loop optimal controller, which includes the ability of autonomously and adaptively setting setpoints, for lower layer controller is designed for the DX A/C system to follow. The design of the MIMO MPC controller steers the DX A/C system to follow the time-varying and optimised setpoints. The AHC performance analysis of the energy efficiency and cost savings of the DX A/C system is given.

Next, an AHDC strategy is carried out for a multi-zone ME A/C system in Chapter 4. The dynamic

models of multiple connected rooms and zones for an ME A/C system are built first, taking into account interconnected neighboring rooms. In this chapter, the designed open loop optimal controller is distributed; it only collects local information from one zone or room, to autonomously and adaptively generate reference points, for closed-loop controllers. This is achieved by optimizing the demand and energy costs of the multi-zone building ME A/C system under a TOU rate structure while meeting the requirements of multi-zones' thermal comfort and IAQ at comfort ranges. The closed-loop controller is also distributed to track the reference points calculated by the upper layer distributed controller. After that, the control performance of AHDC compared with the hierarchical control method in Chapters 2 and 3 is given at the end.

Finally, some general conclusions of this dissertation and ideas for future research topics are given in Chapter 5.

CHAPTER 2   PREDICTIVE CONTROL OF A DX A/C SYSTEM FOR ENERGY EFFICIENCY

2.1   INTRODUCTION

In this chapter, nonlinear control systems with respect to indoor air CO_2 concentration, relative humidity and air temperature, taking into account the coupling effects among them in a DX A/C system are firstly modelled. In order to improve indoor IAQ, thermal comfort, and energy efficiency, a hierarchical control scheme is designed as a regulation MIMO MPC controller and an open loop nonlinear controller based on an energy consumption optimization. For this optimal control strategy, the energy models for a DX A/C system validated by curve-fitting of the experimental data in [116] and the system constraints are formulated. The MIMO MPC controller optimises the indoor CO_2 concentration, relative humidity and air temperature of the DX A/C control system to follow a unique and optimal steady state, which is generated by an open loop optimal controller to minimize the energy consumption of the DX A/C system with the reference indoor CO_2 concentration, relative humidity and air temperature maintained. To show the performance of this hierarchical control scheme, comparisons of energy consumption for setting different indoor CO_2 concentration, relative humidity and air temperature setpoints are developed by a case study. In addition, the setpoints regulation, reference following capability and disturbance rejection are also tested in a DX A/C system to demonstrate the proposed control performance.

2.2   CHAPTER OVERVIEW

This chapter presents a hierarchical control scheme to improve the energy efficiency of the DX A/C system while maintaining indoor CO_2 concentration, air temperature and relative humidity at their desired setpoints. A DX A/C control system and preliminaries are modelled and described in Section 2.3, respectively. Section 2.4 outlines the proposed energy-optimised open loop nonlinear control as well as the linearization of DX A/C control system. The presented MIMO MPC controller and algorithm are presented in Section 2.5. Simulation results through setpoints regulation, reference following capability and disturbance rejection tests are given in Section 2.6. Finally, conclusions are drawn in Section 2.7.

2.3   DX A/C SYSTEM DESCRIPTION

2.3.1   DX A/C system

Fig. 2.1 shows a simplified schematic diagram of a VAV DX A/C system. The VAV DX A/C system consists of two main sections, a DX refrigeration plant (refrigerant side) and an air-distribution sub-system (airside). A variable speed scroll compressor, an EEV, a VAV ventilation, an air-cooled tube-plant-finned condenser and a high-efficiency tube-louvre-finned DX evaporator constitute the major components of the DX refrigeration side. The evaporator inside the supply air duct plays as DX air cooling coil. A variable speed centrifugal supply fan, an air-distribution ductwork with return air dampers and a conditioned thermal space constitute the air-distribution sub-system.

2.3.2   A/C space

In this chapter, the performance of the presented hierarchical control strategy is evaluated by a single room model (that has been employed in the building energy simulation test (BESTEST) [57]).
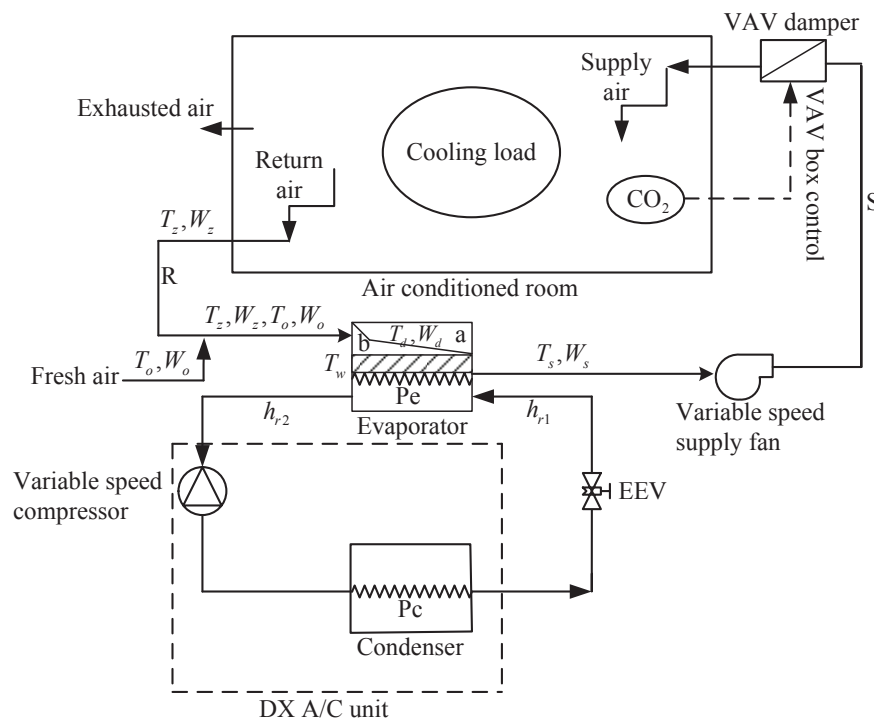
Figure 2.1. Schematics of a VAV DX A/C system.

2.3.3   Single-zone DX A/C model

According to principles of energy and mass conservation balances, the dynamical mathematical model

of the DX A/C system is a highly nonlinear coupling system with regard to indoor CO_2 concentration,

moisture content and air temperature. It is assumed that the DX A/C system is operated in the cooling

mode. The assumptions and basic operation of the DX A/C system are described below. Most of the

following assumptions are standard; they are taken from [103] and are sometimes made for the sake of

simplicity.

(A1) $p\%$ $(0 < p < 100)$ of outside air entering into the system is combined with $(100 - p)\%$ of the

recirculated air at the inlet of the evaporator.

(A2) Before getting conditioned, enough air mixing takes place inside the heat exchangers.

(A3) The air side of the DX evaporator is separated into two areas, including the dry-cooling area

and wet-cooling area. Only the inlet air temperature can be cooled along the dry-cooling area and the

wet-cooling area occurs dehumidify the air. The simplified diagram of the evaporator is displayed in Fig. 2.1. Generally, the dry-cooling area *b* on the air side of the evaporator is very small and it is only used to decrease the inlet air temperature to reach its dewpoint temperature, while the wet region area *a* can be used to couple air dehumidification and cooling.

(A4) Heat losses in air ducts are negligible.

(A5) The supply air enters into the conditioned space to reduce the cooling and pollutant loads acting upon the system.

(A6) In the conditioned room, $(100-p)\%$ of air is recirculated to the system and the rest of the air is exhausted from the air-conditioned room by a damper.

The mass conservation and energy balance mathematical equations of the DX A/C system based on the above assumptions are presented below.

The dynamic mathematical equation based on the principle of energy balance for indoor air temperature in a conditioned room is given as [103]

$$C_a \rho V \frac{\mathrm{d}T_z}{\mathrm{d}t} = C_a \rho v_f (T_s - T_z) + Q_{load}, \tag{2.1}$$

where C_a denotes the specific heat of air; ρ represents the air mass density; V denotes the volume of the air-conditioned room. v_f denotes the air volumetric flow rate of the supply fan, which can be calculated by

$$v_f = k_{fan} S_{fan}, \tag{2.2}$$

where S_{fan} denotes the supply fan speed, k_{fan} represents the gain coefficient of the speed of the supply fan. Q_{load} is the indoor sensible heat load, which is associated with the air temperature in the conditioned space and is mainly relevant to occupants, equipment, electrical devices, supply fan heat gain, external heat load and the ventilation load, etc. The heat emitted from electrical devices, equipment, supply fan heat gain, external heat load and the ventilation load is easy to identify; the main uncertainty of the sensible heat loads are determined by the load related to occupants and can be estimated by the current CO_2 concentration emission in the conditioned space. Hence, a simplified sensible heat load can be calculated by

$$Q_{load} = \mu C_c + \nu + Q_{spl}, \tag{2.3}$$

where C_c represents the indoor CO_2 concentration in the conditioned space; ν is certainty sensible heat load and μ is the gain coefficient of indoor sensible heat load. Q_{spl} is the sensible heat gain generated by the supply fan, which increases due to the air volumetric flow rate. It can be expressed by

$$Q_{spl} = k_{spl}v_f, \tag{2.4}$$

where k_{spl} denotes the coefficient of supply fan heat gain.

The dynamic mathematical equation based on the principle of energy conservation inside the conditioned room with respect to the indoor moisture content can be described as follows [103]:

$$\rho V \frac{dW_z}{dt} = \rho v_f(W_s - W_z) + M_{load}, \tag{2.5}$$

where the moisture loads M_{load} is mainly related to occupants, the fresh air ventilation load from outside air and electrical devices, and can be modelled as

$$M_{load} = \phi C_c + \gamma, \tag{2.6}$$

where γ denotes the certainty of latent heat load and ϕ is the latent heat gain parameter.

Based on the principle of energy balance, the air temperature in the dry-cooling area on the air side of the evaporator is given by

$$C_a\rho V_{h1}\frac{dT_d}{dt} = C_a\rho v_f(p\%T_0 + (1-p\%)T_z - T_d) + \alpha_1 A_1(T_w - \frac{(1-p\%)T_z + p\%T_0 + T_d}{2}), \tag{2.7}$$

where T_w denotes the surface air temperature on the DX evaporator wall; T_d is the air temperature at the end of the dry-cooling area inside the DX evaporator; V_{h1} denotes the air side volume of the DX evaporator on the dry-cooling area; A_1 denotes the heat transfer area in the dry-cooling area of the DX evaporator, α_1 represents the heat transfer coefficient in the dry-cooling area which can be computed by [102]

$$\alpha_1 = j_{e1}\rho v_a \frac{C_a}{Pr^{\frac{2}{3}}}, \tag{2.8}$$

where v_a is the face air velocity, j_{e1} is the Colburn factors; Pr is Prandtl number.

The coupling between sensible and latent heat transfers takes place in the wet-cooling region for air cooling and dehumidification. Therefore, the energy balance law applicable at the wet-cooling area on the air side of the DX evaporator can be written as follows:

$$C_a\rho V_{h2}\frac{dT_s}{dt} + \rho V_{h2}h_{fg}\frac{dW_s}{dt} = C_a\rho v_f(T_d - T_s) + \rho v_f h_{fg}((1-p\%)W_z + p\%W_0 - W_s)$$
$$+ \alpha_2 A_2(T_w - \frac{T_d + T_s}{2}), \tag{2.9}$$

where A_2 is the heat transfer area on the air side of the DX evaporator in the wet-cooling area; V_{h2} denotes the air side volume in the wet-cooling area of the DX evaporator; W_o is the outdoor moisture content; h_{fg} denotes the latent heat of vaporisation of water; α_2 is the heat transfer coefficient in the wet-cooling area calculated by [102]

$$\alpha_2 = j_{e2}\rho v_a \frac{C_a}{Pr^{\frac{2}{3}}}, \tag{2.10}$$

where j_{e2} is the Colburn factors.

The energy balance equation applicable at the DX evaporator wall is modelled by

$$C_w\rho_w V_w \frac{dT_w}{dt} = \alpha_1 A_1 \left(\frac{(1-p\%)T_z + p\%T_0 + T_d}{2} - T_w \right) + \alpha_2 A_2 \left(\frac{T_d + T_e}{2} - T_w \right)$$
$$- m_r(h_{r2} - h_{r1}), \tag{2.11}$$

where ρ_w, C_w, and V_w denote the density of the evaporator wall, the specific heat of air on the evaporator wall and the volume of the evaporator wall, respectively. h_{r1} and h_{r2} are the enthalpies of refrigerants, which associated with the inlet and outlet of the DX evaporator, respectively.

It is assumed that the supply air temperature and moisture content leaving the DX evaporator is about 95% saturated. Then, the connection between them can be obtained by depicting and curve-fitting as [103]

$$\frac{dW_s}{dt} - \frac{2 \times 0.0198T_s + 0.085}{1000} \frac{dT_s}{dt} = 0. \tag{2.12}$$

The dynamic mathematical equation of indoor CO_2 concentration in the conditioned space can be expressed by [37]

$$V\frac{dC_c}{dt} = v_s(C_s - C_c) + C_{load}, \tag{2.13}$$

where v_s is the volume flow rate of air supply; G is the quantity of CO_2 emission rate of one person; P denotes the number of occupants; C_s denotes the supply air CO_2 concentration by the VAV ventilation fan; $C_{load} = GP$ denotes the indoor pollutant load.

The details of the DX A/C control system are modelled by the above nonlinear differential equations (2.1)-(2.13), which can be expressed in a compact format

$$\dot{x} = f(x,u) = D^{-1}f_1(x,u) + D^{-1}f_2(z), \tag{2.14}$$

where $x \triangleq [T_s, T_z, T_d, T_w, W_s, W_z, C_c]^T$, $u \triangleq [v_f, m_r, v_s]^T$, and $z \triangleq [Q_{load}, M_{load}, C_{load}]^T$. The functions f_1, f_2 are defined by $f_1(x,u) = [f_{11}, f_{12}, f_{13}, f_{14}, f_{15}, 0, f_{17}]^T$, $f_2(z) = [Q_{load}, M_{load}, 0, 0, 0, 0, C_{load}]^T$

and

$$f_{11} = C_a \rho v_f (T_s - T_z),$$

$$f_{12} = \rho v_f (W_s - W_z),$$

$$f_{13} = C_a \rho v_f ((1 - p\%)T_z + p\%T_0 - T_d) + \alpha_1 A_1 (T_w - \frac{(1 - p\%)T_z + p\%T_0 + T_d}{2}),$$

$$f_{14} = C_a \rho v_f (T_d - T_s) + \rho v_f h_{fg} ((1 - p\%)W_z + p\%W_0 - W_s) + \alpha_2 A_2 (T_w - \frac{T_d + T_e}{2}),$$

$$f_{15} = \alpha_1 A_1 (\frac{T_d + (1 - p\%)T_z + p\%T_0}{2} - T_w) + \alpha_2 A_2 (\frac{T_d + T_e}{2} - T_w) - m_r (h_{r2} - h_{r1}),$$

$$f_{17} = v_c (C_s - C_c),$$

and the coupling matrix D can be described as

$$D = \begin{bmatrix} 0 & C_a\rho V & 0 & 0 & 0 & 0 & 0 \\ 0 & 0 & 0 & 0 & 0 & \rho V & 0 \\ 0 & 0 & C_a\rho V_{h1} & 0 & 0 & 0 & 0 \\ C_a\rho V_{h2} & 0 & 0 & 0 & \rho V_{h2}h_{fg} & 0 & 0 \\ 0 & 0 & 0 & C_w\rho_w V_w & 0 & 0 & 0 \\ -\frac{2\times 0.0198 T_s + 0.085}{1000} & 0 & 0 & 0 & 1 & 0 & 0 \\ 0 & 0 & 0 & 0 & 0 & 0 & V \end{bmatrix}.$$

The system models in (2.1), (2.5), (2.7), (2.9) and (2.12) supplying no fresh air to the system, have been validated by experimental test reported in [103]. Eq. (2.13) was verified through an on-line learning and model parameter identification estimation approaches with acceptable accuracy [37].

2.4   ENERGY-OPTIMISED OPEN LOOP OPTIMISATION

2.4.1   Open loop optimal controller

An open loop optimal controller is proposed to minimize the energy consumption of a DX A/C system, with given reference point of indoor CO_2 concentration, relative humidity and air temperature for generating a steady state. The energy model for a DX A/C system is given and used as an optimizing objective.

The energy consumed by a DX A/C system mainly entails the power consumption of the compressor P_{comp}, the fan power of the evaporator P_{eva}, the power consumption of the ventilation fan P_{ven}, the

fan power of the condenser P_{con} and the energy consumed by dampers. The energy consumption by the dampers is neglected. Total electric energy consumed by a DX A/C system is consequently expressed

$$P_{tot} = P_{eva} + P_{con} + P_{comp} + P_{ven}, \tag{2.15}$$

where P_{tot} denotes the total consumed energy of a DX A/C system at time t.

The power consumption of the evaporator fan P_{eva} can be presented as a polynomial function of the supply air temperature, the indoor cooling load and the air volumetric flow rate by [116]

$$\begin{aligned} P_{eva} = & a_0 + a_1 v_f + a_2 v_f^2 + a_3 T_s + a_4 T_s^2 + a_5 Q_{cool} + a_6 Q_{cool}^2 + a_7 v_f T_s + a_8 v_f Q_{cool} \\ & + a_9 T_s Q_{cool}, \end{aligned} \tag{2.16}$$

where the coefficients a_i $(i = 0, 1, \ldots, 9)$ are constant; they are obtained by curve-fitting of experimental data. Q_{cool} denotes the room cooling loads, which is the summation of indoor latent and sensible heat loads.

The power consumption of the compressor P_{comp} can be expressed by the empirical expression as follows [117]:

$$P_{comp} = b_0 + b_1 T_d + b_2 T_s + b_3 T_d^2 + b_4 T_d T_s + b_5 T_s^2 + b_6 T_d^3 + b_7 T_d^2 T_s + b_8 T_d T_s^2 + b_9 T_s^3, \tag{2.17}$$

where the coefficients b_i $(i = 0, 1, \ldots, 9)$ are constant and obtained by curve-fitting of the experimental data. It is noted that in [116, 117] the polynomial functions the experimental data better.

The fan power of the condenser P_{con} can be expressed as follows [116]:

$$P_{con} = c_0 + c_1 m_r + c_2 m_r^2, \tag{2.18}$$

where the coefficients c_i $(i = 0, 1, 2)$ are constant; they are obtained by curve-fitting of the experimental data as well.

The power consumption of the ventilation fan to reduce indoor CO_2 concentration is modelled as proportional to a third-order polynomial function of the volume flow rate of the supply air. The connection between the energy consumption of the ventilation fan and the volume flow rate of the supply air can be expressed as follows [37]:

$$P_{ven} = \omega v_s^3, \tag{2.19}$$

where ω is the energy gain coefficient of (2.19) that can be determined by parameter identification.

The coefficients of the energy models (2.16)-(2.18) for the DX A/C system can be determined by a regression analysis technique in this study. The root-mean-square error (RMSE), the relative error (RE) and the coefficient of variance (CV) are introduced and used to validate the fitness of the regression models. In this chapter, these experimental data are cited in [116], and it is shown that the RMSE, CV and RE are 7.16%, 12.89% and 13.43%, respectively. These errors are small and can be accepted. Therefore, the energy models can be used as an optimization objective in this chapter.

With regard to the proposed open loop optimal controller, the DX A/C system is presumed to be in its steady state with the reference of CO_2 concentration, moisture content and air temperature maintained. Therefore, $C_{c,ref}$, $W_{z,ref}$ and $T_{z,ref}$ are defined as the references of indoor CO_2 concentration, moisture content and air temperature in the conditioned space, respectively. The setpoints of indoor moisture content and air temperature can be chosen by a thermal comfort zone. The setpoint of CO_2 concentration is chosen acceptability to the occupants. The indoor thermal comfort level is given by a comfort zone in an American Society of Heating, Refrigerating and Air-Conditioning Engineers (ASHRAE) psychometric chart [118]. Fig. 2.2 shows the ASHRAE comfort zone. $T_{z,ref}$ and $W_{z,ref}$ are the two indicators, which are chosen as the centre point of the comfort zone shown in Fig. 2.2. A steady state of the DX A/C control system (2.14) is obtained by

$$D^{-1}f_1(x,u) + D^{-1}f_2(z) = 0,$$
$$T_z = T_{z,ref},$$
$$W_z = W_{z,ref}, \tag{2.20}$$
$$C_c = C_{c,ref}.$$

To reduce the energy consumption of the DX A/C system, the process is as below: The objective function (2.15) is optimised, while keeping the reference of indoor CO_2 concentration, moisture content and air temperature, to generate an optimised steady state for the DX A/C system. For a simplified purpose, x_i, $i = 1,2,\ldots,7$, represent each variable of the system state vector x, and u_i, $i = 1,2,3$, denote each variable of input vector u. x and u should be satisfied with the following conditions.

(C1) $W_z \in [\underline{W}_z, \overline{W}_z]$, $T_z \in [\underline{T}_z, \overline{T}_z]$. The indoor moisture content and air temperature should be within the comfort bounds, which can be accepted by occupants. The thermal comfort upper and lower bounds $\underline{T}_z, \overline{T}_z, \underline{W}_z$ and $\overline{W}_z$ are the parameters, which are chosen in the light of the thermal comfort zone shown in Fig. 2.2.
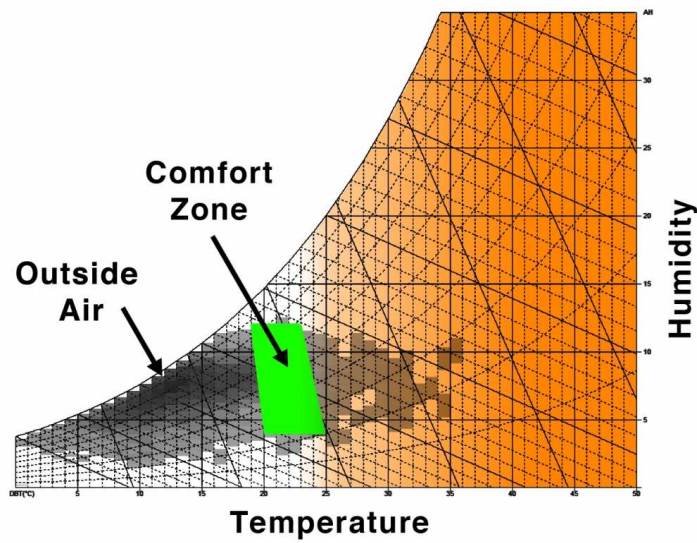
Figure 2.2. ASHRAE comfort range.

(C2) $C_c \in [\underline{C}_c, \overline{C}_c]$. This bound is the requirement range of indoor air CO_2 concentration.

(C3) $W_s \in [\underline{W}_s, \overline{W}_s]$, $T_s \in [\underline{T}_s, \overline{T}_s]$. The DX cooling coils and the physical characteristics of the coils restrict the bounds of supply moisture content and air temperature. Besides, the upper bounds $\overline{T}_s$ and $\overline{W}_s$ are less than the indoor air temperature T_z and indoor moisture content W_z, respectively, due to the DX A/C system operating in the cooling mode.

(C4) $W_s \leq (1-p\%)W_z + p\%W_0$, $T_d \leq (1-p\%)T_z + pT_0$. The inlet moisture content and air temperature across the DX cooling coils can only decrease in reaction to air cooling and dehumidification.

(C5) $T_w \leq T_d$. The air temperature at the DX evaporator wall is less than the air temperature in the dry-cooling region.

(C6) $v_f \in [\underline{v}_f, \overline{v}_f]$, $m_r \in [\underline{m}_r, \overline{m}_r]$, $v_s \in [\underline{v}_s, \overline{v}_s]$. The physical characteristics of the DX A/C system constrain the upper bounds $\overline{v}_f$, $\overline{m}_r$ and $\overline{v}_s$. The lower bounds $\underline{v}_f$, $\underline{m}_r$ and $\underline{v}_s$ are strictly positive to meet the ventilation and operation conditions of the DX A/C requirements.

(C7) $p\% \in [\underline{p}\%, \overline{p}\%)$. The upper and lower bounds constrain the ratio of the fresh air entering the system through the damper.

Thus, the open loop optimal scheduling of the DX A/C control system is a nonlinear programming (NLP) problem with the equality constraints in (2.20), the inequality constraints in (C1)-(C7) and the objective function (2.15). Hence, an optimization problem can be designed below

$$\min P_{total} \tag{2.21}$$

subject to:

$$D^{-1}f_1(x,u) + D^{-1}f_2(z) = 0,$$

$$T_z = T_{z,ref},$$

$$W_z = W_{z,ref},$$

$$C_c = C_{c,ref},$$

$$\underline{T}_s \le T_s \le \overline{T}_s,$$

$$\underline{T}_d \le T_d \le \overline{T}_d,$$

$$\underline{T}_w \le T_w \le \overline{T}_w,$$

$$\underline{W}_s \le W_s \le \overline{W}_s,$$

$$\underline{v}_f \le v_f \le \overline{v}_f,$$

$$\underline{m}_r \le m_r \le \overline{m}_r,$$

$$\underline{v}_s \le v_s \le \overline{v}_s,$$

$$h_i(x) \le 0, \ i = 1, 2,$$

where $h_1(x) = W_s - (1 - p\%)W_z - p\%W_0$ and $h_2(x) = T_d - (1 - p\%)T_z - pT_0$.

In the optimization problem (2.21), the variables $T_s, T_d, T_w, W_s, v_f, m_r$ and v_s are used as the optimising variables to minimize P_{total}. In addition, the three variables T_z, W_z and C_c are also used as the optimising variables that have to satisfy $T_z = T_{z,ref}$, $W_z = W_{z,ref}$ and $C_c = C_{c,ref}$. For solving the above optimization problem (2.21), the researcher employs the Matlab built-in function *fmincon* to obtain optimal solution for $T_{s,s}, T_{z,ref}, T_{d,s}, T_{w,s}, W_{s,s}, W_{z,ref}, C_{c,ref}$ and $v_{f,s}, m_{r,s}, v_{s,s}$.

Remark 2.1 *There are many solutions in (2.20), which can be regarded as steady states. In [103, 110], the authors selected a specific operating point for the DX A/C control system to analyze the MIMO controller design. In [119], the nonlinear HVAC system was linearized around an equilibrium point. It can be obtained by fixing the system input and then solving the state as an equilibrium point, as that in [65, 80]. The researcher's proposal is an open loop optimal controller that minimizes an energy consumption model of the DX A/C system to generate an optimal and unique steady state.*

2.4.2   Linearization for closed-loop control

Let $\delta T_z = T_z - T_{z,ref}$, $\delta W_z = W_z - W_{z,ref}$, $\delta C_c = C_c - C_{c,ref}$, $\delta T_s = T_s - T_{s,s}$, $\delta T_d = T_d - T_{d,s}$, $\delta T_w = T_w - T_{w,s}$, $\delta W_s = W_s - W_{s,s}$, $\delta v_f = v_f - v_{f,s}$, $\delta m_r = m_r - m_{r,s}$ and $\delta v_s = v_s - v_{s,s}$ be the deviations of the system state variables and input variables from their steady states. Let $x_0 \triangleq$ $[T_{s,s}, T_{z,ref}, T_{d,s}, T_{w,s}, W_{s,s}, W_{z,ref}, C_{c,ref}]^T$ and $u_0 \triangleq [v_{f,s}, m_{r,s}, v_{s,s}]^T$ be the optimal steady state of states and inputs, respectively. The dynamic mathematical equation of the DX A/C control system is then linearized around the optimal steady states x_0 and u_0, which can be written as a linear system as

$$\begin{cases} \delta \dot{x} = A_c(x_0, u_0)\delta x + B_c(x_0, u_0)\delta u, \\ y = C\delta x + Cx_0, \end{cases} \tag{2.22}$$

where $\delta x \triangleq [\delta T_s, \delta T_z, \delta T_d, \delta T_w, \delta W_s, \delta W_z, \delta C_c]^T$ denotes the deviation of the state vector x from its optimal steady state of state x_0, $\delta u \triangleq [\delta v_f, \delta m_r, \delta v_s]^T$ denotes the deviation of the input vector u from its optimal steady state of input u_0. $y \triangleq [T_z, W_z, C_c]^T$ are the output variables of the original system, which require to be maintained at their desired setpoints. The system state and input matrices $A_c(x_0, u_0), B_c(x_0, u_0)$ are computed by:

$$A_c(x_0, u_0) = \left. \frac{\partial f(x, u)}{\partial x} \right|_{x=x_0, u=u_0} , \quad B_c(x_0, u_0) = \left. \frac{\partial f(x, u)}{\partial u} \right|_{x=x_0, u=u_0} ,$$

and the system output matrix is

$$C = \begin{bmatrix} 0 & 1 & 0 & 0 & 0 & 0 & 0 \\ 0 & 0 & 0 & 0 & 0 & 1 & 0 \\ 0 & 0 & 0 & 0 & 0 & 0 & 1 \end{bmatrix}.$$

Remark 2.2 *Linearization through the first order approximation of the Taylor expansion is one of the classical approaches to deal with nonlinear control problems in the field of control systems. It is locally valid in a neighborhood of the steady state. The loss of exactness of linearization is determined by the size of the local neighborhood and is normally recompensed deviations by using closed-loop control for the transient dynamics to attain the steady state which is generated by the open loop optimal controller. The designed closed-loop regulation control is an MPC, which is presented in the following section.*

2.5 CLOSED-LOOP CONTROL

2.5.1 Discrete-time linear system

The discrete-time expression of (2.22) is given by:

$$\begin{cases} \delta x(k+1) = A_d(x_0, u_0)\delta x(k) + B_d(x_0, u_0)\delta u(k), \\ y(k) = C\delta x(k) + Cx_0, \end{cases} \tag{2.23}$$

where k denotes the sampling instant, $y(k)$, $x(k)$ and $u(k)$ denote the output vector, input vector and state vector at sampling instant k, respectively. $A_d(x_0, u_0) = e^{A_c(x_0, u_0)T_{sp}}$, $B_d(x_0, u_0) = (\int_0^{T_{sp}} e^{A_c(x_0, u_0)t}dt)B_c(x_0, u_0)$ are the state matrix and input matrix of the discrete system (2.23), respectively. T_{sp} is the sampling period.

2.5.2 Cost function

The aim of the proposed MPC controller for the DX A/C is to maintain indoor CO_2 concentration, moisture content and air temperature at desired setpoints as well as improve energy efficiency. To reach the aim, the objective function is described by

$$\min_{\delta u} J = \min_{\delta u} (J_1 + J_2), \tag{2.24}$$

where

1. $\min J_1 = \min \sum_{i=1}^{N_p}(y(k+i) - r(k))^2$, which is to make sure the indoor air temperature, moisture content and CO_2 concentration are at desired levels;

2. $J_2 = \sum_{i=0}^{N_c-1} \|\delta u(k+i)\|_{\overline{R}}$, which implies the consideration given to the size of the control law u when the cost function J is intended to be as small as possible.

Here, $\overline{R}$ is a positive definite diagonal matrix defined as $\overline{R} = r_w I_{3N_c \times 3N_c}$ $(r_w > 0)$, where I is an identity matrix and r_w is a tuning parameter used to adjust the desired closed-loop control performance.

In the objective function (2.24), $y_1(k)$, $y_2(k)$, $y_3(k)$ are the predicted indoor air temperature, moisture contents and CO_2 concentration at the kth step, respectively. Define the predictive output variables by $Y = [y_1(k+1|k), y_2(k+1|k), y_3(k+1|k), \ldots, y_1(k+N_p|k), y_2(k+N_p|k), y_3(k+N_p|k)]^T$, where $y_1(k+$

$i|k)$, $y_2(k+i|k)$ and $y_3(k+i|k)$ denote the predicted output values of $y_1(k)$, $y_2(k)$ and $y_3(k)$ at step

i $(i = 1, \ldots, N_p)$ at the sampling instant k. Define $R_s = \overbrace{[I_{3\times3}, \ldots, I_{3\times3}]}^{N_p}{}^{T} r(k)$ as the reference point

vector, where $[T_{z,ref}(k), W_{z,ref}(k), C_{c,ref}(k)]^T \triangleq r(k)$ denote the setpoints of indoor air temperature,

moisture content and CO_2 concentration at the kth step. Define the input vector $U = \left[\delta u^T(k), \delta u^T(k+ \right.$

$\left. 1|k), \ldots, \delta u^T(k+N_c-1|k) \right]^T$ as the predicted input vector $\delta u^T(k)$ at time step k. N_p denotes the

prediction horizon, N_c denotes the control horizon.

2.5.3   Constraints

The constraints of the system control variables and the state variables can be used to guarantee that

the MPC algorithm is able to obtain a feasible solution by minimizing the objective function (2.24).

The details of these constraints are described in (C1)-(C6). It is noted that the problem of minimizing

the objective function (2.24) is a standard sequential quadratic programming (QP) problem, namely a

convex optimization problem under a linear constraints condition.

2.5.4   The proposed MPC algorithm

A standard MPC algorithm for the DX A/C system is formulated with the help of the state space model

(2.23), the objective function (2.24) and the constraints in (C1)-(C7). This algorithm can be designed

by

i. Compute the proposed MPC gain matrices as follows:

$$F = \left[\begin{array}{cccc} CA & (CA^2 & \ldots & CA^{N_p} \end{array} \right]^T, \; M = \overbrace{\left[\begin{array}{cccc} C & C & \ldots & C \end{array} \right]}^{N_p}{}^{T},$$

$$\Phi = \left[\begin{array}{cccc} CB & 0 & \ldots & 0 \\ CAB & CB & \ldots & 0 \\ \vdots & \vdots & \ddots & 0 \\ CA^{N_p-1}B & CA^{N_p-2}B & \ldots & CA^{N_p-N_c}B \end{array} \right].$$

$E = \Phi^T\Phi + \overline{R}$, and $H = (F\delta x(k) + Mx_0 - R_s)^T\Phi$.

ii. Based on the MPC design procedure, the predicted output vector Y can be transferred to the input vector U

$$Y = Mx_0 + F\delta x(k) + \Phi U, \qquad (2.25)$$

and minimizes the cost function (2.24) as

$$\min J = \min[(Y - R_s)^T (Y - R_s) + U^T \overline{R} U]$$
$$\Rightarrow \min(U^T EU + 2HU). \qquad (2.26)$$

iii. Optimization: The optimal control series U^* can be obtained by solving the objective function (2.26) under the constraints in (C1)-(C6) satisfied as follows:

$$U^* = \arg \min_U (U^T EU + 2HU), \text{ s.t. } (C1) - (C5) \text{ hold.}$$

iv. Compute the receding horizon controllers:

$$u^*(k) = [I_{3\times3}, 0, \ldots, 0]U^*.$$

v. $u^*(k)$ is used in the system (2.23).

vi. Set time $k = k + 1$, and update the system state variables, input variables and output variables with the optimal input $u^*(k)$ to the system (2.23). Repeat the above steps from i to vi until the output variables attain their desired horizon time.

2.5.5 Features of the proposed MPC strategy

The regulation of the MIMO MPC with an open loop optimal controller to minimize an energy consumption model of a DX A/C system are examined. Fig. 2.3 shows the overall steps of the proposed control approach, which is different from the previous studies. Fig. 2.4 details the framework of the proposed MIMO MPC with an open loop optimization scheme. This figure describes the main dynamic process of controlling the indoor CO_2 concentration, moisture content and air temperature, and the purpose of the open loop optimizing energy consumption.

In addition, to demonstrate the performance of the proposed control strategy, comparisons of different situations are given in the following simulations. The control performance of the proposed MPC under different situations is regarded as the first case. Comparison of control performance on energy

efficiency for the proposed MIMO MPC controller under different operating points based on the same comfort conditions is also investigated. After the simulation tests, more details of control performance will be provided.
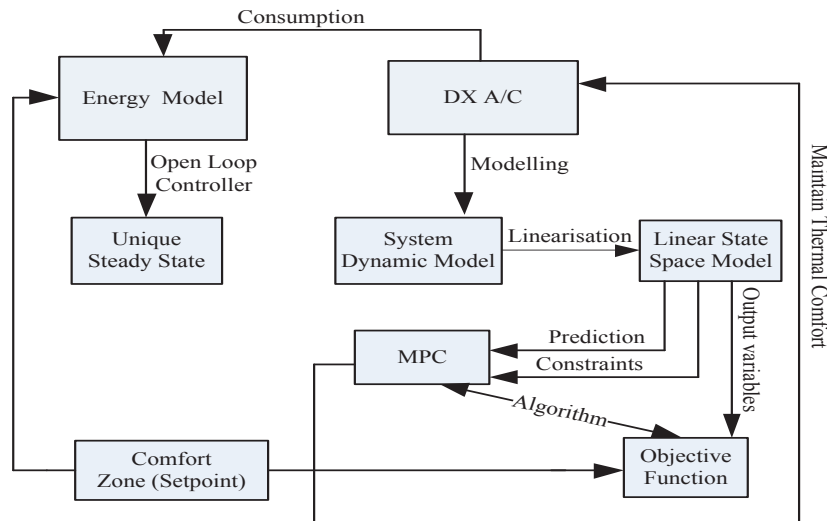
Figure 2.3. Simplified framework of the proposed control scheme.
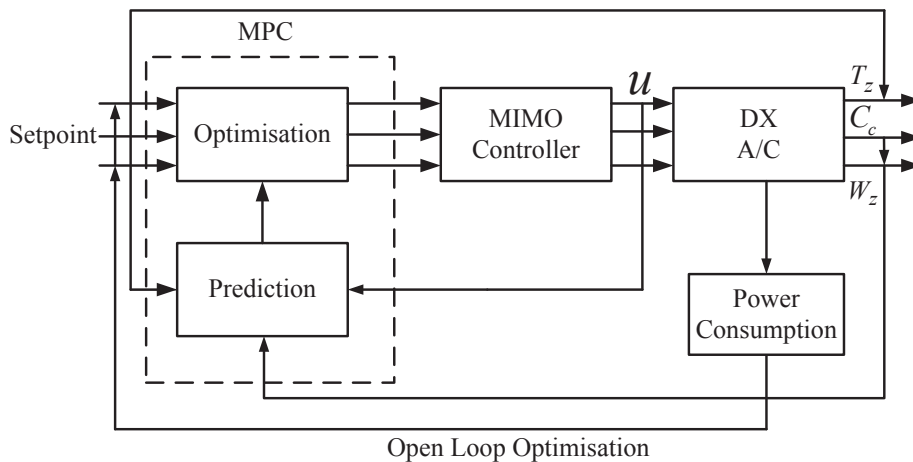
Figure 2.4. Framework of the proposed MIMO MPC with an open loop optimal control scheme.

2.6   RESULTS AND DISCUSSION

In this chapter, the performance of the proposed control method for a DX A/C system can be verified via simulations in a Matlab environment. The experimental data presented in Table 2.1 are taken from [116], which can be adopted to guarantee the validity of the energy models for a DX A/C system. The performance of the proposed control strategy depends on the energy models. A single-zone building is

Table 2.1. Coefficients of energy models.

Notations	Values	Notations	Values
a_0	900.5	a_1	-8.1
a_2	6.18	a_3	-0.15
a_4	-4.61	a_5	0.02
a_6	-0.2	a_7	0.01
a_8	0.12	a_9	0.09
b_0	-6942	b_1	82
b_2	-0.7	b_3	2.4
b_4	-2.5	b_5	2.68
b_6	0.03	b_7	-0.02
b_8	0.04	b_9	0.0001
c_0	138.1	c_1	0.52
c_2	-2.3		

Table 2.2. Parameters of the DX A/C system models.

Notations	Values	Notations	Values
ρ	$1.2 \, \text{kg/m}^3$	h_{fg}	$2450 \, \text{kJ/kg}$
V	$77 \, \text{m}^3$	ε_{win}	0.45
A_2	$18.759 \, \text{m}^2$	V_{h1}	$0.04 \, \text{m}^3$
k_{spl}	$0.0251 \, \text{kJ/m}^3$	C_z	$1.005 \, \text{kJ kg}^{-1} \, {}^\circ\text{C}^{-1}$
A_1	$3.311 \, \text{m}^2$	V_{h2}	$0.16 \, \text{m}^3$
A_0	$22.07 \, \text{m}^2$		

used as the conditioned space to conduct these tests. The system parameters of the DX A/C system listed in Table 2.2, which were validated by experimental data in [103], can be employed in this chapter. To test the proposed MPC strategy with an open-loop optimisation scheme, the DX A/C system's constraints are described in Table 2.3. In this simulation test, the original nonlinear dynamic model (2.14) can be used as the plant to control.

Table 2.3. Values of system constraints.

Notations	Values	Notations	Values
$\overline{T}_z$	26 °C	$\underline{T}_z$	22 °C
$\overline{W}_z$	12.3/1000 kg/kg dry air	$\underline{W}_z$	10.4/1000 kg/kg dry air
$\overline{C}_c$	850 ppm	$\underline{C}_c$	650 ppm
$\overline{T}_s$	22 °C	$\underline{T}_s$	10 °C
$\overline{W}_s$	10.4/1000 kg/kg dry air	$\underline{W}_s$	7.85/1000 kg/kg dry air
$\overline{T}_d$	22 °C	$\underline{T}_d$	10 °C
$\overline{T}_w$	22 °C	$\underline{T}_w$	10 °C
$\overline{v}_f$	0.8 m^3/s	$\underline{v}_f$	0 m^3/s
$\overline{m}_r$	0.11 kg/s	$\underline{m}_r$	0 kg/s
$\overline{v}_s$	3 m^3/s	$\underline{v}_s$	0 m^3/s

2.6.1   MPC with open loop optimal controller

To evaluate the performance of the proposed MIMO MPC with an open loop controller for minimizing an energy consumption of a DX A/C system scheme, three cases are given as follows:

(1) Setpoint regulation.

(2) Reference following.

(3) Disturbances rejection.

2.6.1.1   Setpoint regulation

The simulation case with $p = 25\%$ air volume exhausted is studied in this section. Regarding this simulation test, the researcher chooses the setpoints of indoor CO_2 concentration, moisture content and air temperature as $T_{z,ref} = 24$ °C, $W_{z,ref} = 11.35/1000$ kg kg^{-1} and $C_{c,ref} = 780.5$ ppm, respectively. $T_{z,ref}$ and $W_{z,ref}$ are chosen due to the comfort zone, as showed in Fig. 2.2, and the $C_{c,ref}$ is selected to be satisfied.

When under 25% indoor air volume is exhausted, according to Table 2.2, the researcher obeys the optimization process in (2.21), and the unique and optimised set of steady state is then obtained, which is listed in Table 2.4. The state and input matrices A_c and B_c of the corresponding system (2.22) under this steady state are calculated and given in Appendix A. To test the performance of the proposed MIMO MPC, the control parameters are provided as follows: the prediction horizon is set to $N_p = 24$ and the control horizon is set to $N_c = 24$, respectively; the tuning parameter is $r_w = 0.5$; the sampling interval is set to 2 minutes, and the total simulation time is set to $K = 24$ hours. To optimize the indoor CO_2 concentration, moisture content and air temperature at their desired setpoints, there are several types of constraints in the DX A/C system. To illustrate the robustness of the proposed closed-loop controller, a disturbance factor due to the model error is considered in the simulation test. For testing the MPC algorithm, the initial points of the system state variables are set to 23, 30, 23, 15, 12.44/1000, 13.5/1000 and 0.001, respectively, and the initial points of the system's input variables are set to 0.309, 0.0415 and 0.7, respectively. One per cent (%) is the unit of the relative humidity (RH), and 11.35/1000 kg/kg moisture content is amount to 60% RH in a conditioned room.

Table 2.4. The optimal operation point of the system under $p = 25\%$ exhausted air volume.

Parameter	Value	Parameter	Value
$T_{s,s}$	11.5 °C	$W_{s,s}$	8.665/1000 kg/kg dry air
$T_{z,ref}$	24 °C	$W_{z,ref}$	11.35/1000 kg/kg dry air
$T_{d,s}$	15 °C	$T_{w,s}$	12 °C
$m_{r,s}$	0.045 kg/s	$v_{f,s}$	0.298 m^3/s
$S_{fan,s}$	2102 rpm	$v_{sc,s}$	4243 rpm
$C_{c,ref}$	780.5 ppm	$v_{s,s}$	0.097 m^3/s
v	3.665 kW	γ	1.396 kW
T_0	30 °C	W_0	13.5/1000 kg/kg dry air
C_s	300 ppm		

The proposed MPC performance is displayed in Figs. 2.5-2.6. In Fig. 2.5, it depicts control of the indoor air temperature, relative humidity and CO_2 concentration simultaneously by using the DX A/C system in a conditioned room. It can be observed from Fig. 2.5 that the indoor air temperature, relative humidity and CO_2 concentration are reaching their desired setpoints. From Fig. 2.6, it can be observed that the varying speeds of the supply fan and the compressor and the volume flow rate of supply air can be regulated simultaneously by the proposed MIMO MPC controller for the DX A/C system through

setting relative humidity, indoor air temperature and CO_2 concentration levels. It can be noted that the indoor CO_2 concentration, relative humidity and air temperature are maintained at their desired setpoints afterwards when the setpoint is approached. It can also be noted that the proposed MIMO MPC controller for the DX A/C system steers the indoor CO_2 concentration, relative humidity and air temperature following their desired setpoints as 780.5 ppm, 60% and 24 °C, respectively, after a transient process of 20 minutes. After attaining their setpoints, indoor CO_2 concentration, relative humidity and air temperature are maintained at their desired setpoints with deviations no more than ± 9 ppm, $\pm 5\%$ and ± 0.5 °C, respectively. Hence, the setpoints of indoor CO_2 concentration, relative humidity and air temperature can be simultaneously maintained by using the proposed MPC controller to regulate the varying compressor speed, supply fan speed and volume flow rate of the supply air for the DX A/C system.

2.6.1.2   Reference-following capability test

Regarding the reference-following tests, the researcher expects that after the setpoint changes, the proposed MIMO MPC would respond immediately, such that the changing setpoint can be reached and maintained in a short time and in an optimal way.

The initial setpoints of indoor CO_2 concentration, moisture content and air temperature are set to 780.5 ppm, 11.35/1000 kg/kg and 24 °C, respectively, which are the same as the regulation test. After 12:00, their setpoints are changed to 650 ppm, 10/1000 kg/kg and 20.5 °C, respectively. Then, the current steady state, the variable constraints of the DX A/C system and the linearized system matrices will change correspondingly. Thus, to achieve this control objective, the constraint conditions of indoor CO_2 concentration, moisture content and air temperature are changed below. The output constraints are changed from 600 ppm to 700 ppm, 9.5/1000 kg/kg to 11.5/1000 kg/kg and 18 °C to 22 °C, respectively. The open loop optimal controller is used again with the changed setpoints to optimize the energy consumption model (2.15) to generate the optimised steady state for the MIMO MPC controller. Then the MIMO MPC controller follows the steady state calculated by the open loop controller. Note that this setpoint cannot select according to the comfort zone in this section. It is expected that with the setpoints changing, the proposed controller will be capable of having a reference-following capability. Figs. 2.7-2.8 depict the reference-following test results achieved for the proposed MIMO MPC with regard to the changing setpoints of the indoor CO_2 concentration, relative

(a) Indoor air temperature

(b) Indoor relative humidity

(c) Indoor CO_2 concentration
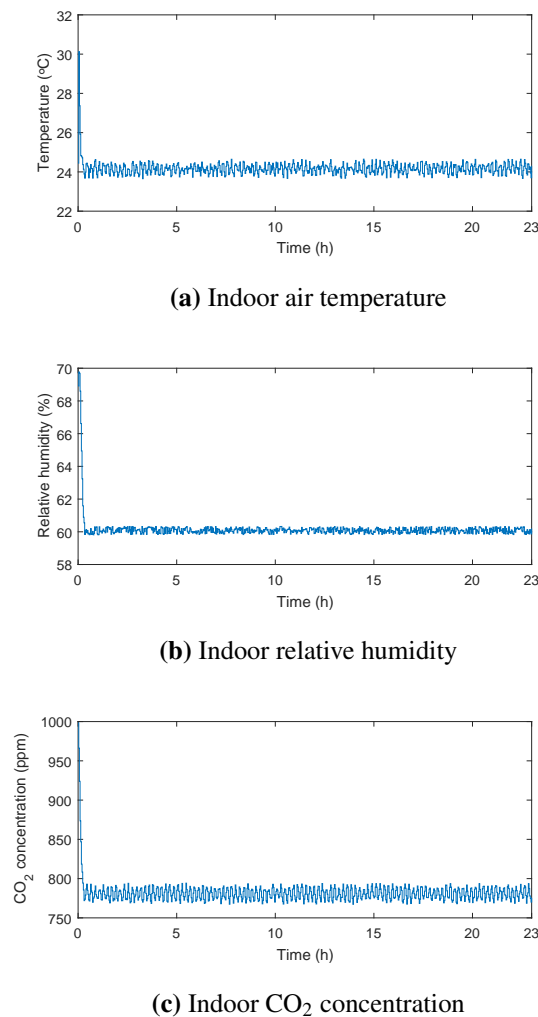
Figure 2.5. Setpoint regulation under 25% exhausted air volume.

humidity and air temperature by varying the speeds of the compressor and supply fan, and the volume flow rate of supply air. When the setpoints of indoor CO_2 concentration, moisture content and air temperature change from 780.5 ppm to 650 ppm, from 11.35/1000 kg/kg to 10/1000 kg/kg and from 24 °C to 20.5 °C, respectively, the steady state operation points of the supply air moisture content and supply air temperature of the DX A/C system have no choice but to change accordingly from 8.665/1000 kg/kg to 7.5/1000 kg/kg and 11.5 °C to 10.4 °C, respectively, by using the proposed open loop optimal controller and the MIMO MPC controller. During the simulation of the first 12 hours, the indoor moisture content, air temperature and CO_2 concentration are maintained at their initial setpoints, simultaneously, at the same time, the varying speeds of the supply fan and compressor and the volume flow rate of the supply air for the DX A/C system are stable at its steady state. At $t = 12 : 00$, when
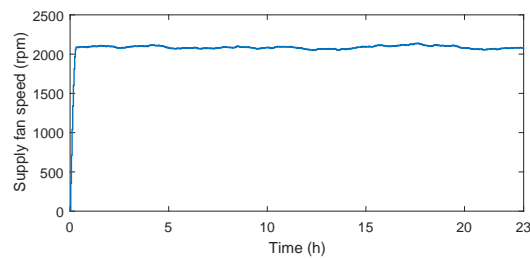
(a) Supply fan speed
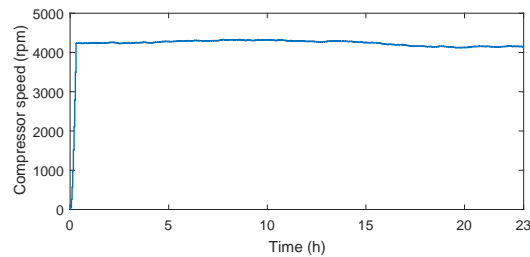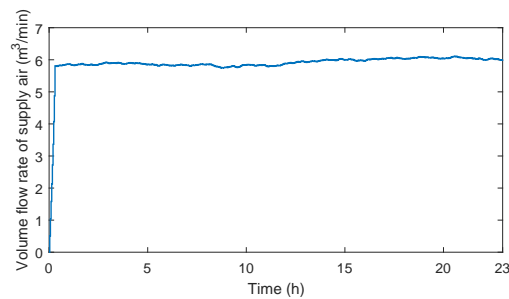
(b) Compressor speed

(c) Volume flow rate of supply air

Figure 2.6. Regulation of the varying speeds of the supply fan and the compressor and volume flow rate of supply air.

the indoor moisture content, air temperature and CO_2 concentration are set to 10/1000 kg/kg, 20.5 °C and 650 ppm, respectively, then these objectives follow their setting references under the proposed MPC controller to immediately by adjusting the speeds of the supply fan and the compressor and the volume flow rate of the supply air for the DX A/C system. In the end, the changes in the setpoints are reached again after a transient process of 16 minutes. It can be noted from Fig. 2.7 that the indoor CO_2 concentration, relative humidity and air temperature can be controlled and maintained at their changing references by the proposed MIMO MPC controller.

From Figs. 2.7 and 2.8, it can be noted that after changing the references to indoor air temperature,

(a) Indoor temperature

(b) Indoor relative humidity

(c) Indoor CO_2 concentration
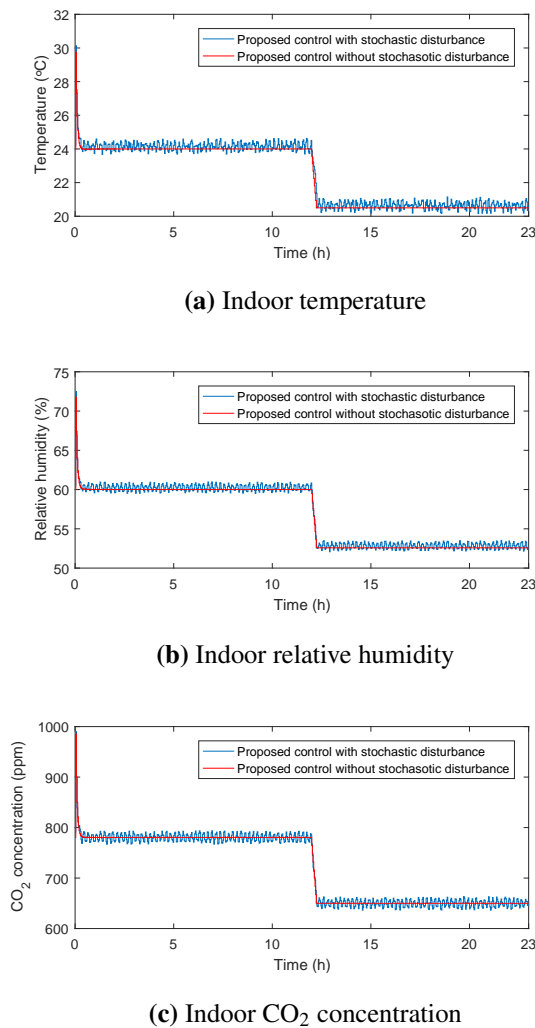
Figure 2.7. Reference following.

relative humidity and CO_2 concentration, the steady state operation points varying. The speed of the compressor, the supply fan speed and the volume flow rate of supply air have no choice but to change accordingly from 2102 rpm to 2500.5 rpm, 4243 rpm to 5468.8 rpm and 5.8 $\mathrm{m^3/min}$ to 8.0 $\mathrm{m^3/min}$, respectively, by the open loop optimal controller and the MIMO MPC controller. After reaching and maintaining the setpoints of the indoor CO_2 concentration, relative humidity and air temperature, the variation ranges are still within ± 9 ppm, $\pm 5\%$ and $\pm 0.5\,^{\circ}\mathrm{C}$, respectively. Consequently, the simulation results demonstrate that the performance of the proposed MIMO MPC strategy on the part of the reference following capability is satisfactory.
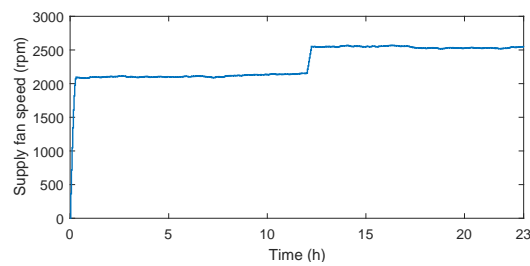
(a) Supply fan speed
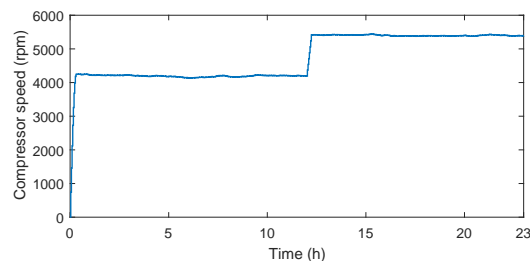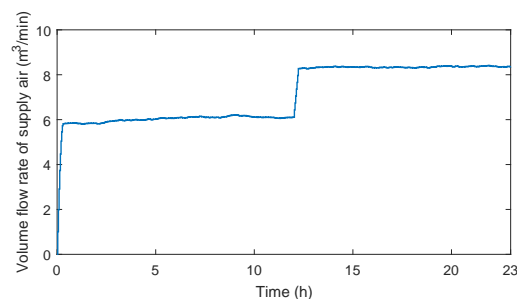
(b) Compressor speed

(c) Volume flow rate of supply air

Figure 2.8. Reference following of the varying speeds of the supply fan and the compressor and volume flow rate of supply air.

2.6.1.3   Disturbance rejection capability test

The indoor CO_2 concentration, relative humidity and air temperature are still kept at their desired setpoints when the conditioned room is affected by the changed disturbances of the pollutant, latent heat and sensible heat loads, which requires robust performance. To test this performance, it is assumed that the profiles of the sensible heat, latent heat and pollutant loads in the total test period are given as shown in Fig. 2.9. Figs. 2.10 and 2.11 display the simulation results of the disturbance rejection capability of the proposed MIMO MPC controller.

The constraints of indoor CO_2 concentration, moisture content and air temperature are given below. They are from 700 ppm to 850 ppm, 10.5/1000 kg/kg to 12.5/1000 kg/kg and 22 °C to 26 °C, respectively. Starting at $t = 8$ h, the indoor sensible heat, latent heat and pollutant loads raise from 4.8 kW to 5.376 kW, 1.397 kW to 1.607 kW and 46.4 m^3/s to 69.6 m^3/s, respectively, as depicted in Fig. 2.9. Thus, the steady state operation points of the DX A/C system have to be changed owing to the increase in the indoor loads and the proposed controller cannot react fast enough to ensure that the indoor CO_2 concentration, relative humidity and air temperature to maintain at their desired setpoints. Fig. 2.10 shows the response profiles of the indoor CO_2 concentration, relative humidity and air temperature. During the first 8 hours of the simulation test, the indoor CO_2 concentration, relative humidity and air temperature are maintained at their desired setpoints as 780.5 ppm, 60% and 24 °C, respectively, before the load changes occur. Afterwards, the indoor CO_2 concentration, relative humidity and air temperature rise from 780.5 ppm to 791 ppm, 60% to 68% and 24°C to 24.5°C, respectively in response to the changes of the thermal loads. Then the supply fan speed, the compressor speed and the volume flow rate of the supply air of the DX A/C system are regulated by the proposed controller to maintain their setpoints, as shown in Fig. 2.10 and Fig. 2.11. The response profiles of the supply fan speed, the compressor speed and volume flow rate of supply air are presented in Fig. 2.11. The volume flow rate of supply air, the speed of the supply fan and the compressor speed increase simultaneously to maintain the indoor CO_2 concentration, relative humidity and air temperature at their desired setpoints. After the return of the indoor CO_2 concentration, relative humidity and air temperature to their setting setpoints, the operation points of the volume flow rate of supply air, the speed of the supply fan and the compressor speed of the DX A/C system are stabilized at 5.82 m^3/s, 4243 rpm and 2103 rpm, respectively, until the end of the test. It can be noted from Fig. 2.10 that, after returning to their setpoints, the variation ranges of the indoor CO_2 concentration, relative humidity and air temperature are no more than ± 9 ppm, $\pm 5\%$ and ± 0.5 °C, respectively. Thereby, the proposed MIMO MPC controller is capable of controlling the indoor CO_2 concentration, relative humidity and air temperature to their desired setpoints by regulating the volume flow rate of the supply air, the compressor speed and the supply fan speed when the indoor thermal loads change, and is satisfactory on the part of disturbance rejection capability.

The proposed energy-optimised open loop controller and the regulation MIMO MPC controller are still capable of reaching the result that a setpoint change is made and the other variables are not allowed to deviate from their setpoints. In fact, the open loop controller can achieve this purpose, and then the closed-loop controller can follow it. This chapter only provides one test to show that the command

(a) Cooling loads

(b) CO_2 pollutant load
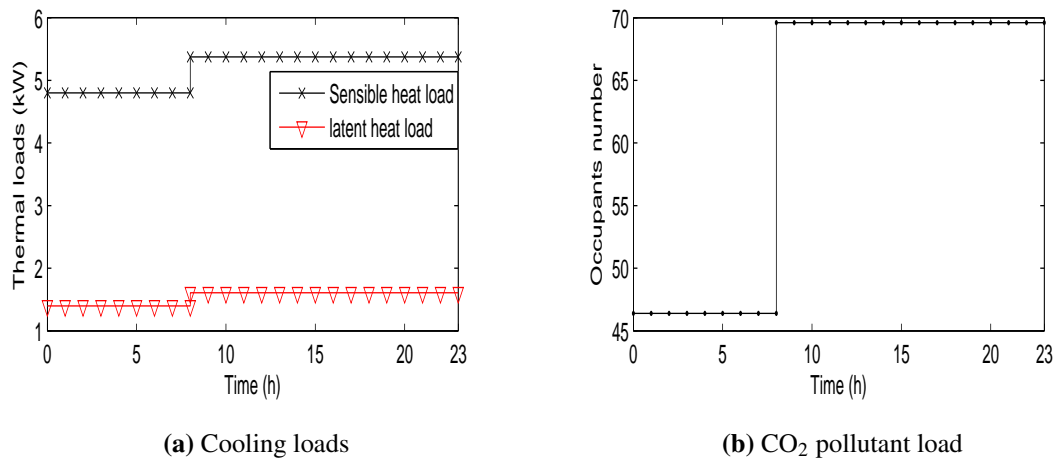
Figure 2.9. The variation profiles of indoor cooling and CO_2 pollutant loads in the disturbance rejection capability test.

following capability is satisfied by the proposed control strategy.

2.6.2   Analysis of energy efficiency

The performance of the proposed control method includes minimizing energy consumption, q, that is computed by the expression formula $q = \sum_{k=0}^{K-1} P_{total}(k)t_s$, where t_s is the sampling interval and P_{total} described in (2.15) is the total power consumption for a DX A/C system. The sampling interval is set to $t_s = 2$ minutes in this chapter. Several ways are provided to verify the energy efficiency performance of the proposed control strategy. The details of comparisons are described as follows.

1) To demonstrate the performance of the proposed MIMO MPC controller and an open loop optimal controller and on energy efficiency, comparisons with previous control methods are given. Table 2.5 summarizes the energy consumption of the DX A/C system under different control methods. The proposed MPC with a given specific operation point strategy is illustrated below: The nonlinear DX A/C system is linearised around a given specific operation point. The MPC controller steers the indoor CO_2 concentration, relative humidity and air temperature following a specific operation point. The MPC with an equilibrium point strategy [119] can be summarized as follows: The state equilibrium point is obtained by fixing the volume flow rate of the supply air, the compressor speed and the speed of the supply fan for the DX A/C system, respectively. Thus, the nonlinear DX A/C system is linearised

(a) Indoor air temperature

(b) Indoor relative humidity

(c) Indoor CO_2 concentration
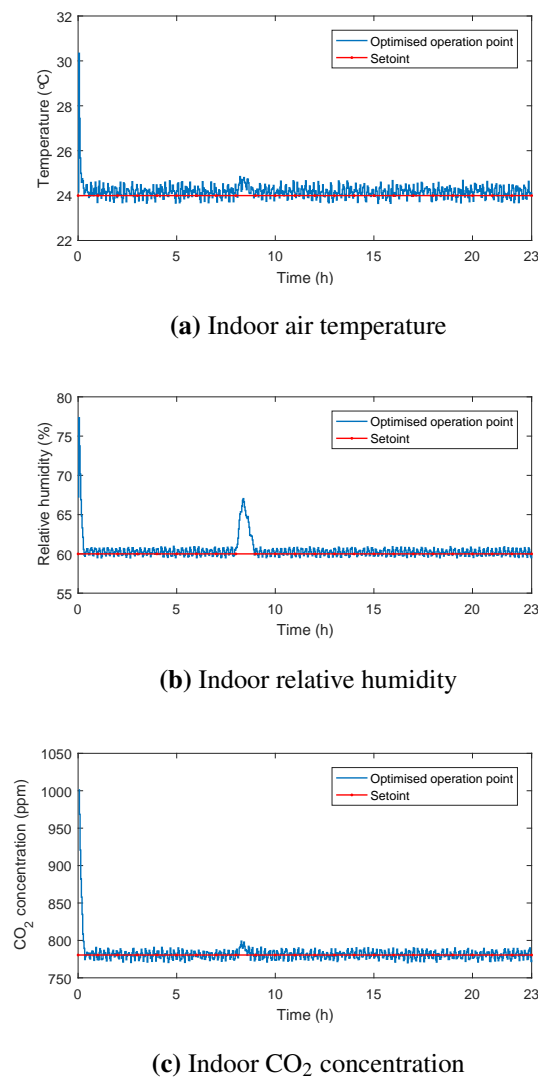
Figure 2.10. Setpoints regulation in the disturbance rejection capability test.

around this equilibrium point. The MPC controller is also used to steer the indoor CO_2 concentration, relative humidity and air temperature reaching this equilibrium point. It can be concluded that the proposed MPC with optimised operation point is superior to that of the other two control approaches in terms of energy efficiency improvement, summarized in Table 2.5.

2) Table 2.6 summarizes energy consumption of a DX A/C system in various situations by the proposed MIMO MPC and the open loop optimal controller. It can be noted that the setpoint regulation method presents the least energy consumption. It is also evident that, in the case of the disturbance rejection capability test, more energy of the DX A/C can be used to lower the heat and improve the IAQ. The
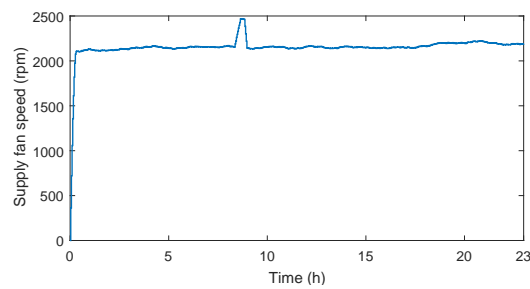
(a) Supply fan speed
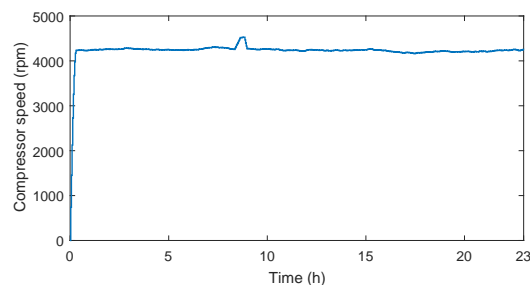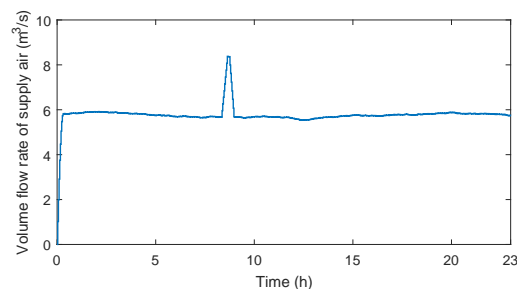
(b) Compressor speed

(c) Volume flow rate of supply air

Figure 2.11. The variation profiles of the varying speeds of the supply fan and the compressor and volume flow rate of the supply air in the disturbance rejection capability test.

DX A/C system consumes the most energy because of the requirement of more cooling capacity in the case of the reference-following capability test.

2.7   CONCLUSION

In this chapter, the researcher proposes a control scheme to maintain the indoor CO_2 concentration, relative humidity and air temperature, simultaneously, at their desired setpoints by regulating the

Table 2.5. Comparison of the energy efficiency of the DX A/C system for the MPC controller under different operation points.

Control method	Energy consumption (kWh/day)
Optimised operation point	17.26
Specific operation point	18.65
Equilibrium point by setting the input	21.96

Table 2.6. Energy consumption under different situations.

Situation	Energy consumption (kWh/day)
Setpoint regulation	17.26
Reference change following	24.15
Setpoint regulation with load disturbances	19.64

volume flow rate of the supply air, the varying speed of the supply fan and the varying speed of the compressor for the DX A/C system and to minimize energy consumption. The proposed control scheme can be formulated by the MIMO MPC control and open loop optimisation of an energy consumption model of a DX A/C system. The main contributions of this chapter are listed as follows: 1) the proposed open loop controller based on a minimizing energy consumption of a DX A/C system and the given setpoint of the indoor CO_2 concentration, relative humidity and air temperature can generate an optimised and unique steady state; 2) the indoor CO_2 concentration, relative humidity and air temperature can be maintained well at their desired setpoints through setpoint regulation, reference-following and disturbance rejection tests by employing the proposed MPC controller; 3) the coupling effects between indoor CO_2 concentration, relative humidity and air temperature have been considered in the DX A/C control system, whereas most previous works investigated energy efficiency in either relative humidity control or air temperature control or CO_2 concentration control; and 4) according to the simulation results, the proposed control strategy for energy efficiency improvement is better than conventional control methods.

It can be noted from both theoretical and simulation results that the DX A/C system used in the proposed MIMO MPC controller yield superior control performance and energy efficiency. It can also be noted that the proposed MPC with the optimised steady state strategy can reduce the energy

consumption by 1.39 kWh/day in comparison with the proposed MPC with a specific operation point in the simulation results. The results also indicated that CO_2 emissions can be reduced by 502.28 kg per annum (saving 1 kWh energy can reduce 0.99 kg CO_2 emissions [1]). Therefore, the proposed control strategy allows effective energy management for building DX A/C systems to lower energy consumption and CO_2 emissions.

For residential and office buildings equipped with a DX A/C system, the regulation of the proposed MIMO MPC and the energy-optimised open loop controller strategies can be adapted to satisfy the needs. In addition, for buildings using other A/C systems, the proposed control strategy can be modified to suit the need.

---

[1]http://www.integratedreport.eskom.co.za/.

CHAPTER 3   AUTONOMOUS HIERARCHICAL CONTROL OF A DX A/C SYSTEM

3.1   INTRODUCTION

Although the energy efficiency of the DX A/C system and both IAQ and thermal comfort improvements are addressed in Chapter 2, the optimized and time-varying reference points of indoor CO_2 concentration, relative humidity and air temperature over a 24-hour period have not been studied so far. In addition, the weather conditions and the allowed volume of outside air entering the system were considered to be constant over a 24-hour period, as in [73] and [115]. In fact, the outside air temperature and humidity are time-varying over a 24-hour period. They are the main objectives of this chapter, which focuses on designing an AHC to deal with these issues. In particular, the researcher proposes the AHC method for a DX A/C system to ensure that occupants' IAQ and thermal comfort are within comfortable levels. This also reduces both energy consumption and cost. The proposed AHC strategy includes two levels: the upper layer and lower layer. The upper level is a nonlinear optimizer that generates the optimised and time-varying trajectory reference points of indoor CO_2 concentration, relative humidity and air temperature within comfort ranges for the lower-layer controller. This controller uses open loop optimal control to minimize the value of the PMV index and the energy cost of the DX A/C system under a TOU price policy over a 24-hour period. Meanwhile, the lower level designs a MIMO MPC controller to adaptively and automatically track trajectory reference points computed by the upper layer. Therefore, the setpoints of the indoor CO_2 concentration, relative humidity and air temperature are not needed owing to the optimized setpoints adaptively feeding into the control system. On the other hand, the allowed volumes of outside air entering the DX A/C system are considered to vary with the environment changing over a 24-hour period. These are optimised by the proposed hierarchical control strategy. Moreover, a supply fan that drives the pressure swing absorption (PSA) with a built-in

PI controller is proposed to lower indoor CO_2 concentration in this chapter. This has the potential to reduce the complexity of computation and the cost of hardware. Furthermore, the PMV index is traditionally used as an indicator of indoor thermal comfort. In this chapter, it is used as an indicator of both thermal comfort and IAQ when the indoor air CO_2 concentration is at its steady state. Finally, to demonstrate the performances of the proposed control strategy, the proposed control strategy and baseline control method are compared in Chapter 2 in a case study.

3.2   CHAPTER OVERVIEW

Autonomous hierarchical controllers are designed in this chapter to lower energy cost and improve the energy efficiency of the DX A/C system while maintaining both IAQ and thermal comfort at comfort levels. This chapter also considers the optimal volume of outside air entering the system. To facilitate the proposed hierarchical controller's design, the nonlinear dynamical system models, the energy consumption models of the DX A/C system, the indoor pollutant and cooling load models are presented first in Section 3.3. An open loop optimal controller and the MIMO MPC tracking controller are designed in Section 3.4. Simulation results are provided in Section 3.5 to demonstrate the effectiveness of the proposed control scheme. Conclusions are drawn in Section 3.6.

3.3   MODIFIED DX A/C SYSTEM

Compared to Chapter 2, the differentiating component of this chapter's DX A/C system is the addition of a PSA box to the supply fan and the removal of the VAV ventilation box for the purposes. Fig. 3.1 shows a simplified schematic diagram of this modified DX A/C system. The PSA box can absorb the CO_2 contaminant concentration to improve IAQ. Therefore, the outside air entering the system and the PSA box coordinate to improve the fresh air ratio of a room.

3.3.1   The DX A/C model

In this chapter, it is also assumed that the DX A/C system is operated in the cooling mode. Most of the basic operation and assumptions of the system are the same as these in Chapter 2 for the purpose of simplicity. Only one assumption is different, as indicated below: It is assumed that there are two areas on the air side of the DX evaporator, that is, a dry-cooling area (sensible heat transfer only) and

Figure 3.1. Simplified diagram of the modified DX A/C system.

Figure 3.2. Simplified schematics diagram of the DX evaporator.

wet-cooling area (sensible and latent heat transfer region). The relationship between the two areas is that the outlet air properties of the first one (dry-cooling region) are the inlet air conditions entering the wet-cooling area. Therefore, the area from zero to A_1 pertains to the dry-cooling area and the rest of the total surface area is the wet-cooling area A_2. The simplified schematic diagram of the DX evaporator is depicted in Fig. 3.2, which is modified from its original one [103]. The boundary between the dry surface and the wet surface in the DX evaporator is determined by the distribution of the surface temperature, which is time-varying under various conditions. The boundary is a bounded and uncertainty parameter.

The dynamic mathematical equations of the DX A/C system for controlling indoor CO_2 concentration, moisture content and air temperature simultaneously are built based on the principles of energy and

mass conservation, which can be modelled in Chapter 2, and compactly written as follows:

$$C_a \rho V \frac{dT_z}{dt} = C_a \rho v_f (T_s - T_z) + Q_{load}, \tag{3.1}$$

$$\rho V \frac{dW_z}{dt} = \rho v_f (W_s - W_z) + M_{load}, \tag{3.2}$$

$$C_a \rho V_{h1} \frac{dT_d}{dt} = C_a \rho v_f ((1 - p\%)T_z + p\%T_0 - T_d) + \alpha_1 A_1 (T_w - \frac{(1-p\%)T_z + p\%T_0 + T_d}{2}), \tag{3.3}$$

$$C_a \rho V_{h2} \frac{dT_s}{dt} + \rho V_{h2} h_{fg} \frac{dW_s}{dt} = C_a \rho v_f (T_d - T_s) + h_{fg} \rho v_f ((1 - p\%)W_z + p\%W_0 - W_s) +$$
$$\alpha_2 A_2 (T_w - \frac{T_d + T_s}{2}), \tag{3.4}$$

$$C_w \rho_w V_w \frac{dT_w}{dt} = \alpha_1 A_1 (\frac{(1-p\%)T_z + p\%T_0 + T_d}{2} - T_w) + \alpha_2 A_2 (\frac{T_d + T_s}{2} - T_w) - (h_{r2} - h_{r1})m_r, \tag{3.5}$$

$$V \frac{dC_c}{dt} = v_s (C_s - C_c) + C_{load}. \tag{3.6}$$

It is assumed that the CO_2 concentration flow rate v_s follows a PI controller

$$v_s = k_P v_f + k_I \int_0^{T_I} v_f ds, \tag{3.7}$$

where k_P and k_I are the two tuned parameters of the PI controller.

Remark 3.1 *In Chapter 2, the three control variables m_r, v_f and v_s are designed to control three state variables, namely C_c, T_z, and W_z. In this chapter, among the three control variables, the third control variable v_s is special, which is described as $v_s = k_P v_f + k_I \int_0^{T_I} v_f ds$. Therefore, the control vector u can be represented by two control variables m_r and v_f. In fact, when manipulating v_f to control indoor humidity, the controller v_f is steering v_s simultaneously to control the concentration of CO_2 concentration via a PI controller. The parameters k_P and k_I of the PI controller are tuned to set and track the CO2 setpoint. The researcher purposely adopted this design in order to 1) reduce hardware requirements of the control implementations, and 2) save energy when combining the VAV damper and the varying speed supply fan as shown in Fig. 2.1. In essence, there are three manipulated variables. This type of control system is still controllable.*

Since the air enthalpy, moisture content and air temperature leaving the evaporator has the following relationship

$$h_s = C_a T_s + h_{fg} W_s. \tag{3.8}$$

Therefore, Eqs. (3.2) and (3.4) can be rewritten as follows:

$$\rho V \frac{dW_z}{dt} = \rho v_f (\frac{h_s - C_a T_s}{h_{fg}} - W_z) + M_{load}, \tag{3.9}$$

$$\rho V_{h2} \frac{dh_s}{dt} = C_a \rho v_f (T_d - T_s) + h_{fg} \rho v_f ((1 - p\%)W_z + p\%W_0 - \frac{h_s - C_a T_s}{h_{fg}}) + \alpha_2 A_2 (T_w - \frac{T_d + T_s}{2}). \tag{3.10}$$

The air side convective heat transfer coefficients of the dry-cooling and wet-cooling regions in the DX evaporator shown in Fig. 3.2 are expressed in (2.8) and (2.10).

The air velocity v_a can be described as follows:

$$v_f = dv_a + \varepsilon, \tag{3.11}$$

where d is the cross-sectional area of the conditioned space and ε is the error vector since the air enters or exits through the door or window.

The left-hand sides of (3.1)-(3.2) are the heat flow into the conditioned room. On the right-hand side of (3.1), the first term denotes the heat transfer from the DX evaporator to the conditioned space. It is operating in the heat mode if $T_s > T_z$ and in the cooling mode if $T_s < T_z$. The other terms mean the indoor sensible heat load needs to be removed by the DX A/C system. Similarly, on the right-hand side of (3.2), the first term represents the wet-bulb temperature transferred to the conditioned room. It is positive if W_s is greater than W_z for the humidification mode and negative if W_s is lesser than W_z for dehumidification mode. The second term represents the moisture load required to be removed by the DX A/C system. Eqs. (3.3), (3.5) and (3.10) mean that the heat transfer takes place inside the DX A/C system. In Eq. (3.3), the first term of the right-hand side represents the heat transfer between the mixed air and the air side at the evaporator. The second term represents the heat transfer between the evaporator wall and the mixed air. Eq. (3.6) denotes the dynamic balance of the indoor CO_2 concentration.

Remark 3.2 *In this chapter, the relationship between the moisture content and air temperature at the outlet of the evaporator in (2.12): $W_s = \frac{0.0198T_s^2 + 0.085T_s + 4.4984}{1000}$ has been released, since it may not be feasible under different operating conditions. In this chapter, the ratio of fresh air entering the system is not fixed according to the changing environment over 24 hours. In a previous study in which the researcher was involved [115], a VAV ventilation fan with an independent PSA was used to improve IAQ. A supply fan to drive the PSA with a built-in PI controller is employed. This leads to one less independent control input.*

3.3.2   Load models

It is known that IAQ and thermal comfort are affected by a set of disturbances, such as solar radiation through opaque, external air and transparent surfaces and internal heat gains due to occupants,

appliances, lights, etc. Consequently, superior performance for controlling indoor CO_2 concentration, relative humidity and air temperature are required to deal with the disturbances. When disturbances are neglected, a large error occurs. Nevertheless, perfect prediction of future disturbances does not happen in reality. Some disturbances such as outside temperature, humidity and CO_2 concentration can be measured. While others such as solar radiation and internal gains cannot but may be estimated. The researcher will subsequently provide more details for estimating indoor sensible heat load Q_{load}, moisture load M_{load} and pollutant load C_{load}.

Sensible heat loads are generally generated by internal loads such as occupants, lighting, equipment, fresh air entering and applications and external loads such as heat transfer conduction mainly through the building roof, floor, walls and doors. Heat transfer by radiation mainly through fenestration such as windows and skylights is also an external load. In this chapter, the researcher assumes the external load, including heat loads by radiation through windows and the fresh air load by ventilation. The moisture load is also generated by occupants, equipment, fresh air ventilation and their applications. The CO_2 pollutant load is directly generated by the occupants' action. The sensible heat load owing to lighting, equipment and applications and the latent heat load from applications are easy to estimate based on electrical characteristics of these devices. The main uncertainties used to estimate the sensible and latent heat loads are due to the loads associated with the occupants in the conditioned space. The sensible heat and moisture loads are determined by occupants through the current CO_2 emission. To predict the sensible heat, moisture and indoor pollutant loads, the following method is proposed

$$Q_{load}(t) = Q_{r,load} + Q_{spl} + \mu C_c + v + Q_{air}, \tag{3.12a}$$

$$M_{load}(t) = \phi C_c + \gamma + M_{air}, \tag{3.12b}$$

$$C_{load}(t) = G \cdot Occp, \tag{3.12c}$$

where the heat gain of the supply fan Q_{spl} is expressed in (2.4). The external heat load by radiation $Q_{r,load}$ through windows is described by the following equation

$$Q_{r,load} = n_{win}\varepsilon_{win}A_{win}Q_{rad}, \tag{3.13}$$

where n_{win} denotes whether the conditioned space has a window, i.e., when $n_{win} = 1$, it has a window, while if $n_{win} = 0$, it does not. The fresh air of the sensible heat load, Q_{air}, and the moisture load, M_{air}, in the conditioned space are expressed as follows:

$$Q_{air} = p\%C_z\rho v_f(T_0 - T_z), \tag{3.14a}$$

$$M_{air} = p\%\rho v_f(W_0 - W_z). \tag{3.14b}$$

Remark 3.3 *In this chapter, the researcher gives a simple way to predict the indoor sensible heat and moisture loads and CO_2 pollutant load. In [64], an alternative method to estimate the cooling loads were presented. Besides, the weather forecast data taken from the weather prediction of Cape Town is qualified for this research, because 1) the current weather station can make exact predictions and 2) the weather conditions and solar radiation are relatively stable in the area, which indicates that the profiles of the predicted outside CO_2 concentration, relative humidity and air temperature are quite representative.*

3.3.3 PMV index

The PMV index is widely used as an indicator of human thermal comfort requirements. This indicator was first proposed by Fanger [120] to predict the average vote of many people on the thermal sensation scale. This sensation can be expressed by relating the integer range [-3,+3] to the qualitative words cold, cool, slightly cool, neutral, slightly warm, warm and hot. The PMV index depends on the following six factors: metabolic rate M (W/m^2), clothing insulating I_{cl} (m^2°C/W), air temperature T_z and humidity H_z, air velocity v_a (m/s) and mean radiant temperature T_r. It is computed by means of a heat-balance equation given by [120]

$$
\begin{aligned}
PMV =& (0.303 \mathrm{e}^{-0.036M} + 0.028)\Big\{ (M-W) - 3.05 \times 10^{-3} [5733 - 6.99(M-W) - P_a] - 0.42[(M-\\
& W) - 58.15] - 1.7 \times 10^{-5} M(5867 - P_a) - 0.0014 M(34 - T_z) - 3.96 \times 10^{-8} f_{cl}[(T_{cl} + 273)^4\\
& - (T_r + 273)^4] - f_{cl} h_c \cdot (T_{cl} - T_z)\Big\},
\end{aligned}
$$

$$(3.15)$$

where W (W/m^2) is the external work, P_a denotes the partial water vapor pressure in Pascal. The surface temperature of clothing, T_{cl}, can be given as follows:

$$
T_{cl} = 35.7 - 0.028(M-W) - I_{cl}\Big\{ 3.96 \times 10^{-8} f_{cl}[(T_{cl} + 273)^4 - (T_r + 273)^4] + f_{cl} h_c (T_{cl} - T_z)\Big\},
$$

$$(3.16)$$

where the convective heat transfer coefficient, h_c, can be expressed by

$$
h_c = \begin{cases} h_c^*, & \text{if } h_c^* > 12.1\sqrt{v_a}, \\ 12.1\sqrt{v_a}, & \text{if } h_c^* < 12.1\sqrt{v_a}. \end{cases}
$$

$$(3.17)$$

The factor h_c^* is given as: $h_c^* = 2.38 \cdot (T_{cl} - T_z)^{0.25}$. Where f_{cl} denotes the ratio of body surface area covered by clothes to the naked surface area. The factor f_{cl} is defined as follows:

$$
f_{cl} = \begin{cases} 1.00 + 1.290 I_{cl} & \text{if } I_{cl} \leq 0.078, \\ 1.05 + 0.645 I_{cl} & \text{if } I_{cl} > 0.078, \end{cases}
$$

$$(3.18)$$

and the mean radiant temperature, T_r, can be determined by [121]

$$T_r = [(T_g + 273)^4 + \frac{1.10 \times 10^8 v_a^{0.6}}{\varepsilon D^{0.4}}(T_g - T_z)]^{1/4} - 273, \tag{3.19}$$

where T_g is the globe temperature; D and ε are the globe diameter in meters and the globe emissivity coefficient, respectively. P_a is related to the relative humidity of the air, H_z, by means of Antoine's equation [122]

$$P_a = 10 H_z e^{(16.6536 - 4030.183/(T_z+235))}, \tag{3.20}$$

where $H_z = 100 W_z / A_{conv}$, A_{conv} is the unit transfer coefficient. The metabolic rate, M, can be determined by [123]

$$M = \lambda G,$$

where the coefficient λ is the unit transfer coefficient. Then the PMV index is rewritten as a function of the following variables

$$PMV = g(T_z, W_z, C_c, v_f, T_r, I_{cl}, T_{cl}). \tag{3.21}$$

Remark 3.4 *There are several existing metrics to measure human (dis)comfort, e.g., temperature constraint violations [64], comfort penalty [85], predicted percentage dissatisfied (PPD) [124], and PMV index [69, 57]. The PMV index has been widely used as an indicator to maintain human comfort temperature in [69] and to represent indoor air temperature and relative humidity in [57]. In this chapter, the function (3.21) suggests that the PMV index can estimate not only indoor thermal comfort, but also the IAQ, and is used to keep them at a certain range. This is subjective and can be regarded as perfect when PMV=0.*

3.3.4 Energy models

More details about energy consumption by different components of a DX A/C system are described in Chapter 2. In this chapter, the researcher only gives the energy model of the total energy consumption as follows:

$$P_{tot} = P_{eva} + P_{con} + P_{comp}, \tag{3.22}$$

Note that in this chapter the energy consumption by the VAV ventilation fan cannot be included in the total energy model since the VAV fan has been substituted by the supply fan with a PI controller.

3.3.5 System constraints

The DX A/C system operation is limited by IAQ, thermal comfort and physical characteristics. Most of the system constraints are listed in (C1)-(C9) in Chapter 2 and the other constraints are defined below.

(C8) $PMV \in [\underline{PMV}, \overline{PMV}]$. The limit of the PMV index can guarantee both thermal comfort and IAQ at comfortable levels.

(C9) The bound of the air enthalpy, h_s, satisfies: $h_s \in [C_z \underline{T}_s + h_{fg} \underline{W}_s, C_z \overline{T}_s + h_{fg} \overline{W}_s]$ because of (3.8).

The system dynamic equations (3.1), (3.3), (3.5)-(3.6) and (3.9)-(3.10) can be expressed compactly below

$$\dot{x}(t) = f(x(t), u(t), w(t)), \tag{3.23}$$

where the *state vector* of the system (3.23) can be defined by

$$x = [h_s, T_z, T_d, T_w, W_z, C_c]^T,$$

the *control vector* by

$$u = [v_f, m_r]^T,$$

the *load vector* by

$$w = [Q_{load}, M_{load}, C_{load}]^T,$$

and the *output vector* by

$$y = [T_z, W_z, C_c]^T.$$

The constraints in (C1)-(C9) can be compactly written by

$$x \in \mathbb{X}, \ u \in \mathbb{U}, \ PMV \in \mathbb{F}, \ p \in \mathbb{P}, \ T_s \in \mathbb{T}_s, \ W_s \in \mathbb{W}_s, \ \text{and } h_i(x) \leq 0, \ i = 1, 2, \tag{3.24}$$

where $\mathbb{X}$, $\mathbb{U}$, $\mathbb{P}$, $\mathbb{T}_s$ and $\mathbb{W}_s$ are bounded sets. $h_i(x)$ is a function of the state variables, which are described in Chapter 2.

3.3.6   TOU strategy

Generally, most electricity companies have implemented the TOU strategy to benefit both electricity companies and consumers. The TOU electricity tariff is a typical program of demand-side management where the electricity price changes over different periods depending on the electricity supply cost. For example, it charges a high price σ_h in peak periods $\mathcal{T}_h$, a medium price σ_m in standard periods $\mathcal{T}_m$, and a low price σ_l in off-peak periods $\mathcal{T}_l$. In this study, the daily TOU electricity prices are known in advance and can be expressed as follows:

$$\sigma(l) = \begin{cases} \sigma_h = 0.20538 \ \$/\text{kW h}, l \in \mathcal{T}_h, \\ \sigma_m = 0.05948 \ \$/\text{kW h}, l \in \mathcal{T}_m, \\ \sigma_l = 0.03558 \ \$/\text{kW h}, l \in \mathcal{T}_l, \end{cases} \tag{3.25}$$

where $\mathcal{T}_h = (8,11] \bigcup (19,21]$, $\mathcal{T}_l = (0,7] \bigcup (23,24]$ and $\mathcal{T}_m = (7,8] \bigcup (11,19] \bigcup (21,23]$. $ is the United States dollar and time $\mathcal{T}$ is the whole period of the day with $l = 1,\ldots,24$. Because of a big difference in energy prices between the peak and off-peak hours, a cost reduction is expected if a significant amount of power consumption is shifted from peak hours to off-peak hours. To reduce the energy cost, some previous optimization control strategies are studied in [60, 62]. In this chapter, the researcher proposes an alternative optimisation control scheme to minimize both the energy cost and energy consumption.

3.4   HIERARCHICAL CONTROL DESIGN

The hierarchical control method is widely used to handle complex problems which can be decomposed into smaller subproblems, and reassemble their solutions in a hierarchical structure. The main idea is to establish a hierarchical control structure consisting of two layers. The two layers are developed by using a control schedule, the simplified scheme of which is depicted in Fig. 3.3. The main principle of hierarchical control can be described as follows: In the upper layer, the objective is to collect information to generate the optimal operational conditions with respect to a performance index based on an economic and environmental criterion over a long-term scale horizon, H_L, with a sampling period, T_L. In this layer, detailed but static and physically original nonlinear models are used. In the lower layer, a simple linear dynamic model is used to design an MPC controller, which guarantees that the targets transmitted from the upper layer can be carried out over a short time horizon, $h_l = T_L$, with a smaller sampling period, $t_l = T_L/n_l$. Fig. 3.3 suggests that the upper layer
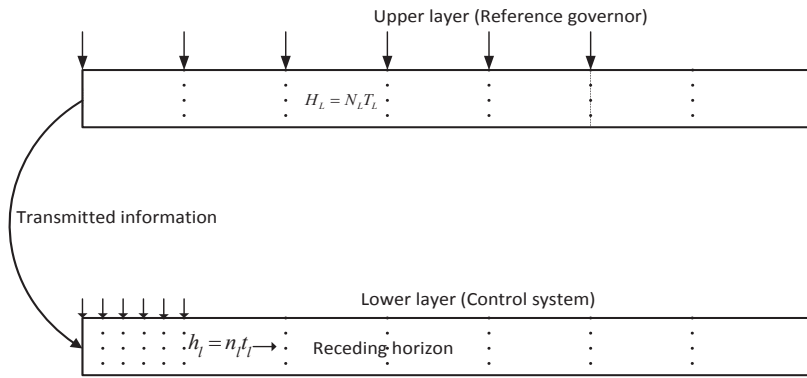
Figure 3.3. Simplified schematic of a two-layer hierarchical structure.
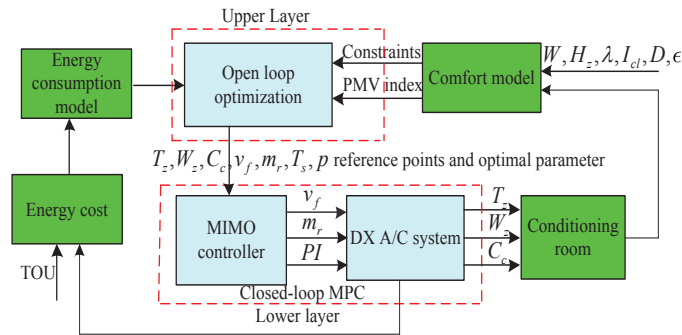
Figure 3.4. Conceptual framework of the proposed hierarchical control scheme.

transmits information to the lower layer at the sampling instant mT_L $(m = 0, 1, \ldots, \infty)$. The lower layer receives the information as a task, and then completes the task within the sampling intervals $[mT_L + qt_l, mT_L + (q+1)t_l)$ $(q = 0, 1, \ldots, n_l - 1)$.

This chapter proposes an AHC approach to obtain a real-time optimisation scheduling strategy to reduce the total energy cost of a DX A/C system while maintaining both the indoor IAQ and thermal comfort within requirement ranges. This control approach is based on a traditional control scheme with a reference governor in the upper layer named the optimization layer. The optimization layer uses a nonlinear optimizer to generate the steady states for a DX A/C system and the optimal proportion of fresh air entering the system by optimising the energy cost of the DX A/C system and the PMV index under the TOU electricity rate over the day. The lower layer receives the steady states as input, and then the MIMO MPC controller is designed to track the trajectory references of indoor CO_2 concentration, moisture content and air temperature. The conceptual framework of the proposed AHC approach is illustrated in Fig. 3.4, with its details to be provided next.

3.4.1 Upper layer

In the upper layer, the reference governor has been defined according to the optimization problem described by (3.26). Note that the PMV index (3.21) and the energy model (3.22) are the two different optimization objective functions, which are described below in (3.26). In the upper layer, the optimisation problem is considered as an open loop optimal control framework. Consider the DX A/C system (3.23) and its constraints (3.24). The researcher formulates the following optimal controller to generate the steady states.

$$\min \ (\alpha |PMV(t_{m_0})| + (1 - \alpha)P_{tot}(t_{m_0})\sigma(t_{m_0})), \tag{3.26}$$

subject to the following constraints:

$$f(x(t_{m_0}), u(t_{m_0}), T_s(t_{m_0}), p(t_{m_0})) = 0, \tag{3.27}$$

$$x(t_{m_0}) \in \mathbb{X}, \ u(t_{m_0}) \in \mathbb{U}, \ PMV(t_{m_0}) \in \mathbb{F}, \ p(t_{m_0}) \in \mathbb{P}, \ T_s(t_{m_0}) \in \mathbb{T}_s, \ W_s(t_{m_0}) \in \mathbb{W}_s, \ h(x(t_{m_0})) \leq 0, \tag{3.28}$$

where α is a weighting factor $(0 < \alpha < 1)$, x, u and $f(\cdot)$ are defined in (3.23). $x(t_{m_0}), u(t_{m_0}), z(t_{m_0})$ are the optimization variables for $m = 0, \ldots, N_L - 1$, where $z = [p, T_s, T_r, T_{cl}]$.

It is assumed that all the variables are within the bounded sets and that feasible solutions exist for the optimization problem (3.26) by using an NLP algorithm. Among all the feasible solutions, let $x_s(t_{m_0}), u_s(t_{m_0}), z_s(t_{m_0})$ be the optimal solution of the optimization problem (3.26), and $x_s(t_{m_0}) \in \boldsymbol{X}_s, \ u_s(t_{m_0}) \in \boldsymbol{U}_s, \ z_s(t_{m_0}) \in \boldsymbol{Z}_s$ for $m = 0, \ldots, N_L - 1$. $\boldsymbol{X}_s, \boldsymbol{U}_s, \boldsymbol{Z}_s$ are the optimal sequence points of the state and input variables. In this chapter, the optimal sequence points are the steady states of equation (3.27) over a 24-hour period.

Remark 3.5 *The weighting factor α is chosen to balance the two objectives, which are the energy cost and comfort levels. Specifically, a relatively large α provides a better comfort level but worse cost savings. In the case that α is relatively large, more effort is taken to optimize the most comfortable indoor air temperature, humidity and CO_2, which causes a loss of balancing capacity. The parameter α can be chosen by utilities to achieve different goals.*

3.4.2   Lower layer

As discussed above, in every sample period, T_L, the upper layer controller calculates the optimal steady state and sends the result to the lower layer. The lower layer then receives the steady state as the trajectory reference including a closed-loop control algorithm trying to drive the DX A/C system to track the trajectory reference. Therefore, in this case, this layer consists of a discrete-time MPC controller with a sampling time of $t_{m_q} \in [mT_L + qt_l, MT_L + (q+1)t_l)$, $m = 0, 1, \ldots, N_L - 1$, $q = 0, 1, \ldots, t_l - 1$, which can be designed to track the reference point of indoor CO_2 concentration, moisture content and air temperature computed by the upper layer.

In the sequel, the researcher makes a commensurate quantization assumption that all variables are quantized in the two sampling schemes, that is, they are represented by the starting values and retain these values in the same sampling interval. The two objective functions $PMV(t)$, $P_{tot}(t)$, the TOU function $\sigma(t)$, and the constraints in (C1)-(C9) are coarsely quantized. This means that they take their corresponding values at mT_L, for all $t \in [mT_L, (m+1)T_L)$. This assumption guarantees that if the steady state $(x_s(t_{m_q}), u_s(t_{m_q}))$ should be obtained from the optimisation (3.26)-(3.28), then one would have $(x_s(t_{m_q}), u_s(t_{m_q})) = (x_s(t_{m_0}), u_s(t_{m_0}))$.

The lower layer receives the trajectory references of state and input vectors defined as: $x_s(t_{m_q}) \triangleq [h_{s,s}(t_{m_q}), T_{z,s}(t_{m_q}), T_{d,s}(t_{m_q}), T_{w,s}(t_{m_q}), W_{z,s}(t_{m_q}), C_{c,s}(t_{m_q})]^T$ and $u_s(t_{m_q}) = [v_{f,s}(t_{m_q}), m_{r,s}(t_{m_q})]^T$. Define $\delta T_z(t_{m_q}) = T_z(t_{m_q}) - T_{z,s}(t_{m_q})$, $\delta W_z(t_{m_q}) = W_z(t_{m_q}) - W_{z,s}(t_{m_q})$, $\delta C_c(t_{m_q}) = C_c(t_{m_q}) - C_{c,s}(t_{m_q})$, $\delta h_s(t_{m_q}) = h_s(t_{m_q}) - h_{s,s}(t_{m_q})$, $\delta T_d(t_{m_q}) = T_d(t_{m_q}) - T_{d,s}(t_{m_q})$, $\delta T_w(t_{m_q}) = T_w(t_{m_q}) - T_{w,s}(t_{m_q})$, $\delta v_f(t_{m_q}) = v_f(t_{m_q}) - v_{f,s}(t_{m_q})$, $\delta m_r(t_{m_q}) = m_r(t_{m_q}) - m_{r,s}(t_{m_q})$, which are the deviations of states and inputs from their trajectory references at sampling period $[mT_L + qt_l, mT_L + (q+1)t_l)$. Thereby, the dynamical mathematical equation of the system (3.23) at time t_{m_q} is linearized and can be written in a linear state-space representation as follows:

$$\begin{cases} \delta\dot{x}(t_{m_q}) = A_c(x_s(t_{m_0}), u_s(t_{m_0}))\delta x(t_{m_q}) + B_c(x_s(t_{m_0}), u_s(t_{m_0}))\delta u(t_{m_q}), \\ y(t_{m_q}) = C\delta x(t_{m_q}) + y_s(t_{m_0}), \end{cases} \tag{3.29}$$

where the state variables $\delta x(t_{m_q}) = x(t_{m_q}) - x_s(t_{m_0}) = [\delta h_s(t_{m_q}), \delta T_z(t_{m_q}), \delta T_d(t_{m_q}), \delta T_w(t_{m_q}), \delta W_z(t_{m_q}),$ $\delta C_c(t_{m_q})]^T$, the input variables $\delta u(t_{m_q}) = u(t_{m_q}) - u_s(t_{m_q}) = [\delta v_f(t_{m_q}), \delta m_r(t_{m_q})]^T$, $y_s(t_{m_0}) = [T_{z,s}(t_{m_0}),$ $W_z(t_{m_0}), C_{c,s}(t_{m_0})]^T$ and $y(t_{m_q}) = [T_z(t_{m_q}), W_{z,s}(t_{m_q}), C_c(t_{m_q})]^T$ are the original output variables. $A(x_s(t_{m_0}), u_s(t_{m_0}))$, $B(x_s(t_{m_0}), u_s(t_{m_0}))$, C are the system state matrix, input matrix and output matrix

at the sampling time t_{m_q}, respectively, which can be calculated by

$$A_c(x_s(t_{m_0}), u_s(t_{m_0})) = \left. \frac{\partial f(x(t_{m_0}), u(t_{m_0}))}{\partial x(t_{m_0})} \right|_{\substack{x(t_{m_0}) = x_s(t_{m_0}) \\ u(t_{m_0}) = u_s(t_{m_0})}},$$

$$B_c(x_s(t_{m_0}), u_s(t_{m_0})) = \left. \frac{\partial f(x(t_{m_0}), u(t_{m_0}))}{\partial u(t_{m_0})} \right|_{\substack{x(t_{m_0}) = x_s(t_{m_0}) \\ u(t_{m_0}) = u_s(t_{m_0})}},$$

and the corresponding output matrix is

$$C = \begin{bmatrix} 0 & 1 & 0 & 0 & 0 & 0 \\ 0 & 0 & 0 & 0 & 1 & 0 \\ 0 & 0 & 0 & 0 & 0 & 1 \end{bmatrix}.$$

The discrete-time version of (3.29) can be written by

$$\begin{cases} \delta x(t_{m_{q+1}}) = A_d(x_s(t_{m_0}), u_s(t_{m_0})) \delta x(t_{m_q}) + B_d(x_s(t_{m_0}), u_s(t_{m_0})) \delta u(t_{m_q}), \\ y(t_{m_q}) = C \delta x(t_{m_q}) + y_s(t_{m_0}), \end{cases} \tag{3.30}$$

where $x(t_{m_q})$, $u(t_{m_q})$ and $y(t_{m_q})$ are the state, input and output vectors at sampling instant $mT_L + qt_l$, $m = 0, 1, \ldots, N_L - 1$, $q = 0, 1, \ldots, n_l - 1$, respectively. $A_d(x_s(t_{m_0}), u_s(t_{m_0})) = e^{A_c(x_s(t_{m_0}), u_s(t_{m_0}))t_l}$, $B_d(x_s(t_{m_0}), u_s(t_{m_0})) = (\int_0^{t_l} e^{A_c(x_s(t_{m_0}), u_s(t_{m_0}))\tau} d\tau) B_c(x_s(t_{m_0}), u_s(t_{m_0}))$ are the discrete-time system state and input matrices, respectively.

The objective of this chapter is to design a MIMO MPC controller to optimise the DX A/C system to reach the trajectory reference points of the indoor CO_2 concentration, moisture content and air temperature and maintain at the required levels with lower energy consumption and cost. To achieve this, the objective function to be minimised is given as follows:

$$\min_{\delta u} J(t_{m_q}) = \underbrace{\sum_{j=1}^{n_p} \left\| y(t_{m_{q+j}}|t_{m_q}) - r(t_{m_{q+j}}) \right\|^2}_{(a)} + R_{\delta u} \underbrace{\sum_{j=0}^{n_c - 1} \left\| \delta u(t_{m_{q+j}}) \right\|^2}_{(b)}, \tag{3.31}$$

subject to:

$$\begin{cases} \delta x(t_{m_{l_1}}|t_{m_{q+1}}) = A_d(x_s(t_{m_0}), u_s(t_{m_0})) \delta x(t_{m_{l_1-1}}|t_{m_q}) + B_d(x_s(t_{m_0}), u_s(t_{m_0})) \delta u(t_{m_{l_1-1}}|t_{m_q}), \\ y(t_{m_{l_1-1}}|t_{m_q}) = C \delta x(t_{m_{l_1-1}}|t_{m_q}) + y_s(t_{m_0}), \end{cases} \tag{3.32}$$

$$\delta x(t_{m_{l_1}}|t_{m_q}) + x_s(t_{m_0}) \in \mathbb{X}, \quad \delta u(t_{m_{l_2}}) + u_s(t_{m_0}) \in \mathbb{U},$$

$$l_1 = q + 1, \ldots, q + n_p, \ l_2 = q, \ldots, q + n_c - 1, \tag{3.33}$$

$$q = 0, 1, \ldots, n_l - 1, \ m = 0, 1, \ldots, N_L - 1.$$

where (a) represents the tracking error of the indoor CO_2 concentration, moisture content and air temperature and (b) denotes the balancing signal tracking error, respectively, in quadratic forms. The current time index, t_{m_q}, defines the current time $mT_L + qt_l$. $|t_{m_q}$ means the predicted value, which is based on the information up to $t = mT_L + qt_l$, $n_p = T_L/t_l$ is the prediction horizon of the lower layer, $n_c = T_L/t_l$ is the control horizon of the lower layer, $r(t_{m_{q+j}})$ denotes the reference vector at step $t_{m_{q+j}}$, $y(t_{m_{q+j}}|t_{m_q})$ is the predicted output vector at step $t_{m_{q+j}}$, and $\delta u(t_{m_{q+j}})$ is the predicted control vector at step $t_{m_{q+j}}$.

Remark 3.6 *The system matrices of the system (3.29) are updated to $A_d(x_s(t_{(m+1)_0}), u_s(t_{(m+1)_0}))$ and $B_d(x_s(t_{(m+1)_0}), u_s(t_{(m+1)_0}))$ when the system transits from the sampling interval $[mT_L + (n_l - 1)t_l, (m + 1)T_L)$ to $[(m+1)T_L, (m+1)T_L + t_l)$. On the other hand, at sampling interval $[(m+1)T_L, (m+1)T_L + t_l)$, the variables $\delta x(t_{m_{n_l-1}})$ and $\delta u(t_{m_{n_l-1}})$ as the initial points are fed to the system (3.32), and the references are updated in (3.31). The convergence for this periodic MPC for an optimisation problem over an infinite time horizon can be proved by using the results [125, 126].*

3.4.3 Algorithm

The researcher proposes the algorithm to solve the above nonlinear steady state optimization problem.

NLP algorithm is used to solve the original nonlinear DX A/C system.

Initialization: Given the initial state values $x(0)$ and $u(0)$, note that the initial state values are set within their bounds.

1: Input the data of the outside condition, pollutant, latent heat and sensible heat loads.

2: The objective function (3.26) and constraints in (3.27) and (3.28) are converted into the following standard NLP so that it can be conveniently solved by the MATLAB built-in functions *fmincon*:

$$\min f_c^T \cdot z \quad s.t. \quad \begin{cases} c(z) \leq 0 \\ ceq(z) = 0 \\ A \cdot z \leq b \\ A_{eq} \cdot z = beq \\ lb \leq z \leq ub \end{cases} \tag{3.34}$$

3: Solve the above minimization problem (3.34).

The proposed MIMO MPC algorithm can be given below.

MPC algorithm to the DX A/C system tracking control.

Initialization: Given an initial state value $x(0)$, and let $t_{m_q} = 0$ ($m = 0, q = 0$).

1: Calculate the optimal feasible solution $\overline{U}(t_{m_0}) = [\overline{u}(t_{m_0}), \overline{u}(t_{m_1}), \ldots, \overline{u}(t_{m_{n_l-1}})]^T$ of the problem formulated in (3.31) and (3.33).

2: Let the MPC controller solution $u_{mpc}(t_{m_0}) = \overline{u}(t_{m_0})$ be the system in the sampling interval $[t_{m_0}, t_{m_0} + t_l)$, where the rest of the solutions $\overline{u}(t_{m_q}), q = 1, \ldots, n_l - 1$ are discarded. $x(t_{m_{q+1}})$ is computed by $x(t_{m_{q+1}}) = f(x(t_{m_q}), u_{mpc}(t_{m_q}))$.

3: Set $t_{m_q} := t_{m_{q+1}}$, and update the system states, inputs and outputs with the control input $u_{mpc}(t_{m_0})$ and the state equation $x(t_{m_{q+1}}) = f(x(t_{m_q}), u_{mpc}(t_{m_q}))$.

4: Until $t_{m_q} := t_{m_{n_l-1}}$, update the system outputs, inputs, states and the state equation; repeat steps 1 and 2, one obtains the control $u_{mpc}(t_{m_{n_l-1}}) = \overline{u}(t_{m_{n_l-1}})$. Apply the MPC control input $u_{mpc}(t_{m_{n_l-1}})$ to the system in the sampling interval $[t_{m_{n_l-1}}, t_{(m+1)_0})$.

5: Set $t_{m_q} := t_{(m+1)_0}$, measure the state value $x(t_{m_{n_l-1}})$ by step $t_{m_q} = t_{m_{n_l-1}}$, and $u_{mpc}(t_{m_{n_l-1}})$ to the system $x(t_{(m+1)_0}) = f(x(t_{m_{n_l-1}}), u_{mpc}(t_{m_{n_l-1}}))$, and update the reference $r(t_{m_0}) := r(t_{(m+1)_0})$ in (3.31).

6: Compute the optimal solution $\overline{U}(t_{(m+1)_0}) = [\overline{u}(t_{(m+1)_0}), \overline{u}(t_{(m+1)_1}), \ldots, \overline{u}(t_{(m+1)_{n_l-1}})]^T$ of the problem formulated in (3.31) and (3.33). Then the MPC controller $u_{mpc}(t_{(m+1)_0}) = \overline{u}(t_{(m+1)_0})$ (the remaining $\overline{u}(t_{(m+1)_q}), q = 1, \ldots, n_l - 1$ are discarded) is used in the system in the sampling interval $[t_{(m+1)_0}, t_{(m+1)_0} + t_l)$ to solve the MIMO MPC solution $x(t_{(m+1)_1}) = f(x(t_{(m+1)_0}), u_{mpc}(t_{(m+1)_0}))$ over the period $[t_{(m+1)_0} + t_l, t_{(m+1)_0} + 2t_l)$.

7: Set $t_{m_q} := t_{(m+1)_1}$ and go to step 1.

Generally, the above MPC algorithm never stops, and it updates the controller at each time interval $[t_{m_q}, t_{m_{q+1}})$ to include feedback information.

3.5   SIMULATION AND RESULTS

Here, the researcher presents a case study to demonstrate the performance of the proposed hierarchical control method of a DX A/C system. The experimental data from [116] is used to calibrate the parameters of the energy models described in Section 3.3.4. Then the DX A/C system model is built up in [103] based on the experimental environment. The proposed AHC strategy is compared with a baseline strategy through simulations over 24 hours.

3.5.1   System setup

In this case study, an office room is regarded as the conditioned space. The volume of the DX conditioned room is 77 m^3. The parameters of the energy models are listed in Table 2.1. The DX A/C system parameters are described in Table 2.2. For the proposed hierarchical control strategy considered below, most of the system constraints are given in Table 2.3, the bound of the air enthalpy h_s is limited in the range of [27.3, 46.3] and one constrains the value of the PMV index in the range of $[-0.5, 0.5]$ to ensure that the DX A/C system is able to maintain both IAQ and thermal comfort at acceptable levels.

In this chapter, data of the outside relative humidity and air temperature over a 24-hour period in a single summer is shown in Fig. 3.5(a). The data was obtained from a meteorological station located in Cape Town, South Africa. The solar radiative heat flux density profile of Cape Town over a 24-hour

(a) Outside air temperature and relative humidity

(b) Radiative heat flux
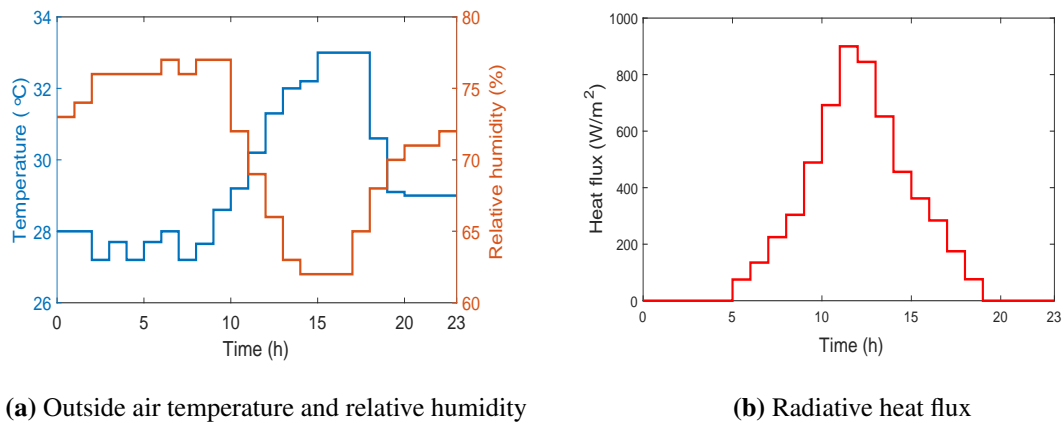
Figure 3.5. Forecast of outside air temperature, relative humidity and radiative heat flux over a 24-hour period.

(a) Cooling loads

(b) Radiative heat flux
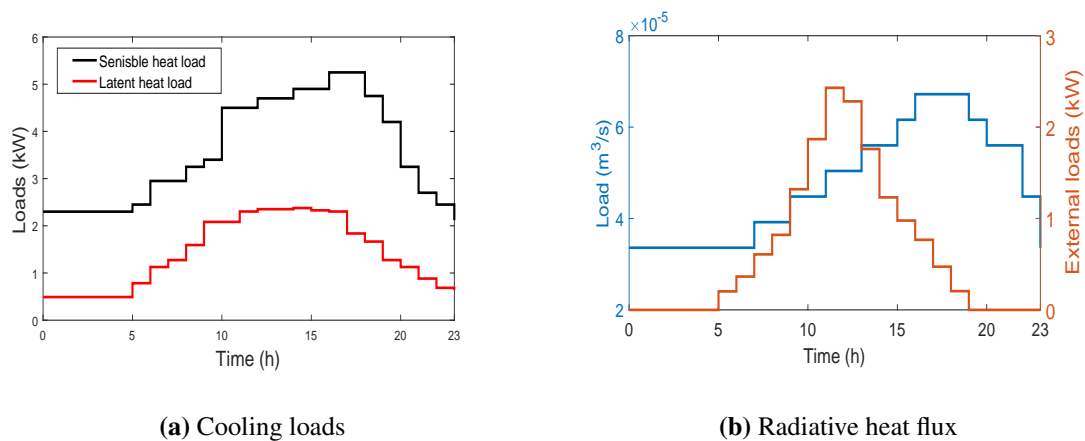
Figure 3.6. Estimation of the certainty internal sensible and latent, pollutant and external sensible heat loads over a 24-hour period.

period is shown in Fig. 3.5(b). The certainty internal sensible and latent heat loads, the external sensible heat load and the pollutant load in a conditioned space are predicted in Fig. 3.6. The values of Figs. 3.5-3.6 at every hour are commensurately quantised. It is assumed that the PI controller would absorb the CO_2 concentration in the air supply, where C_s=360 ppm is used in this chapter.

The TOU electricity prices for summer hours are summarized in (3.25). For simplicity, only the TOU energy charge is considered in this chapter. The original nonlinear systems (3.1)-(3.6) can also be employed as the plant to be controlled in the simulation test of this chapter.

3.5.2   Two control strategies

Here, two strategies to schedule the operation of a DX A/C system are considered in the conditioned space. One is a MIMO MPC controller and an energy-optimised open loop controller, which serves as a baseline strategy [115], and the other is the proposed AHC strategy. To compare the control strategies, the predicted load and outside weather profiles are the same.

1) Baseline: The baseline strategy is described below. The researcher first determines a setpoint for indoor air temperature and relative humidity based on a comfort zone, the psychrometric chart and a setpoint for CO_2 concentration based on the level acceptable to occupants. The ASHRAE comfort zone is taken from [127]. Its details are omitted here because of the space limitations. Under the given reference points of indoor CO_2 concentration, relative humidity and air temperature, one can obtain a unique and optimised steady state of the DX A/C system by solving the optimization problem (3.26) under $\alpha = 0$ and without TOU electricity price at every hour over a 24-hour period. The nonlinear model can then be linearized around the steady state. An MPC is designed for the linearized state-space model. The presented MPC with a sampling period of 2 min is applied that can simultaneously achieve better performance on both thermal comfort and IAQ with superior energy efficiency.

2) Proposed method: For the proposed control strategy, the details are given below. The researcher first uses the open loop controller to solve the optimization problem (3.26) to obtain steady states at every hour by employing NLP. The MIMO MPC is designed to track the references of CO_2 concentration, humidity and air temperature. In the proposed control method, the volume of the outside air entering the indoor space is optimized. The optimal volume of outside air is used in the DX A/C system for the MIMO MPC controller. The sampling period is set to $T_L = 1$ h and the sampling interval is set to $N_L = 24$ in the upper layer. The sampling period for the proposed MPC design is $t_l = 2$ min. The prediction and control horizons are taken as $n_p = n_c = 30$ in the lower layer. At each time step, the open loop controller is repeatedly used to solve the open loop optimization problem (3.26) and then the tradeoff steady states are obtained by the lower layer. In Section 3.5.3, the energy consumption and cost for the baseline and the proposed control strategies are compared in the next section.
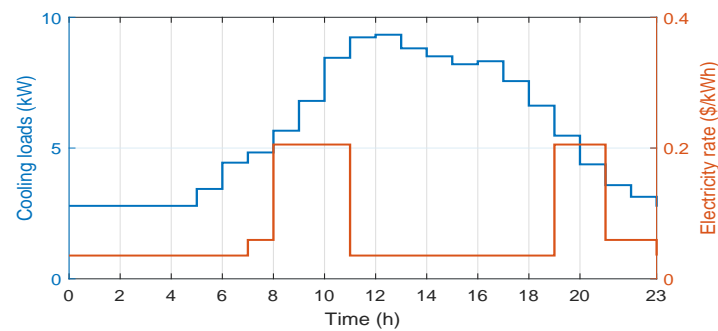
Figure 3.7. Profiles of cooling loads and electricity rates over a 24-hour period.
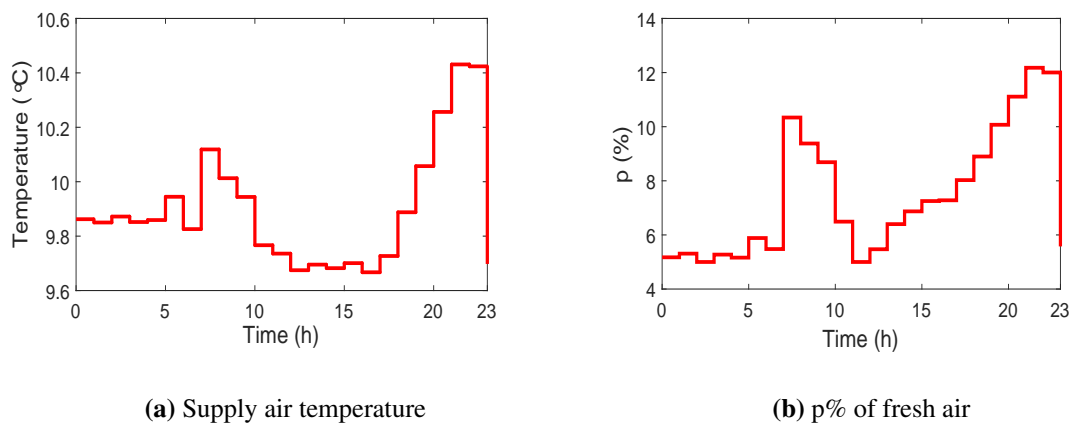
(a) Supply air temperature

(b) p% of fresh air

Figure 3.8. Optimal supply air temperature to the air conditioned room and p% of outside air entering the system over a 24-hour period.

3.5.3   Comparison of two control strategies

The performance of both control strategies is compared with historical weather data of a specific day in Cape Town. The total simulation time is set to $K = 24$ h. The predicted indoor cooling load profile is depicted in Fig. 3.7, overlaid with an electricity rate for summer hours. The researcher duplicates the indoor cooling load profile for the next day to simulate the MPC scheme. The profile of the supply air temperature to the conditioned room and p% of the outside air entering the system over a 24-hour period are shown in Fig. 3.8(a) and 3.8(b). The data can be used in the DX A/C system for the lower layer closed-loop tracking control.

The control calculations from two control strategies are applied to the DX A/C system. The reference points tracking of indoor air temperature in the conditioned space for the proposed strategy together with the setpoint regulation of indoor air temperature for the baseline strategy is shown in Fig. 3.9. The reference points tracking of indoor relative humidity in the conditioned space for the proposed strategy together with the setpoint regulation of indoor relative humidity for the baseline strategy are illustrated in Fig. 3.10. The reference points tracking of indoor CO_2 concentration in the conditioned space for the proposed strategy together with the setpoint regulation of indoor CO_2 concentration for the baseline strategy are simulated in Fig. 3.11. One observes that the indoor CO_2 concentration, relative humidity and air temperature for the proposed strategy can track their reference points well over a 24-hour period through the changing environment. It is also evident that for the proposed strategy, the reference points are tallish during the peak hours for CO_2 concentration, relative humidity and air temperature tracking. The reason is that the proposed controller has automatically adjusted the reference points upward to meet the energy cost and minimize consumption during peak hours, while both the thermal comfort and IAQ are still kept within the acceptable ranges. One further observes that with the baseline strategy under the varying cooling and pollutant loads, the MPC controller always maintains the indoor CO_2 concentration, relative humidity and air temperature at their setpoint by regulating the varying speeds of the supply fan and the compressor. From the local zooming out of Figs. 3.9-3.11, the reference points of indoor CO_2 concentration, relative humidity and air temperature can be reached after a transient process of 18 minutes. After reaching their reference points, the proposed controller maintains the reference points with small variation ranges. The two control variables of the air volumetric flow rate and mass flow rate of refrigerant of the DX A/C over a 24-hour period are shown in Fig. 3.12. The two control variables are varying to drive the indoor air temperature, relative humidity and CO_2 concentration to track their trajectory references according to the changing environment during the day. It can be seen from Fig. 3.12 that the air volumetric flow rate is not increasing, though the indoor cooling loads, pollutant loads and electricity rate are increasing. This is due to the proposed controller adaptively adjusting the setpoint upward for reducing energy consumption. The minimal energy consumption is achieved by optimizing the air volumetric flow rate and the mass flow rate of refrigerant. As is shown in Fig. 3.13, the value of the PMV index for the two control methods is within the expected range [-0.5,0.5].

Fig. 3.14(a) and 3.14(b) show the energy consumption and the energy cost of the DX A/C system operation for the proposed and baseline strategies over a 24-hour period, respectively. One observes from Fig. 3.14(a) and 3.14(b) that, both control strategies consume almost the same energy cost from
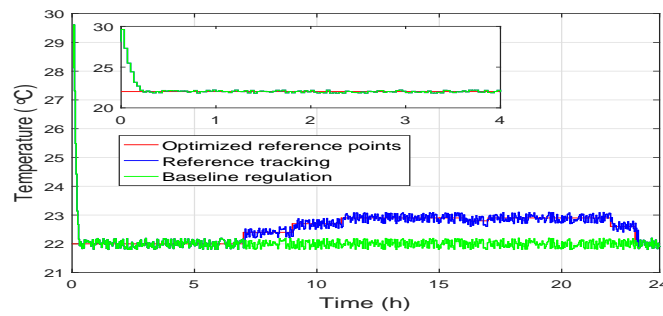
Figure 3.9. Reference tracking of indoor air temperature over a 24-hour period.
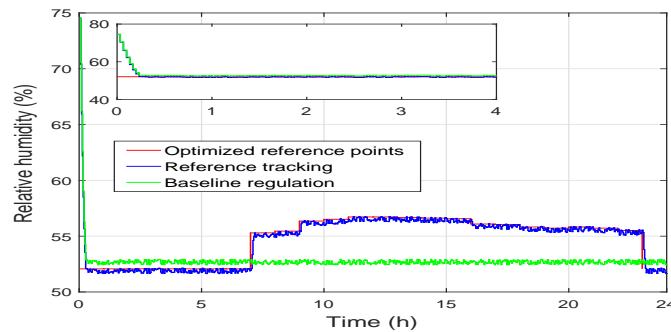
Figure 3.10. Reference tracking of indoor air humidity over a 24-hour period.
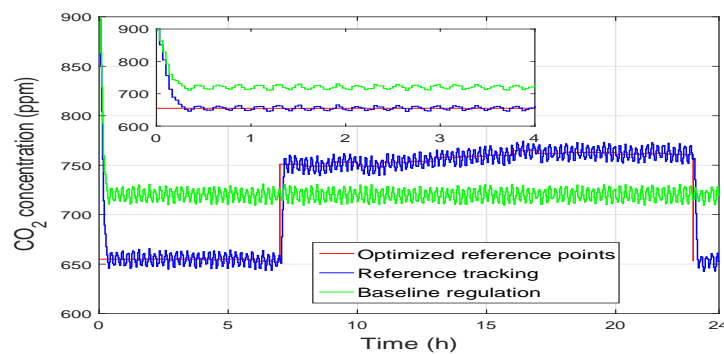
Figure 3.11. Reference tracking of indoor CO_2 concentration over a 24-hour period.

0:00 to 7:00. The indoor CO_2 concentration, relative humidity and air temperature reference points stay at the lower bound of the PMV index during off-peak hours without a higher energy cost. After 8:00, the energy cost of the baseline and proposed control strategies starts increasing since increased pollutant and cooling loads are required to be removed and the power price is increased. Compared to

(a) Air volumetric flow rate

(b) Mass flow rate of refrigerant
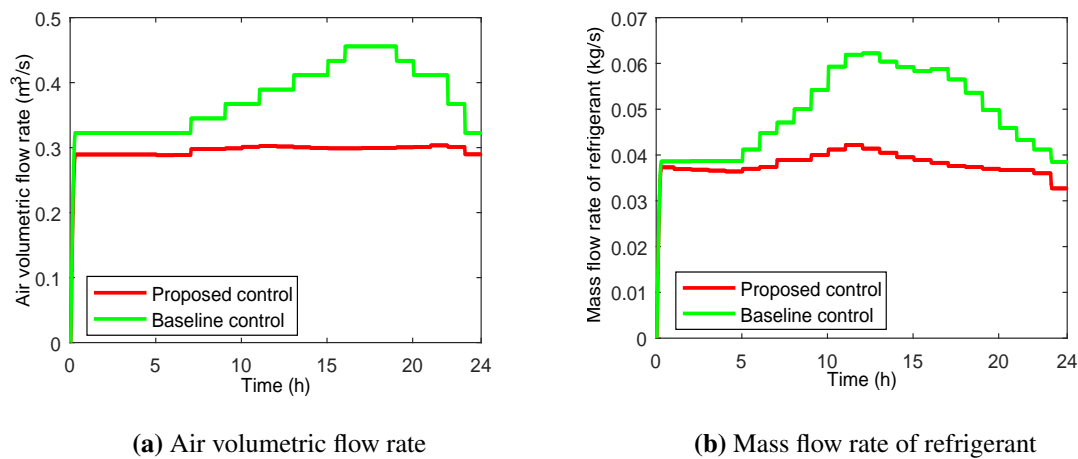
Figure 3.12. Profiles of the variation in the two control variables over a 24-hour period.
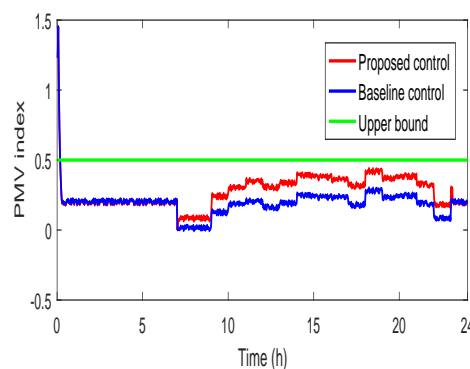
Figure 3.13. Profile of the value of the PMV index over a 24-hour period.

the baseline strategy, Fig. 3.14(a) shows that the proposed method consumes less energy. Comparing the two strategies, one also observes that energy costs under the proposed method are reduced further during peak hours. This is due to the proposed controller, which automatically adjusts the reference points upward such that the energy consumption and cost are minimized during peak hours while maintaining both IAQ and thermal comfort at the required levels. From the simulation, it can be seen that the major energy consumption and cost have been verified to reduce effectively during the peak hour. The total energy consumption and cost over a 24-hour period are summarized in Table 3.1. According to the findings, the proposed AHC strategy performs better than the baseline by around 31.38% of total energy consumption, and by around 33.85% of total energy cost for a DX A/C system operation. It can be observed from Table 3.1 that the proposed control strategy shows a lower energy consumption and costs compared to the baseline control strategy. The table also displays that the total

(a) Energy consumption   **(b)** Energy cost
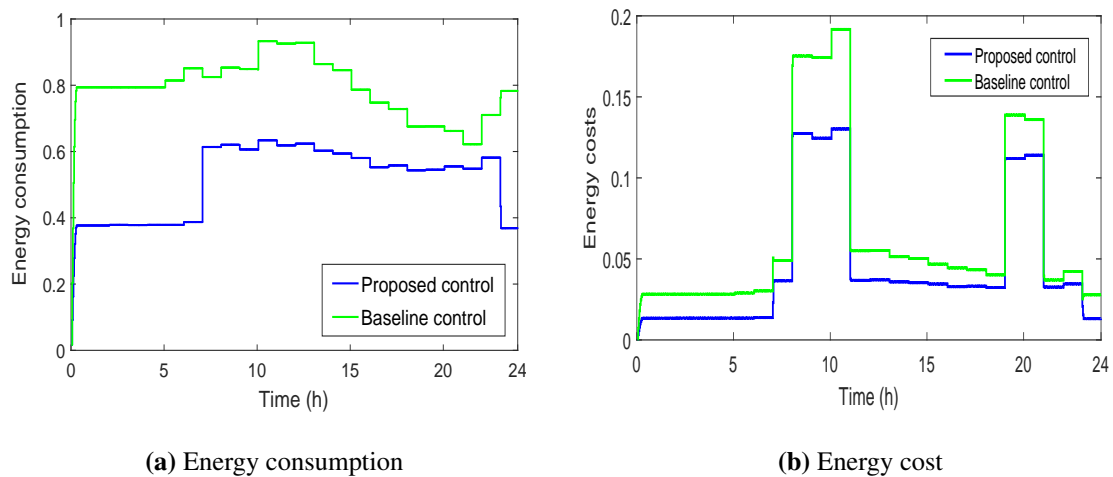
Figure 3.14. Profiles of the energy consumption and cost of a DX A/C system for the proposed and baseline controllers over a 24-hour period.

Table 3.1. Comparison of the proposed and baseline control strategies.

Strategy	Energy consumption (kWh)	Energy cost ($)	$\sum |PMV|$
Baseline control	20.52	1.734	103.33
Proposed control	14.08	1.147	162.32
Saving (%)	31.38	33.85	

values of the PMV index over a 24-hour period for the proposed control strategy are higher than that of the baseline control strategy. It is expected that the proposed control strategy will reduce energy consumption and cost at the expense of comfort level, which will nevertheless still be reasonably and optimally regulated to the required levels. Therefore, the utilities can choose the two control approaches to implement building DX A/C systems based on their different aims.

Though it is desirable to compute the energy cost savings brought about by the proposed control strategy over the baseline control strategy, it is an impossible task for real buildings simply to compare the cost values of two control strategies in one day, because load factors, outside temperature and relative humidity cannot be the same every day. When demonstrating the effectiveness of the proposed AHC scheme in different weather conditions, the proposed testing days happened to be much warmer than the baseline testing days in this test. The weather conditions of the testing days are listed in

Table 3.2. The energy consumption on the testing days is obtained and described in Fig. 3.15. From this comparison, all proposed control testing days present much lower power consumption, showing successful energy efficiency improvement by the proposed control strategy.

Table 3.2. Different weather conditions for the testing days

Date	Control	Average T_0	Average H_0	T_0^{max}	H_0^{max}
12/30	Baseline	28.6	72.4%	33.9	80%
12/31	Proposed	29.2	71.6%	34.2	81%
01/01	Proposed	28.8	72.1%	32.2	79%
01/02	Proposed	28.9	72.4%	33.2	81%
01/03	Proposed	28.1	73.2%	32.0	82%
01/04	Baseline	28.0	72.3%	32.4	79%
01/05	Baseline	27.6	73.4%	32.0	80%
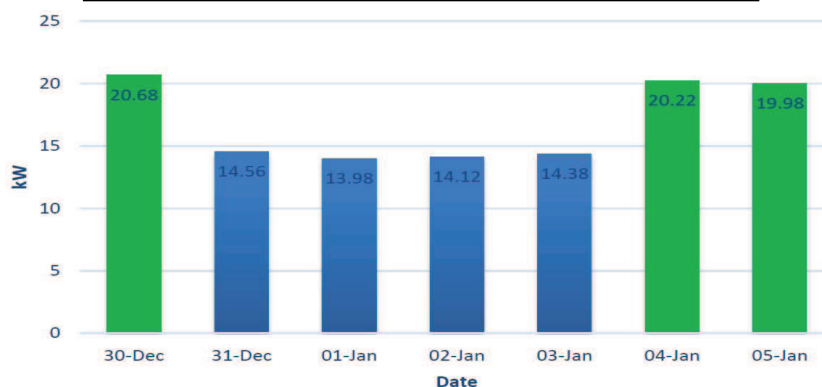
Figure 3.15. Energy consumption on testing days for the baseline and proposed approaches.

3.5.4   Sensitivity analysis

The simulation results presented are obtained in this chapter under the assumption that the parameters are accurate and the DX A/C systems can perfectly describe the real system. However, in reality, there are usually uncertainties in parameters and models. In this chapter, a simple uncertainty analysis is considered to illustrate how the uncertainty parameter would affect the control performance of the proposed AHC strategy. Here, the uncertainties of some major parameters of the DX A/C system are considered, namely the heat transfer area on the dry-cooling region in the DX evaporator A_1 and the heat transfer area on the wet-cooling region in the DX evaporator A_2. However, the total area
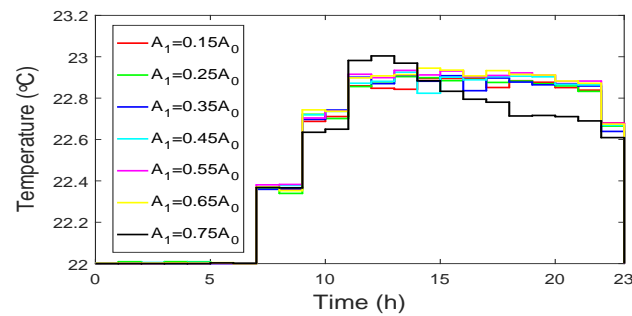
Figure 3.16. Steady state of indoor air temperature optimised by the proposed open loop controller under different system parameters over a 24-hour period.

$A_0 = A_1 + A_2$ is known. Hence, it is only necessary to consider that the uncertainty parameter A_1 would affect the performance of the proposed control strategies. The open loop optimal controller and the tracking of the MIMO MPC with different values of the uncertainty parameter A_1 are verified through simulation. For the case study considered here, the simulations for the indoor air temperature optimized by the proposed open loop optimal controller and the MIMO MPC temperature tracking under different parameter values are shown in Figs. 3.16-3.17, and the results for the open loop optimal controller under all different ranges of the uncertainty parameter are displayed in Table 3.3. The standard deviations for the steady state of indoor air temperatures are less than 0.2 °C. The standard deviations for the objective function values of the open loop controller are less than 6%. The results suggest that the fluctuation of the control performance affected by the parameter uncertainty A_1 is relatively small. Thus, the proposed autonomous hierarchical control strategy is not very sensitive to the modelling parameter A_1 specified here.

3.6 CONCLUSION

This chapter proposes an autonomous hierarchical control method to reduce the total energy consumption and cost of a DX A/C system while maintaining both thermal comfort and IAQ at required levels. It proposes an efficient control algorithm to solve the autonomous hierarchical control problem based on an open loop optimal controller and the MIMO MPC scheme. The optimal and time-varying reference points of indoor CO_2 concentration, relative humidity and air temperature for the DX A/C system are generated by the upper layer. The lower layer MIMO MPC is then proposed to steer the DX A/C system to follow the reference points, whereas energy consumption and costs are minimized.
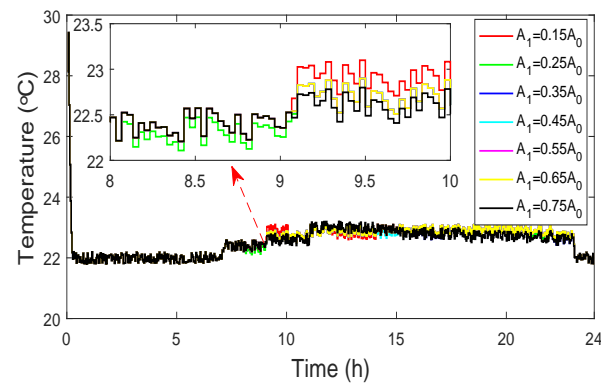
Figure 3.17. The MIMO MPC temperature tracking under different system parameters over a 24-hour period.

The results show that the proposed control method could achieve an energy consumption saving of 33.9% and energy cost reduction of 33.85% while keeping the value of the PMV index in the range of [-0.5,0.5]. The performance of the proposed control is obtained under the assumption that the models and parameters can express the real system perfectly. However, in reality, there are usually uncertainties. Hence, the researcher has made a parameter sensitivity analysis in this chapter. The simulation results suggest that the performance of the proposed control method is satisfactory because the standard deviations of energy saving are less than 5% in comparison with around 35% energy saving for normal values. Therefore, the proposed control method is significant when applied in theoretical and practical applications.

Table 3.3. Open loop optimization results under different dry-cooling regions.

Objective function value of open loop optimization	Area of dry region	Portion of A_1 m^2	Derivation %
43.04	$(0, 0.05A_0]$	$0.05A_0$	2.14%
44.23	$(0.05A_0, 0.10A_0]$	$0.10A_0$	0.57%
43.98	$\mathbf{(0.1A_0, 0.15A_0]}$	$\mathbf{0.15A_0}$	
43.00	$(0.15A_0, 0.20A_0]$	$0.20A_0$	2.23%
43.20	$(0.2A_0, 0.25A_0]$	$0.25A_0$	1.77%
43.48	$(0.25A_0, 0.30A_0]$	$0.30A_0$	1.14%
42.87	$(0.3A_0, 0.35A_0]$	$0.35A_0$	2.52%
41.57	$(0.35A_0, 0.40A_0]$	$0.40A_0$	5.48%
42.54	$(0.4A_0, 0.45A_0]$	$0.45A_0$	3.27%
42.47	$(0.45A_0, 0.50A_0]$	$0.50A_0$	3.43%
42.21	$(0.50A_0, 0.55A_0]$	$0.55A_0$	4.02%
42.26	$(0.55A_0, 0.60A_0]$	$0.65A_0$	3.91%
44.00	$(0.60A_0, 0.70A_0]$	$0.70A_0$	0.04%
42.22	$(0.70A_0, 0.75A_0]$	$0.75A_0$	4.00%
41.91	$(0.75A_0, 0.80A_0]$	$0.80A_0$	4.71%
41.60	$(0.80A_0, 0.85A_0]$	$0.85A_0$	5.41%
41.52	$(0.85A_0, 0.90A_0]$	$0.90A_0$	5.59%
41.70	$(0.90A_0, 0.95A_0]$	$0.95A_0$	5.18%

CHAPTER 4   DISTRIBUTED CONTROL OF AN ME A/C SYSTEM

4.1   INTRODUCTION

Although the energy efficiency improvement and energy cost reduction, as well as comfort level improvement, have been investigated in a single-zone DX A/C system presented in Chapters 2 and 3, reducing the energy consumption, energy cost, communication resources, computational complexity and conservativeness simultaneously for a multi-zone building's ME A/C system while maintaining multi-zones' IAQ and thermal comfort at comfort ranges have not been studied so far. They are the main objectives of this chapter, which focus on designing advanced controllers to solve the issues. In particular, we propose an AHDC method for a multi-zone building's ME A/C system. This control strategy includes two levels. The upper level involves open-loop scheduling that only collects local measurement information and operational profiles, formulates and solves a distributed coordination steady-state optimization problem by optimizing the energy cost and demand charge of operating a multi-zone building's ME A/C system under the TOU price structures over a 24-hour period to generate trajectory references adaptively and autonomously for lower-layer controllers. In this chapter, it is assumed that the occupancies, functions and purposes in multi-zones are similar; in this situation, one can distributively design an optimal scheduler, which scheduling generates time-varying reference points and communicates with the whole connected network via neighbors. All rooms then transmit their reference points to the lower-layer controllers. The lower layer designed as MIMO DMPC controllers only uses local information to formulate and solve local optimization problems for the ME A/C system to track autonomously and adaptively the trajectory reference points, which are calculated by the upper layer, autonomously and adaptively. Therefore, for large-scale systems, the researcher first proposes a two-layer distributed control strategy, which is capable of reducing more communication

resources, computational complexity and conservativeness compared with the previous distributed and non-distributed control strategies [85, 86, 87, 89, 88, 90, 93].

In the proposed distributed control scheme, communication can be done with reduced hardware of cheaper and shorter-range communication modules and depend on the communication topology, a receiver only. While in the conventional control schemes [78, 80, 81, 82, 89, 91], it may require full-swing communication modules, which requires external service providers in long-range data communication. It may also require that both transmitter and receiver for the implement.

In view of energy efficiency, the peak demand reduction of building's DX A/C systems based on demand response (DR) action has not been considered by the hierarchical controllers designed in Chapters 2 and 3. Thereby, another purpose of the ME A/C control system designed in this chapter is to shift the peak demand to off-peak hours to improve the energy efficiency and reduce the energy cost of the ME A/C system.

Another contribution of this chapter is that the researcher proposes autonomous demand-side management scheduling for office buildings, which is beneficial for both occupancy and buildings. The idea of the ADSMS is based on the two-layer distributed controllers for a multi-zone building's ME A/C system and helps us understand how to use this control scheme in practical applications.

To illustrate the performance of the designed two-layer distributed control schemes over previous controllers on energy efficiency and cost savings, and reduction of communication resources, computational complexity and conservativeness simultaneously for a multi-zone building's ME A/C system, a case study is provided to validate them.

4.2 CHAPTER OVERVIEW

This chapter presents a new hierarchical control system for a multi-zone building's ME A/C system including an upper-layer distributed nonlinear controller and lower-layer distributed controllers. Whereas the multi-zone building's ME A/C system is an extension number evaporators to a single-zone DX A/C system reported in Chapters 2 and 3, the controller for a multi-zone building's ME A/C system is newly designed in this chapter. Moreover, the upper-layer distributed nonlinear controller only collects

local measurement information to generate an optimized signal profile and communicates with the whole connected network through neighbors by an open loop manner, and the lower layer distributed controllers use the signals as inputs in a closed-loop manner. Further, the controllers designed in this chapter consider the demand peak reduction, which was not studied in Chapters 2 and 3. In summary, two-layer distributed controllers are designed to improve energy efficiency and reduce energy cost, demand, communication resources, computational complexity and conservativeness while maintaining multi-zones' thermal comfort and IAQ at comfort ranges.

Section 4.3 presents nonlinear multi-zone dynamical models and energy models for a multi-zone building's ME A/C system. The proposed control strategy for the multi-zone building's ME A/C system is designed in Section 4.4. Simulation results are described in Section 4.5. Conclusions are drawn in Section 4.6.

4.3   ME A/C SYSTEM

4.3.1   Description of an ME A/C system

A diagram schematic of an ME A/C system is illustrated in Fig. 4.1. The components of the ME A/C system are dampers, DX evaporators, an air-cooled tube-plate-finned condenser, a variable speed compressor, EEVs, variable speed centrifugal supply fans with PSA boxes, and a damper for mixing the return air from the building with the outside air. The supply fan regulates its own speed based on the air flow rate/opening controlled by the EEV to control cooled air to each room. Each indoor unit placed in the room has an EEV and an evaporator. The PSA box absorbs CO_2 contaminant concentration of mixed air to improve the fresh air ratio. Each indoor unit is connected to the compressor and the outlet of the condenser. The indoor air unit recirculates return air from building spaces and mixes it with fresh outside air. The proportion of return air to outside air is controlled by damper positions in the ME A/C system. The mixed air is cooled by the DX cooling coil. In this chapter, the ME A/C system is also assumed to operate in the cooling mode.

Because of the complex nature of the air flow and heat transfer process, ME A/C systems are usually modelled as time-varying nonlinear partial differential equations [128], which are not suitable
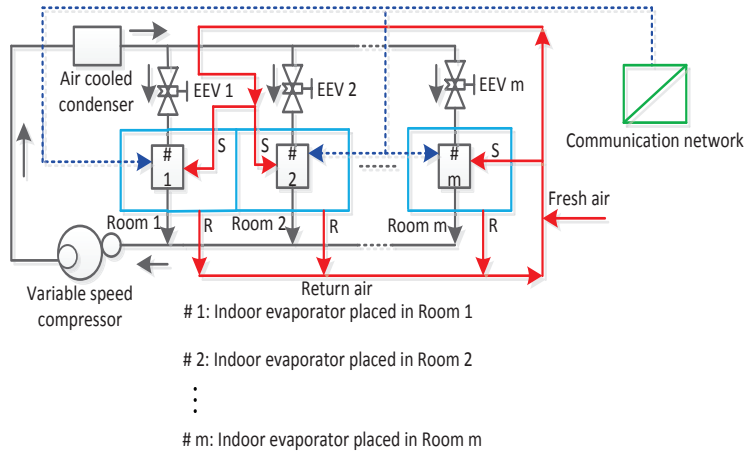
Figure 4.1. Schematic diagram of the ME A/C system with control box.

for control and optimization. Therefore, the following assumptions are provided to simplify the modelling.

1) The air in each room and outdoor environment is well mixed immediately so that the CO_2 concentration, relative humidity and air temperature distributions are uniform.

2) The heat capacity of the air is constant.

4.3.2 Dynamic model of an ME A/C system

Based on the above configuration, the researcher uses an undirected connected graph structure to represent the rooms and their dynamic couplings in the following way; The i-th room is associated with the i-th node of the system. The mathematical dynamic models for the multi-zone building's ME A/C system via the relationship among air enthalpy, air temperature and the moisture content leaving the evaporator i of unit i as $h_{s,i} = C_a T_{s,i} + h_{fg} W_{s,i}$ are described as below. In this chapter, only the interaction between rooms in terms of sensible heat gain is considered.

$$C_a \rho V_i \frac{dT_{z,i}}{dt} = \sum_{j=1}^{m} \frac{T_{z,j} - T_{z,i}}{R_{ij}} + \frac{T_0 - T_{z,i}}{R_i} + C_a \rho v_{f,i}(T_{s,i} - T_{z,i}) + Q_{load,i}, \qquad (4.1)$$

$$\rho V_i \frac{dW_{z,i}}{dt} = \rho v_{f,i}(\frac{h_{s,i} - C_a T_{s,i}}{h_{fg}} - W_{z,i}) + M_{load,i}, \qquad (4.2)$$

$$C_a \rho V_{h1,i} \frac{dT_{d,i}}{dt} = C_a \rho v_{f,i}(T_{mix} - T_{d,i}) + \alpha_{1,i} A_{1,i}(T_{w,i} - \frac{T_{mix} + T_{d,i}}{2}) \qquad (4.3)$$

$$\rho V_{h2,i} \frac{dh_{s,i}}{dt} = \alpha_{2,i} A_{2,i}(T_{w,i} - \frac{T_{d,i} + T_{s,i}}{2}) + h_{fg} \rho v_{f,i}(W_{mix} - \frac{h_{s,i} - C_a T_{s,i}}{h_{fg}}) + C_a \rho v_{f,i}(T_{d,i} - T_{s,i}), \quad (4.4)$$

$$C_w \rho_w V_w \frac{dT_{w,i}}{dt} = \alpha_{1,i} A_{1,i} \left(\frac{T_{mix} + T_{d,i}}{2} - T_{w,i} \right) + \alpha_{2,i} A_{2,i} \left(\frac{T_{d,i} + T_{s,i}}{2} - T_{w,i} \right) - (h_{r2,i} - h_{r1,i}) m_{r,i}, \quad (4.5)$$

$$V_i \frac{dC_{c,i}}{dt} = \left(k_P v_{f,i} + k_I \int_0^{T_I} v_{f,i} ds \right) (C_s - C_{c,i}) + G_i \cdot Occp_i. \quad (4.6)$$

where $i = 1, 2, \ldots, m$, $T_{z,j}$ is the air temperature of room j. These notations of the system states and parameters in a single zone or an evaporator are defined. These notations in a multi-zone and multi-evaporator are therefore omitted here. $R_{ij} = R_{ji}$ is the thermal resistance of the wall between rooms i and j and R_i is the thermal resistance of the wall between room i and the outside area. If R_{ij} and R_i are not known from the design specification, they can be obtained through model identification reported in [129, 130]. T_{mix} and W_{mix} are the mixed air temperature and moisture content before the DX evaporator cooling coils, respectively. The mixed air temperature and humidity are calculated by

$$
\begin{aligned}
T_m &= \delta T_0 + (1 - \delta) \frac{\sum_{i=1}^m \rho v_{f,i} T_{z,i}}{\sum_{i=1}^m \rho v_{f,i}}, \\
W_m &= \delta W_0 + (1 - \delta) \frac{\sum_{i=1}^m \rho v_{f,i} W_{z,i}}{\sum_{i=1}^m \rho v_{f,i}},
\end{aligned}
\quad (4.7)
$$

where δ is the mixing ratio between the outside air and the return air. It is assumed that the return air temperature and moisture content are the weighted sums of the zone temperatures and moisture contents with weights being the air volumetric flow rate to the corresponding zones. The return air is not recirculated when $\delta = 0$, and no outside fresh air is used when $\delta = 1$. δ can be used to save energy through recirculation, but it has to be less than one to guarantee minimal outside fresh air allowed to the zones. Note that the first equation in (4.7) was reported in [64]. It is assumed that the mixed moisture content has a similar description in the second equation of (4.7). The airside convective heat transfer coefficients in both the dry-cooling $\alpha_{1,i}$ and wet-cooling $\alpha_{2,i}$ regions at the evaporator i in unit i are expressed in (2.8) and (2.10), respectively. The air velocity $v_{a,i}$ of zone i is described in (3.11).

The dynamic mathematical models (4.1)-(4.5) without considering outside air temperature and relative humidity entering system for a single zone were modelled in [103]. The mathematical dynamic models (4.1)-(4.6) absorbing the zone's CO_2 concentration by an independent PSA box for a single zone are reported in Chapter 2. The mathematical dynamic models (4.1)-(4.6) with absorbing CO_2 concentration by using a PI controller based on a supply fan for a single zone were modeled in Chapter 3. On the right-hand side of (4.1), the first term represents the heat transfer between zone i and all neighbours of zone i; the second term denotes the heat transfer between zone i and outside wall.

Remark 4.1 *Higher-order resistance-capacitance (RC) models were modeled in [78, 80]. For simplicity, this study only considers a first-order RC model in this chapter.*

Remark 4.2 *One of the predictions for a single zone DX A/C system's cooling and pollutant loads was expressed in [92] and used as measurement information in this chapter. The multi-zone loads are affected by some parameters (such as T_0, W_0, $Q_{rad,i}$, $Occp_i$, internal heat gain $Q_{int,i}$ and moisture ventilation load $M_{int,i}$). The prediction of these parameters is obtained through a weather forecast station, historical data and schedules. Though multi-zone building's cooling and pollutant loads cannot be accurately predicted, the closed-loop distributed controller is capable of handling these prediction errors.*

To make the ME A/C system cooperatively control multi-zones' IAQ and thermal comfort at acceptable levels, we assume that the ME A/C system is equipped with a communication network based on wireless sensors. In this network, they can share information (e.g., $T_{z,i}$, $W_{z,i}$ and $C_{c,i}$) with each other, which is shown in Fig. 4.1. The information flow between them is modelled as a network connected graph $\mathcal{G} = (\mathcal{V}, \vartheta, \mathcal{A})$, where $\mathcal{V} = \{1, 2, \ldots, m\}$ is the index set of different rooms and zones of the ME A/C system, $\vartheta \subset \mathcal{V} \times \mathcal{V}$ is the edge set of ordered pairs of the ME A/C system, and $\mathcal{A} = [a_{ij}] \in \mathbb{R}^{m \times m}$ is the adjacency matrix with entries $a_{ij} = 1$ or $a_{ij} = 0$. If the ME A/C subsystem i can receive information from the ME A/C subsystem j, then $(j, i) \in \vartheta$, $a_{ij} = 1$ and the ME A/C subsystem j is called the network neighbor of the ME A/C subsystem i, defined by $j \in \mathcal{V}_i$, where $\mathcal{V}_i = \{j \in \mathcal{V} | a_{ij} = 1\}$. If the ME A/C subsystem i cannot have access to the information of the ME A/C subsystem j, then $(j, i) \notin \vartheta$, $a_{ij} = 0$ and $j \notin \mathcal{V}_i$. Self-connection is not considered for $\mathcal{G}$, ie., $a_{ii} = 0$, $\forall i \in \mathcal{V}$. A graph $\mathcal{G}$ is undirected if $a_{ij} = a_{ji}$ for any $i, j \in \mathcal{V}$. In this chapter, the network connected graph $\mathcal{G} = (\mathcal{V}, \vartheta, \mathcal{A})$ of the ME A/C system is assumed to be undirected and connected [131].

The ME A/C subsystems adjust their comfort levels adaptively by acquiring the adjacent information. The neighbors of an ME A/C subsystem can be denoted in many different ways. In this chapter, the following one is based on the effect of thermal resistance and expressed as follows:

$$\mathcal{V}_i = \{j : |R_{ij}| < \varepsilon_0, i \neq j\}, \tag{4.8}$$

where ε_0 is a predefined threshold.

The system dynamic equations (4.1)-(4.6) can be written in compact form as follows:

$$\dot{x}_i = f_i(x_i, x_{-i}, u_i, \omega_i), \quad i = 1, 2, \ldots, m, \tag{4.9}$$

where the vector $x_i \triangleq [h_{s,i}, T_{z,i}, T_{d,i}, T_{w,i}, W_{z,i}, C_{c,i}]^T$ is the state of the subsystem S_i; $u_i = [v_{f,i}, m_{r,i}]^T$ are the constrained control signals; $\omega_i \triangleq [Q_{load,i}, M_{load,i}, C_{load,i}]^T$ denote the load variables of room i; and

x_{-i} concatenate the states of all subsystems S_j ($j \in \mathcal{V}$) of the subsystem S_i, i.e., $x_{-i} = (\ldots, x_j, \ldots)$. The functions $f_i(x_i, x_{-i}, u_i, \omega_i)$ ($i = 1, 2, \ldots, m$) are expressed as follows:

$$f_i(x_i, x_{-i}, u_i, \omega_i) = \begin{bmatrix} \frac{\alpha_{2,i}A_{2,i}(T_{w,i} - \frac{T_{d,i}+T_{s,i}}{2}) + h_{fg}\rho v_{f,i}(W_{mix} - \frac{h_{s,i}-C_a T_{s,i}}{h_{fg}}) + C_a \rho v_{f,i}(T_{d,i} - T_{s,i})}{\rho V_{h2,i}} \\ \frac{\sum_{j=1}^{m} \frac{T_{z,j}-T_{z,i}}{R_{ij}} + \frac{T_0 - T_{z,i}}{R_i} + C_a \rho v_{f,i}(T_{s,i} - T_{z,i}) + Q_{load,i}}{C_a \rho V_i} \\ \frac{C_a \rho v_{f,i}(T_{mix} - T_{d,i}) + \alpha_{1,i}A_{1,i}(T_{w,i} - \frac{T_m + T_{d,i}}{2})}{C_a \rho V_{h1,i}} \\ \frac{\alpha_{1,i}A_{1,i}(\frac{T_{mix}+T_{d,i}}{2} - T_{w,i}) + \alpha_{2,i}A_{2,i}(\frac{T_{d,i}+T_{s,i}}{2} - T_{w,i}) - (h_{r2,i} - h_{r1,i})m_{r,i}}{C_{w,i}\rho_{w,i}V_{w,i}} \\ \frac{\rho v_{f,i}(\frac{h_{s,i}-C_a T_{s,i}}{h_{fg}} - W_{z,i}) + M_{load,i}}{\rho V_i} \\ \frac{(k_P v_{f,i} + k_I \int_0^{T_I} v_{f,i}\,ds)(C_{s,i} - C_{c,i}) + G_i \cdot Occp_i}{V_i} \end{bmatrix}. \tag{4.10}$$

4.3.3 Simplified energy models of an ME A/C system

The power consumers of the ME A/C system include the dampers, condenser fan, compressor, and DX cooling coils. The power to drive the dampers is assumed to be negligible. The condenser fan power P_{con} is approximated as a second-order polynomial function of the total mass flow rate of refrigerant ($m_r = \sum_{i=1}^{m} m_{r,i}$) driven by the fan

$$P_{con} = c_0 + c_1 m_r + c_2 m_r^2, \tag{4.11}$$

where the coefficients c_0, c_1 and c_2 are given in Table 2.1.

The power consumption of the evaporator fans is calculated as follows:

$$P_{eva} = \sum_{i=1}^{m} (a_0 + a_1 v_{f,i}, + a_2 v_{f,i}^2 + a_3 T_{s,i} + a_4 T_{s,i}^2 + a_5 Q_{c,i} + a_6 Q_{c,i}^2 + a_7 v_{f,i}T_{s,i} +$$
$$a_8 v_{f,i}Q_{c,i} + a_9 T_{s,i}Q_{c,i}), \tag{4.12}$$

where the coefficients a_i ($i = 0, 1, \ldots, 9$) are also listed in Table 2.1. $Q_{c,i}$ is the summation of the sensible and latent heat loads of room i.

The power consumption of the compressor P_{comp} is expressed by

$$P_{comp} = \sum_{i=1}^{m} \frac{m_{r,i}(h_{r2,i} - h_{r1,i})}{\overline{\eta}}, \tag{4.13}$$

where $\overline{\eta}$ is the combined total efficiency of the compressor (known parameters).

The total electric power consumption of the ME A/C system is expressed in (3.22).

4.3.4 PMV index

The details of the PMV index are described in 3.3.3. In this chapter, the researcher considers multi-zones' thermal comfort and air quality. Based on the equation in (4.6), the metabolic rate of room i denoted by M_{r_i} under a steady state of the CO_2 concentration in room i can be rewritten as follows [92]:

$$M_i = \frac{\lambda}{Occp_i}(k_P v_{f,i} + k_I \int_0^{T_I} v_{f,i} ds)(C_{c,i} - C_{s,i}), \ i = 1, 2, \ldots, m.$$

If PMV_i denotes the thermal comfort and IAQ indicator of room i, the PMV_i is then the function of the following variables

$$PMV_i = g_i(T_{z,i}, W_{z,i}, C_{c,i}, v_{f,i}, I_{cl}, T_r), \ i = 1, 2, \ldots, m. \tag{4.14}$$

4.3.5 Constraints

The ME A/C system is subject to IAQ, thermal comfort and cooling operational constraints. Most of the constraints of each room should be satisfied in (C1)-(C3), (C6), (C8)-(C9) and the other constraints are listed below.

(C10) $\delta \in [\underline{\delta}, \overline{\delta})$. Both upper and lower bounds limit the ratio of the outside fresh air entering the system.

(C11) $\sum_{i=1}^{m} v_{f,i} T_{s,i} \leq \sum_{i=1}^{m} v_{f,i} T_m$, $\sum_{i=1}^{m} v_{f,i} W_{s,i} \leq \sum_{i=1}^{m} v_{f,i} W_m$, $i = 1, 2, \ldots, m$. The mixed air temperature and moisture content after each DX evaporator can only decrease.

(C12) $T_{d,i} \leq T_m$, $T_{w,i} \leq T_{d,i}$, $W_{s,i} \leq W_m$, $i = 1, 2, \ldots, m$. The mixed air temperature and moisture content after each DX dry-cooling and wet-cooling region can only decrease.

The constraints in (C1)-(C3), (C6), (C8)-(C12) can be compactly written as

$$x_i \in \mathbb{X}, \ u_i \in \mathbb{U}, \ h_{3,i}(x_i, u_i) \leq 0, \ h_{4,i}(x_i) \leq 0 \text{ and } PMV_i \in \mathbb{F}, \ i = 1, 2, \ldots, m. \tag{4.15}$$

where $\mathbb{X}$, $\mathbb{U}$, $\mathbb{P}$ and $\mathbb{F}$ are bounded sets. The functions $h_{3,i}(x_i, u_i)$ and $h_{4,i}(x_i)$ correspond to the constraints in (C11) and (C12), respectively.

4.4 CONTROLLER DESIGN

To facilitate the description of the hierarchical distributed control algorithm for the nonlinear systems (4.9), the notation ^{u} will be defined for the upper-layer control while ^{l} will be defined for the lower-layer MPC. The researcher will also abbreviate the upper-layer open loop optimal controller to UOPC, and the lower-layer DMPC for one of room i as LDMPCi for short. t_k^u represents the sampling time instant of the UOPC, and t_k^l denotes that of the lower-lower DMPCs; define $c(k,q) \triangleq kN+q$, where N is a positive integer number corresponding to the number of sampling instants of LMPC between two sampling instants of UOPC; $t_k^u \triangleq t_{k,0}^l$; $\delta^u \triangleq t_{k+1}^u - t_k^u$, $\delta^l \triangleq t_{k+1}^l - t_k^l$ represent the sampling period of the UOPC and LDMPC, respectively; $\delta^u = M\delta^l$. T^l represents the prediction horizon of the LDMPC that satisfies $T^u \geq T^l + \delta^u$.

Throughout the rest of this chapter, the researcher defines the long-term scale horizon as $[0, K^u]$, and $K^u = n\delta^u$ $(n \in N^+)$.

4.4.1 Upper level: Steady state optimization problem

In reality, each zone has desired CO_2 concentration, relative humidity and air temperature, the trajectory references of which are determined by users. The aims of the upper layer considered in this chapter are to minimize the total electricity bills in the building, which consist of demand and energy costs under a TOU rate structure, and provide optimal reference points of air temperature, relative humidity and CO_2 concentration for each zone in the lower layer. More specifically, the following centralized steady-state optimization problem is considered

$$x^*(t_k^u) = \arg \min_{x(t_k^u), u(t_k^u)} \left(\underbrace{\sum_{i=1}^{m} [w_1 \sum_{k=1}^{n} \left(E_c(t_k^u) P_{tot,i}(t_k^u) \delta^u \right)}_{\text{energy cost}} + \underbrace{w_2 (D_c(t_k^u) \max_{1 \leq k \leq n} \{ P_{tot,i}(t_k^u) \})]}_{\text{demand cost}} \right),$$

$$(4.16a)$$

subject to the following constraints:

$$f_i(x_i(t_k^u), x_{-i}(t_k^u), u_i(t_k^u), \omega_i(t_k^u)) = 0, \ i = 1, 2, \ldots, m, \qquad (4.16b)$$

$$|PMV_i(t_k^u)| \leq \beta, \ i = 1, 2, \ldots, m, \qquad (4.16c)$$

$$x_i(t_k^u) \in \mathbb{X}_i, \; u_i(t_k^u) \in \mathbb{U}_i, \; h_{3,i}(x_i(t_k^u), u_i(t_k^u)) \le 0, \; h_{4,i}(x_i(t_k^u)) \le 0, \; t_k^u \in [0, K^u], \; i = 1, 2, \ldots, m,$$

(4.16d)

where $x(t_k^u) = [x_1(t_k^u), \ldots, x_m(t_k^u)]^T$ is the system state vector and $u(t_k^u) = [u_1(t_k^u), \ldots, u_m(t_k^u)]^T$ is the control input vector. The total energy consumption P_{tot} for the ME A/C system is expressed in (3.22) and the PMV function is expressed in (4.14). The parameter β is the comfort bound of the PMV index. $E_c(t_k^u)$ is the TOU electricity energy charge rate at time step t_k^u, and $D_c(t_k^u)$ is the demand charge rate at time step t_k^u. w_i $(i = 1, 2)$ represent the weighting factors and $f_i(x_i(t_k^u), x_{-i}(t_k^u), u_i(t_k^u), \omega_i(t_k^u))$ are given in (4.10). $x^*(t_k^u)$ denotes a global optimal solution of the optimization problem (4.16).

Before studying the distributed steady state optimization problem, the researcher makes an assumption on the system model.

Assumption 4.1 *The optimal problem (4.16) admits a solution, of which the steady state of CO_2 concentration, relative humidity and air temperature for each zone are almost the same.*

This assumption is valid in many practical situations where different zones serve the same functions and purposes, such as in an office environment; the comfort requirements are subject to the same standards, ambient conditions and energy regulatory and pricing structure; therefore, they are normally the same.

Secondly, under a steady state, the total heat gain from neighboring zones is sometimes less dominant compared with that from the outside heat gain plus the indoor heat gain in every zone. As reported [92], the TOU rate structure is also the main factor to dominate the steady state optimization solutions. Therefore, in the optimization problem (4.16), one can ignore the interaction terms $\Sigma_{j=1, j \ne i}^{m} \frac{T_{z,j} - T_{z,i}}{R_{ij}}$ in (4.1) or $\Sigma_{j=1, j \ne i}^{m} \frac{T_{z,j} - T_{z,i}}{R_{ij}}$ in (4.16b). A simplified optimization problem (4.17) can be formulated for one zone i only as follows:

$$x_i^r(t_k^u) = \arg \min_{x_i(t_k^u), u_i(t_k^u)} \left(w_1 \underbrace{\sum_{k=1}^{n} \left(E_c(t_k^u) P_{tot,i}(t_k^u) \delta^u \right)}_{\text{energy cost}} + \underbrace{w_2 (D_c(t_k^u) \max_{1 \le k \le n} \{P_{tot,i}(t_k^u)\})}_{\text{demand cost}} \right),$$

(4.17a)

subject to the following constraints:

$$\widetilde{f}_i(x_i(t_k^u), u_i(t_k^u), \omega_i(t_k^u)) = 0,$$

(4.17b)

$$|PMV_i(t_k^u)| \leq \beta, \tag{4.17c}$$

$$x_i(t_k^u) \in \mathbb{X}_i, \ u_i(t_k^u) \in \mathbb{U}_i, \ h_{3,i}(x_i(t_k^u), u_i(t_k^u)) \leq 0, \ h_{4,i}(x_i(t_k^u)) \leq 0, \ t_k^u \in [0, K^u], \tag{4.17d}$$

where $x_i^r(t_k^u)$ is a local optimal solution, and i means that the optimization problem (4.17) only needs the measurement information from room i. Here, $\widetilde{f}_i(x_i, u_i, \omega_i)$ can be described by

$$\widetilde{f}_i(x_i, u_i, \omega_i) = \begin{bmatrix} \dfrac{\alpha_{2,i}A_{2,i}(T_{w,i} - \frac{T_{d,i}+T_{s,i}}{2}) + h_{fg}\rho v_{f,i}(W_{mix} - \frac{h_{s,i}-C_aT_{s,i}}{h_{fg}}) + C_a\rho v_{f,i}(T_{d,i}-T_{s,i})}{\rho V_{h2,i}} \\[2ex] \dfrac{\frac{T_0-T_{z,i}}{R_i} + C_a\rho v_{f,i}(T_{s,i}-T_{z,i}) + Q_{load,i}}{C_a\rho V_i} \\[2ex] \dfrac{C_a\rho v_{f,i}(T_{mix}-T_{d,i}) + \alpha_{1,i}A_{1,i}(T_{w,i} - \frac{T_m+T_{d,i}}{2})}{C_a\rho V_{h1,i}} \\[2ex] \dfrac{\alpha_{1,i}A_{1,i}(\frac{T_{mix}+T_{d,i}}{2} - T_{w,i}) + \alpha_{2,i}A_{2,i}(\frac{T_{d,i}+T_{s,i}}{2} - T_{w,i}) - (h_{r2,i}-h_{r1,i})m_{r,i}}{C_{w,i}\rho_{w,i}V_{w,i}} \\[2ex] \dfrac{\rho v_{f,i}(\frac{h_{s,i}-C_aT_{s,i}}{h_{fg}} - W_{z,i}) + M_{load,i}}{\rho V_i} \\[2ex] \dfrac{(k_P v_{f,i} + k_I \int_0^{T_I} v_{f,i}\mathrm{d}s)(C_{s,i} - C_{c,i}) + G_i \cdot Occp_i}{V_i} \end{bmatrix}. \tag{4.18}$$

The researcher has five important remarks to make on the optimization problem (4.16a).

- In (4.17a), the term regarding the end-user services contains two parts, i.e., the energy cost of the multi-zone building's ME A/C system given by $\sum_{k=1}^{n}\left[E_c(t_k^u)P_{tot,i}(t_k^u)\delta^u\right]$ (weighted by w_1) aims to minimize energy cost; the peak demand $D_c(t_k^u)\max_{1\leq k\leq n}\{P_{tot,i}(t_k^u)\}$ (weighted by w_2) aims to reduce demand cost.

- The weighting factors w_1, w_2, which are determined by users, are to balance the two objectives. Specifically, if preferring more demand reduction, they can increase w_2 and decrease w_1 and vice versa.

- It can be seen in (4.17a) that the energy and demand charge rates $E_c(t_k^u)$ and $D_c(t_k^u)$ depend on the TOU price policy. The rate structures are determined by utilities for various tuples of customers. For some rate plans, customers have the flexibility to choose peak periods so that they can save energy cost by optimizing the energy use during specific time periods.

- This steady state optimization problem is different from that in previous studies [115, 92]. In [115], an open loop optimal control algorithm was proposed to minimize energy consumption by setting air temperature, relative humidity and CO_2 concentration. In [92], an open loop steady state optimal control algorithm is designed to optimize air temperature, relative humidity and CO_2 concentration references, which could be time-varying to minimize energy cost and the

PMV index in possible. This chapter reaches the same conclusions as [92] in scheduling the time-varying reference setpoints.

- The optimal solution applies to one zone, and the resulting reference setpoints are then communicated to the whole network through connecting neighbors. Therefore, the scheduling is implementable in a distributed manner.

Fig. 4.2 is a architecture on how to implement the proposed control strategy.

The ADSMS is a hierarchical distributed way that aims at achieving energy and cost savings in ME A/C operations without compromising occupancy comfort levels. The information communication for the simplified ADSMS is illustrated in Fig. 4.2. The idea here is to consider comfort as a service for occupancies, which is provided by the ME A/C system. The zones (using zone modules (ZMs)) are where the people seeking this service (called a token), and a distribution system operator (DSO) is the service provider (called as provider). There are four steps in the ADSMS that are explained in the following.

- Master: The DSO collects one room's measurement information (cooling and pollutant loads, weather and occupancy), computes and transmits optimal reference signals to this zone by a communication network.

- Slave: The neighboring zones receive communication information using numerous ZMs from the driving system. Then its neighbouring zones then communicate to whole zones by connecting neighbors. This way can easily be applied in engineering and reduce communication cost or sources.

- Token requests: The main aim of the ZM is to run an MPC using forecast information (weather condition, occupancy and cooling and pollutant loads) plus sensor readings (temperature and humidity, thermostat and CO_2 sensors) to compute the minimal energy consumption and cost required without breaching the comfort ranges.

- Coordination: After each room receives communication information, each DX unit employs a DMPC algorithm to optimise the transient process to reach the IAQ and thermal comfort
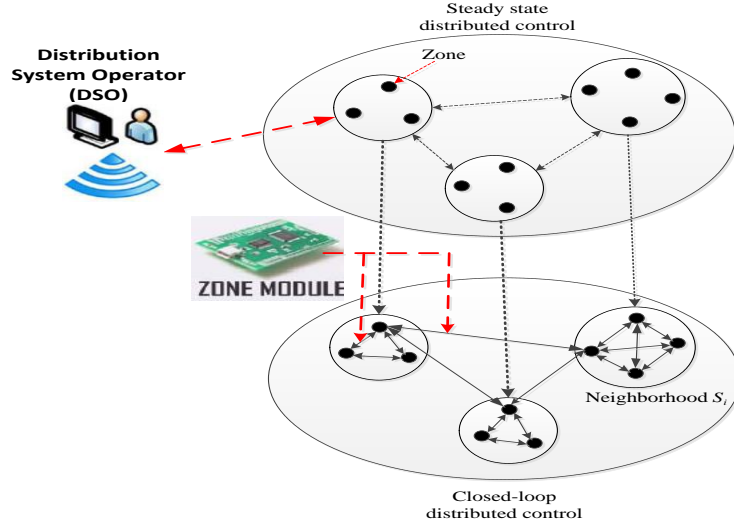
Figure 4.2. Autonomous demand-side management scheduling architecture.

demands while minimizing energy consumption and costs.

Remark 4.3 *For ease of implementation, the min-max problem in (4.17a) is converted into the following standard NLP so that it can be conveniently solved by the Matlab built-in functions. A new variable $z_{P,i}$ is introduced to denote the peak demand of the day for zone i as following:*

$$z_{P,i} = max_{1 \le k \le n}\{P_{tot,i}(t_k^u)\}. \tag{4.19}$$

By simplifying the objective to the form in Eq. (4.20), the optimization problem in (4.17a) can be rewritten as follows:

$$min \left(w_1 \sum_{k=1}^n E_c(t_k^u)P_{tot,i}(t_k^u)\delta^u + w_2 D_c(t_k^u)z_{P,i} \right). \tag{4.20}$$

4.4.2   Lower level: DMPC

In brief, the aim is to design the tracking rule $u_i(t_k^u)$ $(i \in \mathcal{N})$ in a distributed way such that the systems (4.9) can reach their time-varying trajectory references according to the changing environment during the day, which are the optimal solutions to the optimization problem (4.17).

The UOPC transmits the reference signals, $x^r(s;t_k^u) = [x_1^r(s;t_k^u),\ldots,x_m^r(s;t_k^u)]^T, u^r(s;t_k^u) = [u_1^r(s;t_k^u),\ldots,u_m^r(s;t_k^u)]^T, T_{s,i}^r(s;t_k^u), \delta(s;t_k^u)$, to the LDMPC for $s \in [t_k^u, t_{(k+1)}^u), i = 1,2,\ldots,m$. Here, $x^r(t_k^u) \triangleq x^r(t_k^u;t_k^u)$. In the lower layer, the MIMO DMPC controllers are designed to drive multi-zone buildings'

ME A/C system to track their time-varying trajectory references, which are calculated by the UOPC. The linearized dynamics of the subsystem S_i around their trajectory references at the sampling time instant $t^l_{c(k,q)}$ can be written as below. In (4.21), the interacting terms in non-neighboring zones are ignored owing to the definition of neighbors in (4.8).

$$\begin{cases} \delta \dot{x}_i(s) = A_{ii}(t^l_{c(k,q)})\delta x_i(s) + \sum_{j \in \mathcal{V}_i} A_{ij}(t^l_{c(k,q)})\delta x_j(s) + B_i(t^l_{c(k,q)})\delta u_i(s), \\ y_i(s) = C_{ii}\delta x_i(s) + y^0_i(s), \quad s \in [t^l_{c(k,q)}, t^l_{c(k+1,q)}), \end{cases} \quad (4.21)$$

where $A_{ii}(t^l_{c(k,q)}) = \frac{\partial f_i}{\partial x_i}(x^r_i(t^l_{c(k,q)}), u^r_i(t^l_{c(k,q)}))$, $A_{ij}(t^l_{c(k,q)}) = \frac{\partial f_i}{\partial x_j}(x^r_i(t^l_{c(k,q)}), u^r_i(t^l_{c(k,q)}))$, $B_i(t^l_{c(k,q)}) = \frac{\partial f_i}{\partial u_i}(x^r_i(t^l_{c(k,q)}), u^r_i(t^l_{c(k,q)}))$ for $j \in \mathcal{V}_i$. δx_i and δu_i are respectively the deviations of the state and input vectors from their trajectory references of the subsystem S_i; $y_i = [T_{z,i}, W_{z,i}, C_{c,i}]^T$ are the original output variables and $y^r_i = [T^r_{z,i}, W^r_{z,i}, C^r_{c,i}]^T$ are the trajectory references of the subsystem S_i.

The predicted linearized dynamics of the subsystem S_i can be written as follows:

$$\begin{cases} \delta \dot{x}^p_i(s; t^l_{c(k,q)}) = A_{ii}(s; t^l_{c(k,q)})\delta x^p_i(s; t^l_{c(k,q)}) + \sum_{j \in \mathcal{V}_i} A_{ij}(t^l_{c(k,q)})\delta \widehat{x}_j(s; t^l_{c(k,q)}) + \\ \qquad\qquad B_i(s; t^l_{c(k,q)})\delta u^p_i(s; t^l_{c(k,q)}), \\ y^p_i(s; t^l_{c(k,q)}) = C_{ii}\delta x^p_i(s; t^l_{c(k,q)}) + y^r_i(s; t^u_k), \quad s \in [t^l_{c(k,q)}, t^l_{c(k,q)} + T^l), \quad i = 1, 2, \dots, m, \end{cases} \quad (4.22)$$

where $\delta x^p_i(s; t^l_{c(k,q)})$, $\delta u^p_i(s; t^l_{c(k,q)})$ and $y^p_i(s; t^l_{c(k,q)})$ are the predicted state, input and output trajectories at time step $t^l_{c(k,q)}$, $\delta \widehat{x}_j(s; t^l_{c(k,q)})$ is the assumed state sequence of S_i at time step $t^l_{c(k,q)}$.

The MIMO MPC algorithm is designed for the lower-layer controllers to minimize the optimization objective after reaching trajectory references as well as to handle external disturbances to the building and to compensate for the model mismatch. Let

$$\delta u^p_i(s; t^l_{c(k,q)}) = -\sum_{j \in \mathcal{V}_i} K_j(s; t^l_{c(k,q)})\delta \widehat{x}_j(s; t^l_{c(k,q)}) + v^p_i(s; t^l_{c(k,q)}), \quad i = 1, 2, \dots, m, \quad (4.23)$$

where $v_i(s; t^l_{c(k,q)})$ is a new input variable for zone i, (4.22) can be then converted to (4.24) as follows:

$$\begin{cases} \delta \dot{x}^p_i(s; t^l_{c(k,q)}) = A_{ii}(s; t^l_{c(k,q)})\delta x^p_i(s; t^l_{c(k,q)}) + B_i(t^l_{c(k,q)})v^p_i(s; t^l_{c(k,q)}), \\ y^p_i(s; t^l_{c(k,q)}) = C_{ii}\delta x^p_i(s; t^l_{c(k,q)}) + y^r_i(s; t^u_k), \quad s \in [t^l_{c(k,q)}, t^l_{c(k,q)} + T^l), \quad i = 1, 2, \dots, m. \end{cases} \quad (4.24)$$

Many standard approaches exist in [86, 88] for the system (4.24), which depends entirely on one zone i. In this study, the researcher uses previous results achieved in [92] in the MPC design, then the proposed optimization objective is given by

$$\min_{v^p_i(s; t^l_{c(k,q)})} \overline{J}^l_i = \int_{t^l_{c(k,q)}}^{t^l_{c(k,q)} + T^l} \left(\left\| y^p_i(s; t^l_{c(k,q)}) - y^r_i(s; t^u_k) \right\|^2_{Q_i} + \left\| v^p_i(s; t^l_{c(k,q)}) \right\|^2_{R_i} \right) ds \quad (4.25a)$$

$$+ \left\| y^p_i(t^l_{c(k,q)} + T^l; t^l_{c(k,q)}) - y^r_i(t^l_{c(k,q)} + T^l) \right\|^2_{P_i}, \quad i = 1, 2, \dots, m,$$

subject to:

$$\delta \dot{x}_i^p(s;t_{c(k,q)}^l) = A_{ii}(s;t_{c(k,q)}^l)\delta x_i^p(s;t_{c(k,q)}^l) + B_i(s;t_{c(k,q)}^l)v_i^p(s;t_{c(k,q)}^l), \; i = 1,2,\ldots,m, \quad (4.25b)$$

$$y_i^p(s;t_{c(k,q)}^l) = C_{ii}\delta x_i^p(s;t_{c(k,q)}^l) + y_i^r(s;t_k^u), \; s \in [t_{c(k,q)}^l, t_{c(k,q)}^l + T^l), \; i = 1,2,\ldots,m, \quad (4.25c)$$

$$x_i^p(s;t_{c(k,q)}^l) \in \mathbb{X}, \; v_i^p(s;t_{c(k,q)}^l) \in \mathbb{V}, \; s \in [t_{c(k,q)}^l, t_{c(k,q)}^l + T^l], \; i = 1,2,\ldots,m, \quad (4.25d)$$

where the controllers $\delta u_i^p(s;t_{c(k,q)}^l)$ obtained are distributed. Q_i, R_i, P_i are the weighting matrix, $\mathbb{V}$ is the bounded set of the new input variable v_i. The convergence for the above finite horizon periodic MPC optimization problem (4.25) can be proved by the results in [125, 126].

4.4.3 Algorithm

The implementation strategy of the proposed AHDC algorithms for a multi-zone building's ME A/C system is summarized as follows:

The upper layer distributed steady state optimization algorithm can be solved by the standard NLP algorithm (3.34) in Chapter 3.

The lower layer DMPC algorithm can be given below.

1) At sampling time instant t_k^u, $k = 0,1,\ldots,n$, UOPC receives each local neighbor measurement information.

2) UOPC computes the state trajectory $x^r(t_k^u) = [x_1^r(t_k^u),\ldots,x_m^r(t_k^u)]^T$, $s \in [t_k^u, t_k^u + T^u)$ and its corresponding control input trajectory $u^r = [u_1^r(t_k^u),\ldots,u_m^r(t_k^u)]$, $s \in [t_k^u, t_k^u + T^u)$, which are transmitted to LDMPC, to obtain linearized systems (4.24).

3) At sampling time instant $t_{c(k,q)}^l$, LDMPCi receives the state measurement $x_i(t_{c(k,q)}^l)$ and $x_{-i}(s,t_{c(k,q)}^l)$ from its neighbors, gives an initial point $x_i(0)$ ($k = q = 0$) and computes the optimal control input $v_i^*(s;t_{c(k,q)}^l)$ of the optimization problems (4.25) over the prediction horizon $[t_{c(k,q)}^l, t_{c(k,q)}^l + T^l]$.

4) The first solution $v_i^*(s;t_{c(k,q)}^l)$ is used through (4.23) to update $\delta u_i^p(s;t_{c(k,q)}^l)$ as the initial condition over the next prediction horizon $[t_{c(k,q+1)}^l, t_{c(k,q)}^l + \delta^l]$.

5) If $0 \leq q < M$, $q = q + 1$ and go to 3); else $k = k + 1$, $q = 0$ and go to 1).

4.5   CASE STUDY

In this section, a six-room model is used to test the performance of the proposed AHDC strategy in special climate conditions in Cape Town, South Africa. The simulations are conducted during normal operation of an office building with normal occupancy. The six rooms are connected and the undirected graph is $\mathcal{G} = \{\mathcal{V}, \mathcal{A}\}$ where $\mathcal{V} = \{1, 2, 3, 4, 5, 6\}$ and $\varepsilon_0 = 5$. $R_{12} = R_{21} = R_{23} = R_{32} = R_{34} = R_{43} = R_{45} = R_{54} = R_{56} = R_{65} = R_{61} = R_{16} = 4 < \varepsilon_0$, $R_{13} = R_{31} = R_{24} = R_{42} = R_{35} = R_{53} = R_{46} = R_{64} = R_{51} = R_{15} = R_{62} = R_{26} = 8 > \varepsilon_0$, $R_{14} = R_{41} = R_{25} = R_{52} = R_{36} = R_{63} = 12 > \varepsilon_0$, then the neighbors of zone i are shown in Table 4.1. It can be verified that the network is connected.

Table 4.1. The neighborhood definition of zones

Room (i)	Neighbors ($\mathcal{V}_i$)	Room (i)	Neighbors ($\mathcal{V}_i$)
1	2,6	2	1,3
3	2,4	4	3,5
5	4,6	6	5,1

4.5.1   Parameter selection

The volume of each room is 77 m^3. The model parameters of the ME A/C system are given in Table 2.2, taken from [103]. $R_{ij} = 4°$C/kW and R_i=15°C/kW. The coefficients of the power consumption for the condenser (4.11) and evaporators (4.12) are calibrated through the regression analysis of the available measured data reported in [116], which are depicted in Table 2.1. It is supposed that the combined total efficiency of the compressor is $\overline{\eta} = 0.85$. Each room has a window with an area of 4 m^2. For the proposed AHDC strategy considered below, the system variable constraints of each room are given by bounds in Tables 4.2, and this study constrains the PMV index of each room in the range of $[-0.5, 0.5]$, which refers to an international standard, to guarantee that the ME A/C system is able to control both the IAQ and thermal comfort of each room within the required ranges for occupants. The weighting factors of the upper layer optimization objective are defined as $w_1 = 1$, $w_2 = 1$. The matrix Q_i, R_i, P_i are selected as an identity matrix. In the previous study [92], the simulation results illustrated that the

Table 4.2. Values of system constraints.

Notations	Values	Notations	Values
$\overline{T}_{s,i}$	22 °C	$\underline{T}_{s,i}$	10 °C
$\overline{T}_{z,i}$	26 °C	$\underline{T}_{z,i}$	22 °C
$\overline{T}_{d,i}$	22 °C	$\underline{T}_{d,i}$	10 °C
$\overline{T}_{w,i}$	22 °C	$\underline{T}_{w,i}$	8 °C
$\overline{W}_{z,i}$	12.3/1000 kg/kg	$\underline{W}_{z,i}$	9.85/1000 kg/kg
$\overline{C}_{c,i}$	800 ppm	$\underline{C}_{c,i}$	650 ppm
$\overline{W}_{s,i}$	9.85/1000 kg/kg	$\underline{W}_{s,i}$	7.85/1000 kg/kg
$\overline{v}_{f,i}$	0.8 m³/s	$\underline{v}_{f,i}$	0 m³/s
$\overline{m}_{r,i}$	0.11 kg/s	$\underline{m}_{r,i}$	0 kg/s
$\overline{h}_{s,i}$	46.3 kJ/kg	$\underline{h}_{s,i}$	27.3 kJ/kg
β	0.5		

open loop optimal controller and the MIMO MPC strategies are not sensitive to the system parameters A_1 and A_2 of a single-zone DX A/C system within any ranges of $[aA_0, bA_0]$ where $0 \leq a, b \leq 1$ and $a \leq b$. This result can be extended to the multi-zone building's ME A/C system. Hence, $A_{1,i} = 0.15A_{0,i}$ and $A_{2,i} = 0.85A_{0,i}$, $i \in \mathcal{V}$ are chosen in this chapter.

Since the outside air temperature, relative humidity and radiation determine zones' thermal comfort and IAQ, the data would be exacted better. However, the data cannot be predicted accurately, while the LMPC is capable of dealing with the uncertainty disturbance rejection. The simulation time runs from 0:00 to 23:59. The outside air temperature and relative humidity information are obtained from a meteorological station located in Cape Town, South Africa. The predicted ambient air temperature and relative humidity profiles over a 24-hour period are plotted in Fig. 3.5(a). The predicted solar radiative heat flux density profiles over a 24-hour period are shown in Fig. 3.5(b). The estimation of the external sensible heat load of each room over a 24-hour period is depicted in Fig. 3.6(b). The certainty internal sensible heat load, latent heat load and the CO_2 pollutant load of six rooms over a 24-hour period are predicted in Fig. 4.3. The values of Fig.4.3 at every hour are also commensurately quantized. Though the data cannot be exactly predicted and estimated, the robust DMPC is employed and capable of handling the prediction errors.

(a) Certainty sensible heat load (b) Certainty moisture heat load (c) CO_2 pollutant load
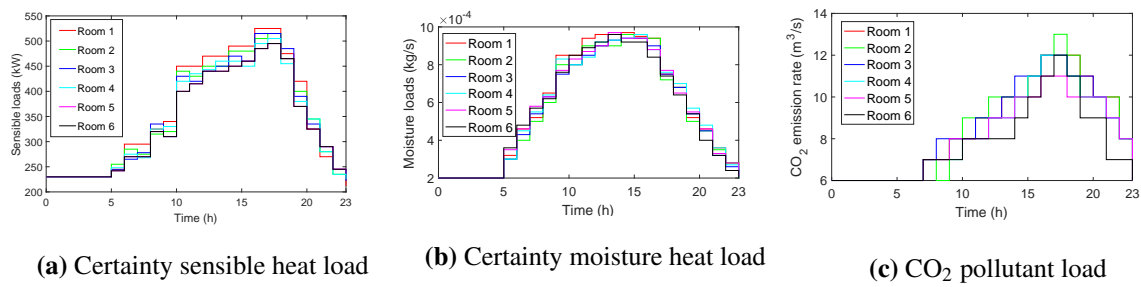
Figure 4.3. Profiles of the forecast certainty sensible heat, certainty moisture heat and CO_2 pollutant loads over a 24-hour period.

It is assumed that multi-zone building's ME A/C system operates according to the TOU rate plan, as shown in Table 4.3. It can be seen from the table that there is a big difference in the demand charges from peak hours to non-peak hours. Energy cost savings can be expected if significant amounts of peak energy consumption are shifted to non-peak hours.

Table 4.3. Time-of-use electricity rates.

Summer	Period	Energy charge ($/kWh)	Demand charge ($/kWh)
Peak	12:00-18:00	0.20538	11.889
Standard	08:00-12:00, 18:00-21:00	0.05948	2.352
Off-Peak	21:00-08:00	0.03558	1.007

4.5.2 Comparison of optimal scheduling control strategies

To demonstrate the performance of the proposed AHDC, comparisons with other control strategies are studied here to schedule the operation of the ME A/C system. The first approach is a DMPC algorithm based on the given setpoints of a zone's CO_2 concentration, relative humidity and air temperature, aiming at energy consumption in [115], referred as S1. The second method is the DMPC algorithm based on energy cost and the value of the PMV index minimization reported in [92], referred as S2. The proposed control scheme is the DMPC algorithm based on demand charge and energy costs minimization, referred to as S3. To simplify the comparison study among the three strategies, the multi-zone building's ME A/C system operation profiles are generated by the NLP algorithm with the same outside and inside conditions. The control parameters are listed below: The sampling time

$\Delta = 2$ min is used to discretize the dynamic model of the ME A/C system. The predictive horizon for the DMPC algorithm in the lower layer is set as $N = 15$; the sampling periods of the UOPC and LMPCi are 1 h and 2 min, respectively. Total simulation time is $K = 24$ hours. Table 4.4 summarizes the combinations of the optimizations and strategies of the three scenarios studied. The simulation test results for the three scenarios are given in Section 4.5.3.

Table 4.4. Comparison of different control strategies.

Scenarios	Upper layer optimization	Low layer control	Setpoint	DR action
S1	Energy consumption	DMPC	Given	
S2	Energy cost+PMV	DMPC	Autonomous	
S3	Energy cost+demand cost	DMPC	Autonomous	✓

4.5.3 Simulation test for proposed control strategy

The performance of the three scenarios is compared by MATLAB simulations with historical weather data for a special day. Fig. 4.4 shows the time-varying steady state profiles of each room's air temperature, relative humidity and CO_2 concentration, which can be obtained by solving the distributed coordination steady state optimization problem (4.17) and the centralized steady state optimization problem (4.16). It can be observed from Fig. 4.4 that the distributed steady state is close to the centralized steady states of each room, and their deviations are small and can be accepted by occupants (Assumption 1 is valid). Therefore, the proposed scheduling is effective.
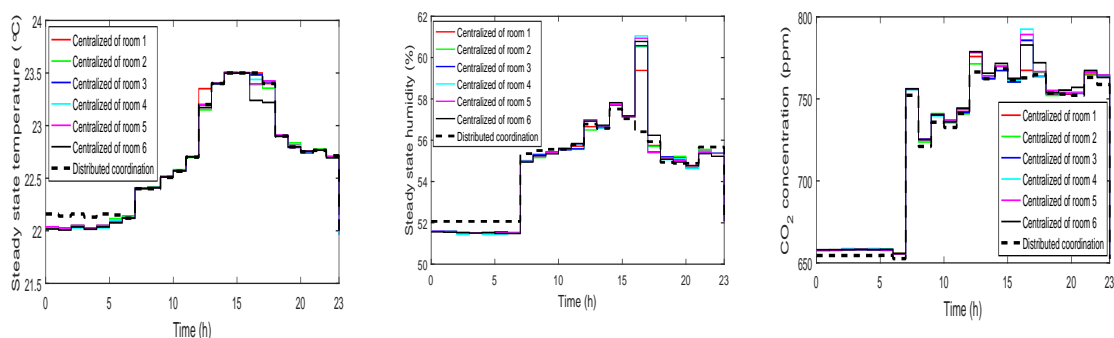

Figure 4.4. The steady state profiles in each room under the distributed and centralized optimal controllers.

The tracking reference points of air temperature for each room with the three control approaches are illustrated in Fig. 4.5 over a 24-hour period. The tracking reference points of relative humidity for each room with the three control approaches are depicted in Fig. 4.6 over a 24-hour period. The tracking reference points of CO_2 concentration for each room with the three control approaches are shown in Fig. 4.7. Figs. 4.5-4.7 also show that the optimized reference points are adaptively and automatically preprogrammed by adopted scenarios S2 and S3. One observes that the air temperature, relative humidity and CO_2 concentration of each room are tracked by the proposed control strategy and maintain their time-varying reference points. It can also be seen from Figs. 4.5-4.7 that the time-varying reference points of air temperature, relative humidity and CO_2 concentration of each room with scenarios S2 and S3 are tallish during standard hours. The reason is that scenarios S2 and S3 automatically adjust their reference points upward during standard hours because of the TOU energy price policy and DR action, respectively, such that energy consumption and cost are minimized while both IAQ and thermal comfort are maintained at acceptable ranges. The pre-cooling and pre-decreasing CO_2 contaminant concentration automatically starts in the morning simultaneously. This is because the energy costs for operating a multi-zone building's ME A/C system during off-peak hours are lower than in other periods. In the morning, the time-varying reference points of CO_2 concentration, relative humidity and air temperature for each room are kept at the lower bounds of the comfort regions to store cooling and lower CO_2 contaminant concentration until the peak hours. As soon as the peak hours start, the reference points increase to the upper bounds, hence reducing the peak demand in the afternoon by taking DR action. After more cooling and pollutant loads occur simultaneously during peak hours, the reference points are automatically set higher to turn off the cooling and increase the CO_2 contaminant concentration. One also observes that the time-varying reference points of CO_2 concentration, relative humidity and air temperature for each room are always maintained at comfort levels over a 24-hour period with the proposed control strategy. It is furthermore clear that after reaching their reference points, the proposed controllers maintain the reference points with small variation ranges. Therefore, the proposed control strategy is capable of handling the changing cooling and pollutant loads and weather conditions over a 24-hour period and maintaining both thermal comfort and IAQ at acceptable levels.

To show the advantage of the proposed AHDC strategy over the other two control strategies in shifting demands from peak periods to non-peak periods, the power consumption under different time periods for the three control strategies is shown in Fig. 4.8. The total energy consumption and cost for the multi-zone building's ME A/C system under the three control strategies are depicted in Table 4.5.
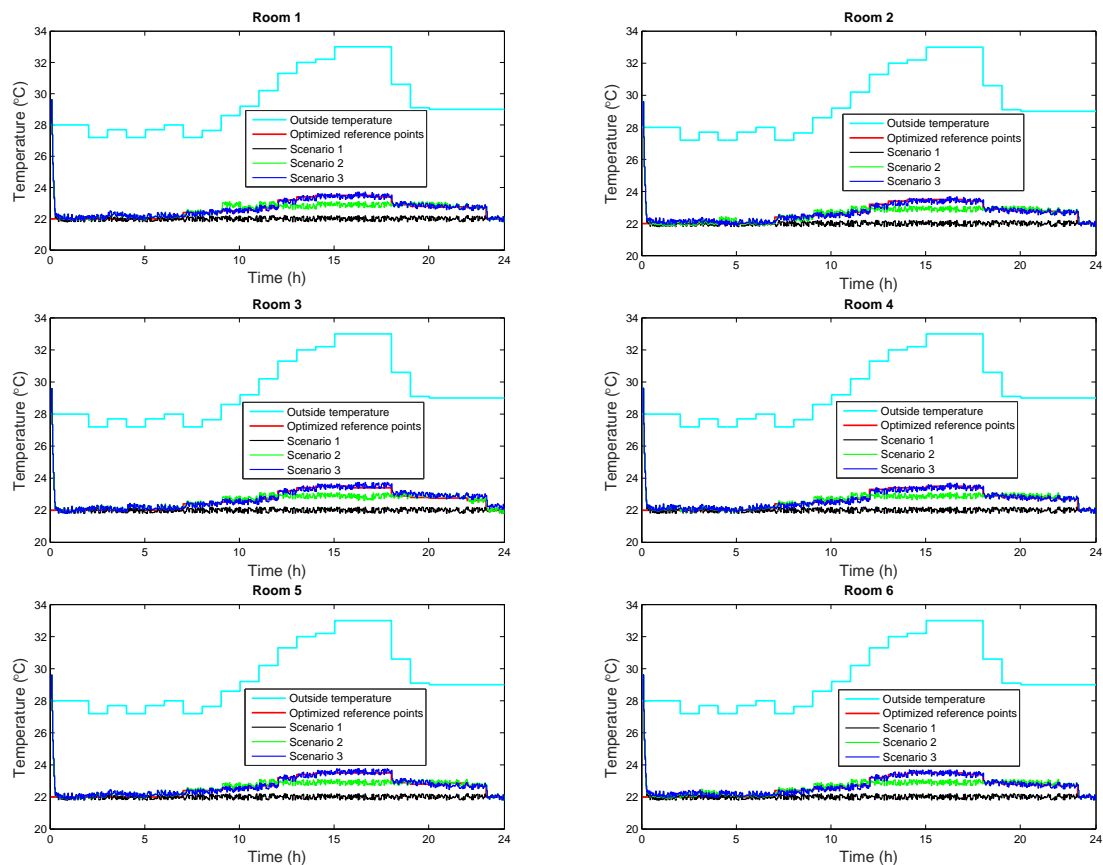
Figure 4.5. Each zone's temperature profile for a 24-hour period.

It can be seen from Table 4.5 that with control strategies S2 and S3, more energy consumption and costs can be saved in comparison with control strategy S1. The reason is that the CO_2 concentration, relative humidity and air temperature reference points of each room are adaptively and optimally preprogrammed under control strategies S2 and S3. It can be observed from Fig. 4.5 that the energy consumption with control strategies S2 and S3 is almost the same, while the energy cost is different. This implies that the proposed control strategy S3 is capable of saving more energy costs but not saving energy consumption in comparison with control strategy S2. It can be seen from Fig. 4.8 that the under the proposed control strategy S3 with DR action, more energy costs are reduced during peak hours in comparison with control strategies S1 and S2. The reason is that the proposed control strategy S3 automatically shifts the peak demands from peak periods to non-peak periods. Meanwhile, energy consumption with the proposed control strategy S3 is more than that with control strategy S2 during standard periods since the energy charge in standard periods is lower than that in peak periods. Therefore, the total energy cost saving and shifting demand is achieved over a 24-hour period while maintaining both thermal comfort and IAQ at the required levels. According to the above comparisons,
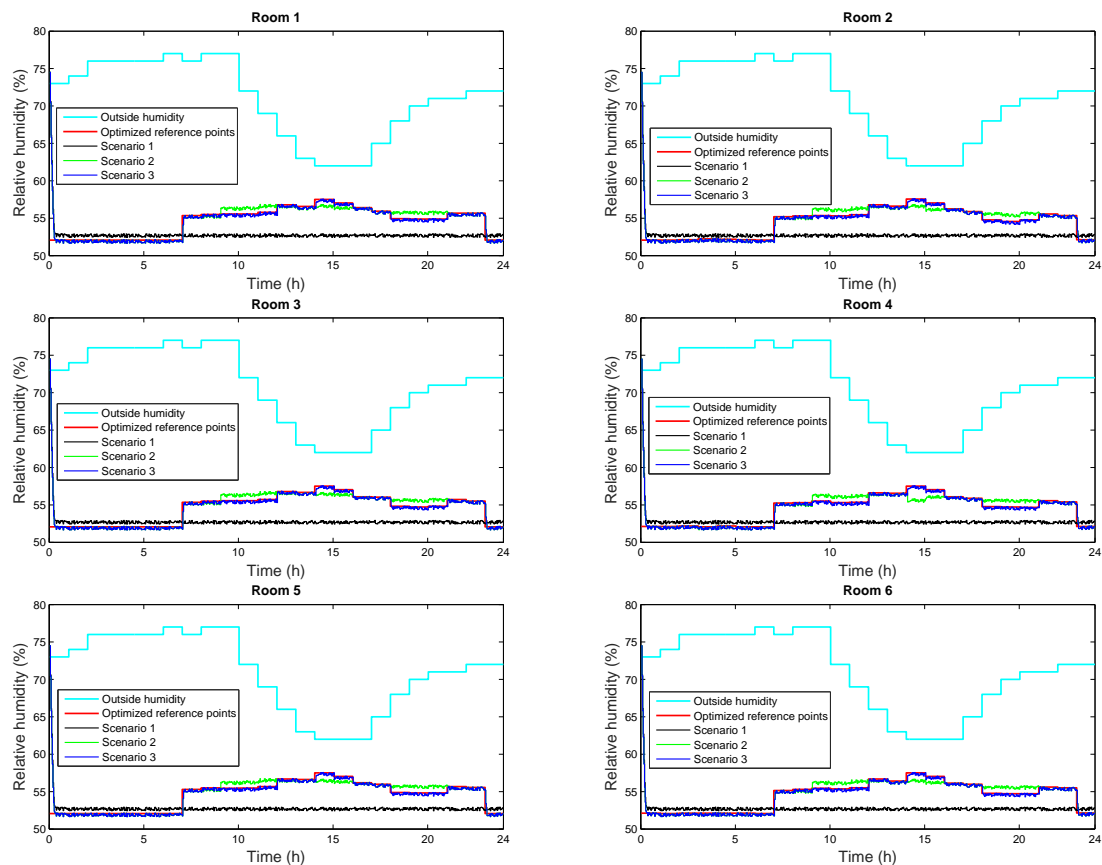
Figure 4.6. Each zone's relative humidity profile for a 24-hour period.

the proposed control strategy S3 thus has a lower proportion of demand cost during peak hours and shows successful demand shifting and energy cost.

Table 4.5. Comparison of control performance.

Strategy	Energy consumption (kWh)	Energy cost ($)
S1	124.56	10.67
S2	80.34	6.98
S3	79.78	5.66

4.6   CONCLUSION

This chapter proposes an AHDC approach to the problem of minimizing demand and energy cost as well as reducing communication resources, computational complexity and conservativeness simul-
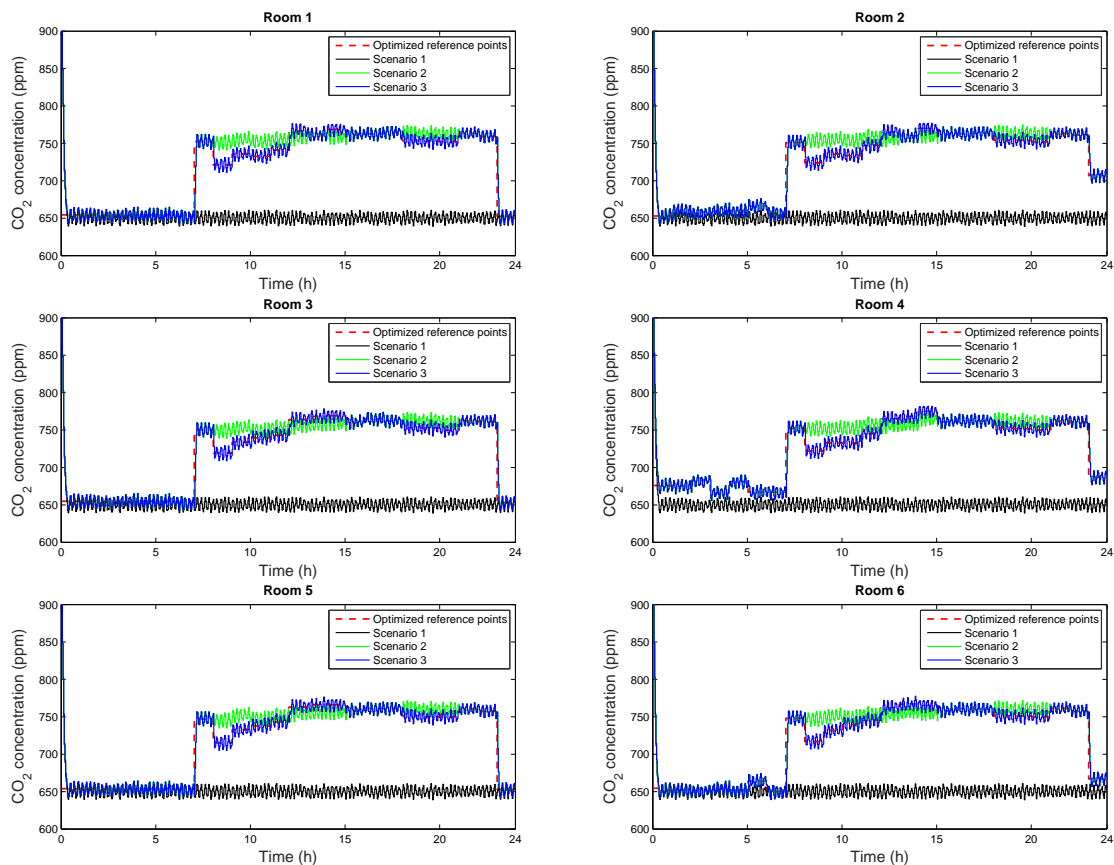
Figure 4.7. Each zone's CO_2 concentration profile for a 24-hour period.
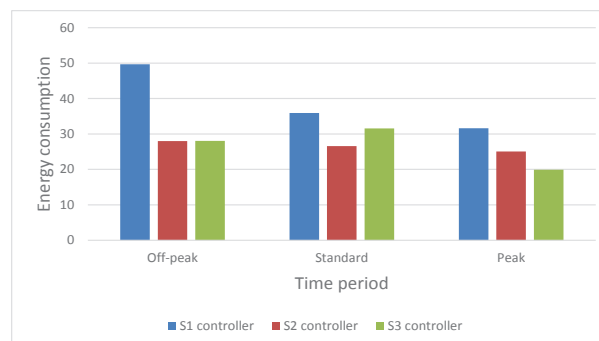
Figure 4.8. Energy consumption on three time periods with the three control strategies.

taneously for a multi-zone building's ME A/C system, while maintaining both thermal comfort and IAQ at acceptable ranges. The developed control strategy is an improvement over the current control approaches, in which the indoor CO_2 concentration, relative humidity and air temperature reference points of each zone are adaptively and optimally preprogrammed to improve the operational profile for the multi-zone building's ME A/C system by minimizing the energy and demand costs. The lower-layer

MIMO DMPC controllers steer the multi-zone building's ME A/C system to follow and maintain the autonomously preprogrammed references, meanwhile, the energy and demand costs are reduced and shifted for the multi-zone building's ME A/C system from peak hours to non-peak hours. The simulation results show that the designed DMPC controllers optimise the transient processes reaching the steady state. They also showed that the proposed AHDC strategy gave the distributed controllers the ability to deal with the model parameter uncertainty of the ME A/C and time-varying weather conditions. The proposed AHDC strategy is distributed suitably for a cluster of similar purposed buildings, which requires less and cheaper communication resources to implement.

CHAPTER 5   CONCLUSIONS

This dissertation focuses on two conflicting issues of building DX A/C systems, namely energy efficiency and indoor comfort levels, due to the contribution of long-term economic and environmental benefits. These two conflicting issues have been completely investigated for improving them are proposed. In particular, a hierarchical control scheme is developed to address energy efficiency improvement and control systems taking into account of indoor CO_2 concentration, relative humidity, air temperature and the coupling effects between them as well as thermal comfort and IAQ. This section outlines the major contributions of this thesis and a brief overview of a future research topic in this area.

5.1   FINDINGS

In this thesis, research on investigating both the thermal comfort and IAQ of building DX A/C systems, improving energy efficiency has been successfully undertaken and reported. The main contributions and findings of these chapters are reflected in the following section.

For indoor comfort and energy efficiency improvement, a MIMO MPC and an energy-optimised open loop controller scheme for the nonlinear dynamic system of a DX A/C system were designed in Chapter 2. It can be observed that the control methods can control indoor CO_2 concentration, relative humidity and air temperature to their setpoints, with small deviations. It is found that the control strategy can effectively reduce the energy consumption and improve both IAQ and thermal comfort of a DX A/C system. The present MPC strategy with the optimized steady state can save 1.39 kWh/day more energy compared to conventional control strategies. It is also noted that a single room's CO_2 emissions can be lowered by 502.28 kg per annum. This control strategy will also be suitable for residential and office buildings using HVAC systems.

For indoor comfort improvement and energy consumption and cost reduction, an AHC strategy, including an open loop optimal controller and a closed-loop tracking MPC controller, was designed in Chapter 3. Though this control strategy is motivated in Chapter 2, both controllers that have been designed are superior to the current control strategies for a DX A/C system in terms of reducing energy consumption and cost. The open loop optimal controller adaptively and autonomously generates time-varying and optimal setpoints by optimizing the PMV index and the TOU time-varying electricity structure with comfort range over a 24-hour period, for a lower-layer controller. The closed-loop MPC controller is designed to follow the scheduled setpoints of CO_2 concentration, relative humidity and air temperature. At the same time, energy consumption and cost are minimized. It is expected that this control strategy could be implemented in the application; the system's parameter sensitivity analysis showed that the proposed control scheme is not sensitive to the model parameters. According to Chapter 3, the energy consumption and cost can be reduced by 31.38% and 33.85%, respectively, while both thermal comfort and IAQ are maintained at acceptable levels. To this end, it can be concluded that the AHC is a suitable control approach for controlling the DX A/C system.

Lastly, for multi-zones' thermal comfort and IAQ and energy efficiency improvement, an AHDC strategy was designed in Chapter 4. This control strategy included two-layer distributed controllers to control a multi-zone building ME A/C system. The AUDC strategy has shifted demand from peaks hours to off-peak hours by taking DR action for a multi-zone building ME A/C system. With the AUDC strategy to autonomously and adaptively generate optimality and time-varying reference points over a 24-hour period, more energy consumption and cost have been reduced compared with the strategies designed in Chapters 2 and 3. It is also found that this hierarchical control method can reduce computational complexity and conservativeness and requires less and cheaper communication resources to implement. Though it is assumed that the multi-zones are similar in occupancies, functions and purposes, in this way, the designed distributed scheduler and the closed-loop DMPC have been verified by a case study to show its effectiveness.

5.2   FUTURE WORK

A number of future studies with respect to the research work in this thesis are suggested:

- For buildings using other A/C units with chilled water systems, the proposed control strategy

can be modified to suit the need. Indoor CO_2 concentration, humidity and air temperature may be controlled simultaneously by varying the opening of the chilled water valve and the supply fan equipped with a PI controller.

• Most DX A/C systems have been widely applied in small to medium-scale buildings. It is assumed that the control strategies that have been developed and advanced can be used to control a large-scale office equipped with a multi-evaporator A/C system. Then the dynamic model will be much more complicated than that reported in Chapter 4, and the control problems will be more difficult.

• Since many factors have an impact on the heat and mass transfer between air and refrigerant inside the evaporator of a DX A/C system, including heat and fluid flow geometries, there is no uniform local heat transfer rate or heat conduction along tube walls, etc. Therefore, it is impossible to consider all these factors in physical models; however, empirical-based models based on the training operating data method are able to find the physical parameters. It is expected that the proposed controller may achieve high control accuracy and sensitivity for a DX A/C system by combining both the physical-based model method and empirical-based model training method.

• Common control strategies are used to control the nonlinear control system by the first order approximation of the Taylor method based on linearization, which brings model derivation for controlling a nonlinear system. It is expected that a dynamic feedback control method will solve this problem based on feedback linearization.

• The researcher hopes that the hierarchical control method that has been developed can be tested by experiment and reported in the future to have been applied successfully in real-time DX air-conditioner.

REFERENCES

[1] International Energy Agency, "World energy outlook 2010," 2010. [Online]. Available: https://www.iea.org/publications/freepublications/publication/weo2010.pdf.

[2] X. Xia and J. Zhang, "Energy efficiency and control systems-from a POET perspective," *IFAC Proceedings Volumes*, vol. 43, no. 1, pp. 255–260, 2010.

[3] X. Xia, J. Zhang, and W. Cass, "Energy management of commercial buildings-A case study from a POET perspective of energy efficiency," *Journal of Energy in Southern Africa*, vol. 23, pp. 23–31, 2012.

[4] D. Setlhaolo and X. Xia, "Optimal scheduling of household appliances with a battery storage system and coordination," *Energy and Buildings*, vol. 94, pp. 61–70, 2015.

[5] S. M. Sichilalu and X. Xia, "Optimal power dispatch of a grid tied-battery-photovoltaic system supplying heat pump water heaters," *Energy Conversion and Management*, vol. 102, pp. 81–91, 2015.

[6] A. J. Bijker, X. Xia, and J. Zhang, "Active power residential non-intrusive appliance load monitoring system," in *AFRICON 2009*, 2009, pp. 1–6.

[7] H. Tazvinga, X. Xia, and J. Zhang, "Minimum cost solution of photovoltaic-diesel-battery hybrid power systems for remote consumers," *Solar Energy*, vol. 96, pp. 292–299, 2013.

[8] B. Zhu, H. Tazvinga, and X. Xia, "Switched model predictive control for energy dispatching

of a photovoltaic-diesel-battery hybrid power system," *IEEE Transactions on Control Systems Technology*, vol. 23, no. 3, pp. 1229–1236, 2015.

[9] E. M. Wanjiru, S. M. Sichilalu, and X. Xia, "Optimal control of heat pump water heater-instantaneous shower using integrated renewable-grid energy systems," *Applied Energy*, vol. 201, pp. 332–342, 2017.

[10] U. E. Ekpenyong, J. Zhang, and X. Xia, "An improved robust model for generator maintenance scheduling," *Electric Power Systems Research*, vol. 92, pp. 29–36, 2012.

[11] H. Carstens, X. Xia, and X. Ye, "Improvements to longitudinal clean development mechanism sampling designs for lighting retrofit projects," *Applied Energy*, vol. 126, pp. 256–265, 2014.

[12] X. Ye, X. Xia, L. Zhang, and B. Zhu, "Optimal maintenance planning for sustainable energy efficiency lighting retrofit projects by a control system approach," *Control Engineering Practice*, vol. 37, pp. 1–10, 2015.

[13] X. Ye, X. Xia, and J. Zhang, "Optimal sampling plan for clean development mechanism energy efficiency lighting projects," *Applied Energy*, vol. 112, pp. 1006–1015, 2013.

[14] X. Ye, X. Xia, and J. Zhang, "Optimal sampling plan for clean development mechanism lighting projects with lamp population decay," *Applied Energy*, vol. 136, pp. 1184–1192, 2014.

[15] Y. Fan and X. Xia, "A multi-objective optimization model for energy-efficiency building envelope retrofitting plan with rooftop PV system installation and maintenance," *Applied Energy*, vol. 189, pp. 327–335, 2017.

[16] Y. Fan and X. Xia, "Energy-efficiency building retrofit planning for green building compliance," *Building and Environment*, vol. 136, pp. 312–321, 2018.

[17] E. M. Malatji, J. Zhang, and X. Xia, "A multiple objective optimisation model for building energy efficiency investment decision," *Energy and Buildings*, vol. 61, pp. 81–87, 2013.

[18] B. Wang, X. Xia, and J. Zhang, "A multi-objective optimization model for the life-cycle cost analysis and retrofitting planning of buildings," *Energy and Buildings*, vol. 77, pp. 227–235, 2014.

[19] B. Wang, Z. Wu, and X. Xia, "A multistate-based control system approach toward optimal maintenance planning," *IEEE Transactions on Control Systems Technology*, vol. 25, no. 1, pp. 374–381, 2017.

[20] E. M. Wanjiru and X. Xia, "Energy-water optimization model incorporating rooftop water harvesting for lawn irrigation," *Applied Energy*, vol. 160, pp. 521–531, 2015.

[21] E. M. Wanjiru, L. Zhang, and X. Xia, "Model predictive control strategy of energy-water management in urban households," *Applied Energy*, vol. 179, pp. 821–831, 2016.

[22] Z. Wu and X. Xia, "Optimal motion planning for overhead cranes," *IET Control Theory Applications*, vol. 8, no. 17, pp. 1833–1842, 2014.

[23] S. Zhang and X. Xia, "A new energy calculation model of belt conveyor," in *AFRICON 2009*, 2009, pp. 1–6.

[24] A. Chatterjee, L. Zhang, and X. Xia, "Optimization of mine ventilation fan speeds according to ventilation on demand and time of use tariff," *Applied Energy*, vol. 146, pp. 65–73, 2015.

[25] L. Zhang, X. Xia, and J. Zhang, "Improving energy efficiency of cyclone circuits in coal beneficiation plants by pump-storage systems," *Applied Energy*, vol. 119, pp. 306–313, 2014.

[26] N. Wang, J. Zhang, and X. Xia, "Desiccant wheel thermal performance modeling for indoor humidity optimal control," *Applied Energy*, vol. 112, pp. 999–1005, 2013.

[27] B. Thomas, M. Soleimani-Mohseni, and P. Fahlén, "Feed-forward in temperature control of buildings," *Energy and Buildings*, vol. 37, no. 7, pp. 755–761, 2005.

[28] A. Ruano, E. Crispim, E. Conceição, and M. Lúcio, "Prediction of building's temperature using neural networks models," *Energy and Buildings*, vol. 38, no. 6, pp. 682–694, 2006.

[29] J. Toftum and P. Fanger, "Air humidity requirements for human comfort," *ASHRAE Transactions*, vol. 105, pp. 641–647, 1999.

[30] D. Westphalen, K. Roth, J. Dieckmann, and J. Brodrick, "Improving latent performance," *ASHRAE Transactions*, vol. 46, pp. 73–75, 2004.

[31] J. Hill and S. Jeter, "Use of heat pipe exchangers for enhanced dehumidification," *ASHRAE Transactions*, vol. 100, pp. 91–102, 1994.

[32] A. Gasparella, G. A. Longo, and R. Marra, "Combination of ground source heat pumps with chemical dehumidification of air," *Applied Thermal Engineering*, vol. 25, no. 2, pp. 295–308, 2005.

[33] A. Capozzoli, P. Mazzei, F. Minichiello, and D. Palma, "Hybrid HVAC systems with chemical dehumidification for supermarket applications," *Applied Thermal Engineering*, vol. 26, no. 8, pp. 795–805, 2006.

[34] R. Tu, X. Liu, and Y. Jiang, "Irreversible processes and performance improvement of desiccant wheel dehumidification and cooling systems using exergy," *Applied Energy*, vol. 145, pp. 331–344, 2015.

[35] G. Jahedi and M. Ardehali, "Wavelet based artificial neural network applied for energy efficiency enhancement of decoupled HVAC system," *Energy Conversion and Management*, vol. 54, no. 1, pp. 47–56, 2012.

[36] D. K. Lim, B. H. Ahn, and J. H. Jeong, "Method to control an air conditioner by directly measuring the relative humidity of indoor air to improve the comfort and energy efficiency," *Applied Energy*, vol. 215, pp. 290–299, 2018.

[37] S. Wang and X. Jin, "Model-based optimal control of VAV air-conditioning system using genetic algorithm," *Building and Environment*, vol. 35, no. 6, pp. 471–487, 2000.

[38] S. Atthajariyakul and T. Leephakpreeda, "Real-time determination of optimal indoor-air condition for thermal comfort, air quality and efficient energy usage," *Energy and Buildings*, vol. 36, no. 7, pp. 720–733, 2004.

[39] S. Lin, S. Chiu, and W. Chen, "Simple automatic supervisory control system for office building based on energy-saving decoupling indoor comfort control," *Energy and Buildings*, vol. 86, pp. 7–15, 2015.

[40] K. Gladyszewska-Fiedoruk, "Correlations of air humidity and carbon dioxide concentration in the kindergarten," *Energy and Buildings*, vol. 62, pp. 45–50, 2013.

[41] A. H. Mohsenian-Rad, V. W. S. Wong, J. Jatskevich, R. Schober, and A. Leon-Garcia, "Autonomous demand-side management based on game-theoretic energy consumption scheduling for the future smart grid," *IEEE Transactions on Smart Grid*, vol. 1, no. 3, 2010.

[42] W. Surles and G. P. Henze, "Evaluation of automatic priced based thermostat control for peak energy reduction under residential time-of-use utility tariffs," *Energy and Buildings*, vol. 49, pp. 99–108, 2012.

[43] M. Kii, K. Sakamoto, Y. Hangai, and K. Doi, "The effects of critical peak pricing for electricity demand management on home-based trip generation," *IATSS Research*, vol. 37, no. 2, pp. 89–97, 2014.

[44] H. T. Nguyen, D. T. Nguyen, and L. B. Le, "Energy management for households with solar assisted thermal load considering renewable energy and price uncertainty," *IEEE Transactions on Smart Grid*, vol. 6, no. 1, pp. 301–314, 2015.

[45] P. Xu, P. Haves, M. A. Piette, and J. E. Braun, "Peak demand reduction from pre-cooling with zone temperature reset in an office building," in *2004 ACEEE Summer Study on Energy Efficiency in Buildings*, Pacific Grove, CA, 2004.

[46] J. E. Braun, "Load control using building thermal mass," *Journal of Solar Energy Engineering*, vol. 125, no. 3, pp. 292–301, 2003.

[47] K. Lee and J. E. Braun, "Development of methods for determining demand-limiting setpoint trajectories in buildings using short-term measurements," *Building and Environment*, vol. 43, no. 10, pp. 1755–1768, 2008.

[48] R. Tang, S. Wang, K. Shan, and H. Cheung, "Optimal control strategy of central air-conditioning systems of buildings at morning start period for enhanced energy efficiency and peak demand limiting," *Energy*, vol. 151, pp. 771–781, 2018.

[49] M. Wallace, R. McBride, S. Aumi, P. Mhaskar, J. House, and T. Salsbury, "Energy efficient model predictive building temperature control," *Chemical Engineering Science*, vol. 69, no. 1, pp. 45–58, 2012.

[50] J. Cigler, S. Prívara, Z. Váňa, E. Žáčeková, and L. Ferkl, "Optimization of predicted mean vote index within model predictive control framework: Computationally tractable solution," *Energy and Buildings*, vol. 52, pp. 39–49, 2012.

[51] G. Mantovani and L. Ferrarini, "Temperature control of a commercial building with model predictive control techniques," *IEEE Transactions on Industrial Electronics*, vol. 62, no. 4, pp. 2651–2660, 2015.

[52] F. Oldewurtel, A. Parisio, C. N. Jones, D. Gyalistras, M. Gwerder, V. Stauch, B. Lehmann, and M. Morari, "Use of model predictive control and weather forecasts for energy efficient building climate control," *Energy and Buildings*, vol. 45, pp. 15–27, 2012.

[53] A. Elaiw and X. Xia, "HIV dynamics: Analysis and robust multirate MPC-based treatment schedules," *Journal of Mathematical Analysis and Applications*, vol. 359, no. 1, pp. 285–301, 2009.

[54] L. Zhang, X. Xia, and B. Zhu, "A dual-loop control system for dense medium coal washing processes with sampled and delayed measurements," *IEEE Transactions on Control Systems*

Technology, vol. 25, no. 6, pp. 2211–2218, 2017.

[55] X. Xia, J. Zhang, and A. Elaiw, "A model predictive control approach to dynamic economic dispatch problem," in *2009 IEEE Bucharest PowerTech*, 2009, pp. 1–7.

[56] Z. Wu, X. Xia, and B. Zhu, "Model predictive control for improving operational efficiency of overhead cranes," *Nonlinear Dynamics*, vol. 79, no. 4, pp. 2639–2657, 2015.

[57] R. Z. Freire, G. H. Oliveira, and N. Mendes, "Predictive controllers for thermal comfort optimization and energy savings," *Energy and Buildings*, vol. 40, no. 7, pp. 1353–1365, 2008.

[58] S. Prívara, J. Široký, L. Ferkl, and J. Cigler, "Model predictive control of a building heating system: The first experience," *Energy and Buildings*, vol. 43, no. 2, pp. 564–572, 2011.

[59] J. Álvarez, J. Redondo, E. Camponogara, J. Normey-Rico, M. Berenguel, and P. Ortigosa, "Optimizing building comfort temperature regulation via model predictive control," *Energy and Buildings*, vol. 57, pp. 361–372, 2013.

[60] J. Ma, S. J. Qin, and T. Salsbury, "Application of economic MPC to the energy and demand minimization of a commercial building," *Journal of Process Control*, vol. 24, no. 8, pp. 1282–1291, 2014.

[61] T. Salsbury, P. Mhaskar, and S. J. Qin, "Predictive control methods to improve energy efficiency and reduce demand in buildings," *Computers and Chemical Engineering*, vol. 51, pp. 77–85, 2013.

[62] J. Ma, J. Qin, T. Salsbury, and P. Xu, "Demand reduction in building energy systems based on economic model predictive control," *Chemical Engineering Science*, vol. 67, no. 1, pp. 92–100, 2012.

[63] H. Huang, L. Chen, and E. Hu, "A new model predictive control scheme for energy and cost savings in commercial buildings: An airport terminal building case study," *Building and Environment*, vol. 89, pp. 203–216, 2015.

[64] Y. Ma, J. Matuško, and F. Borrelli, "Stochastic model predictive control for building HVAC systems: Complexity and conservatism," *IEEE Transactions on Control Systems Technology*, vol. 23, no. 1, pp. 101–116, 2015.

[65] M. Maasoumy and A. Sangiovanni-Vincentelli, "Total and peak energy consumption minimization of building HVAC systems using model predictive control," *IEEE Design Test of Computers*, vol. 29, no. 4, pp. 26–35, 2012.

[66] M. Avci, M. Erkoc, A. Rahmani, and S. Asfour, "Model predictive HVAC load control in buildings using real-time electricity pricing," *Energy and Buildings*, vol. 60, pp. 199–209, 2013.

[67] D. Kolokotsa, A. Pouliezos, G. Stavrakakis, and C. Lazos, "Predictive control techniques for energy and indoor environmental quality management in buildings," *Building and Environment*, vol. 44, no. 9, pp. 1850–1863, 2009.

[68] M. Castilla, J. Álvarez, M. Berenguel, F. Rodríguez, J. Guzmán, and M. Pérez, "A comparison of thermal comfort predictive control strategies," *Energy and Buildings*, vol. 43, no. 10, pp. 2737–2746.

[69] M. Castilla, J. Álvarez, J. N. Rico, and F. Rodríguez, "Thermal comfort control using a nonlinear MPC strategy: A real case of study in a bioclimatic building," *Journal of Process Control*, vol. 24, no. 6, pp. 703–713, 2014.

[70] Z. Váňa, J. Cigler, J. Široký, E. Žáčeková, and L. Ferkl, "Model-based energy efficient control applied to an office building," *Journal of Process Control*, vol. 24, no. 6, pp. 790–797, 2014.

[71] X. Jin, H. Ren, and X. Xiao, "Prediction-based online optimal control of outdoor air of multizone VAV air conditioning systems," *Energy and Buildings*, vol. 37, no. 9, pp. 939–944, 2005.

[72] X. Xu, S. Wang, Z. Sun, and F. Xiao, "A model-based optimal ventilation control strategy of multi-zone VAV air-conditioning systems," *Applied Thermal Engineering*, vol. 29, no. 1, pp. 91–104, 2009.

[73] Y. Zhu, X. Jin, X. Fang, and Z. Du, "Optimal control of combined air conditioning system with variable refrigerant flow and variable air volume for energy saving," *International Journal of Refrigeration*, vol. 42, pp. 14–25, 2014.

[74] Y. Zhu, X. Jin, Z. Du, X. Fang, and B. Fan, "Control and energy simulation of variable refrigerant flow air conditioning system combined with outdoor air processing unit," *Applied Thermal Engineering*, vol. 64, no. 1, pp. 385–395, 2014.

[75] M. Gruber, A. Trüschel, and J.-O. Dalenbäck, "Model-based controllers for indoor climate control in office buildings-Complexity and performance evaluation," *Energy and Buildings*, vol. 68, pp. 213–222, 2014.

[76] A. Kusiak, F. Tang, and G. Xu, "Multi-objective optimization of HVAC system with an evolutionary computation algorithm," *Energy*, vol. 36, no. 5, pp. 2440–2449, 2011.

[77] M. Kavgic, D. Mumovic, Z. Stevanovic, and A. Young, "Analysis of thermal comfort and indoor air quality in a mechanically ventilated theatre," *Energy and Buildings*, vol. 40, no. 7, pp. 1334–1343, 2008.

[78] M. Maasoumy, M. Razmara, M. Shahbakhti, and A. S. Vincentelli, "Handling model uncertainty in model predictive control for energy efficient buildings," *Energy and Buildings*, vol. 77, pp. 377–392, 2014.

[79] J. Hu and P. Karava, "A state-space modeling approach and multi-level optimization algorithm for predictive control of multi-zone buildings with mixed-mode cooling," *Building and Environment*, vol. 80, pp. 259–273, 2014.

[80] M. Razmara, M. Maasoumy, M. Shahbakhti, and R. Robinett, "Optimal exergy control of building HVAC system," *Applied Energy*, vol. 156, pp. 555–565, 2015.

[81] E. Atam, "Decentralized thermal modeling of multi-zone buildings for control applications and investigation of submodeling error propagation," *Energy and Buildings*, vol. 126, pp. 384–395, 2016.

REFERENCES

[82] V. Chandan and A. G. Alleyne, "Decentralized predictive thermal control for buildings," *Journal of Process Control*, vol. 24, no. 6, pp. 820–835, 2014.

[83] X. Zhang, W. Shi, B. Yan, A. Malkawi, and N. Li, "Decentralized and distributed temperature control via HVAC systems in energy efficient buildings," *CoRR*, vol. abs/1702.03308, 2017. [Online]. Available: http://arxiv.org/abs/1702.03308

[84] Y. Zheng, S. Li, and H. Qiu, "Networked coordination-based distributed model predictive control for large-scale system," *IEEE Transactions on Control Systems Technology*, vol. 21, no. 3, pp. 991–998, 2013.

[85] P. D. Morosan, R. Bourdais, D. Dumur, and J. Buisson, "Building temperature regulation using a distributed model predictive control," *Energy and Buildings*, vol. 42, no. 9, pp. 1445–1452, 2010.

[86] Y. Ma, G. Anderson, and F. Borrelli, "A distributed predictive control approach to building temperature regulation," in *Proceedings of the 2011 American Control Conference*, 2011, pp. 2089–2094.

[87] P.-D. Moroşan, R. Bourdais, D. Dumur, and J. Buisson, "A distributed MPC strategy based on benders' decomposition applied to multi-source multi-zone temperature regulation," *Journal of Process Control*, vol. 21, no. 5, pp. 729–737, 2011.

[88] H. Scherer, M. Pasamontes, J. Guzmán, J. Álvarez, E. Camponogara, and J. Normey-Rico, "Efficient building energy management using distributed model predictive control," *Journal of Process Control*, vol. 24, no. 6, pp. 740–749, 2014.

[89] M. S. Elliott and B. P. Rasmussen, "Decentralized model predictive control of a multi-evaporator air conditioning system," *Control Engineering Practice*, vol. 21, no. 12, pp. 1665–1677, 2013.

[90] Y. Long, S. Liu, L. Xie, and K. H. Johansson, "A hierarchical distributed MPC for HVAC systems," in *2016 American Control Conference (ACC)*, 2016, pp. 2385–2390.

[91] A. Zafra-Cabeza, J. Maestre, M. A. Ridao, E. F. Camacho, and L. Sánchez, "A hierarchical distributed model predictive control approach to irrigation canals: A risk mitigation perspective," *Journal of Process Control*, vol. 21, no. 5, pp. 787–799, 2011.

[92] J. Mei and X. Xia, "An autonomous hierarchical control for improving indoor comfort and energy efficiency of a direct expansion air conditioning system," *Applied Energy*, vol. 221, pp. 450–463, 2018.

[93] N. Radhakrishnan, S. Srinivasan, R. Su, and K. Poolla, "Learning-based hierarchical distributed HVAC scheduling with operational constraints," *IEEE Transactions on Control Systems Technology*, pp. 1–9, 2017.

[94] G. Y. Yun, J. Choi, and J. T. Kim, "Energy performance of direct expansion air handling unit in office buildings," *Energy and Buildings*, vol. 77, pp. 425–431, 2014.

[95] K. Krakow, S. Lin, and Z. Zeng, "Temperature and humidity control during cooling and dehumidifying by compressor and evaporator fan speed variation," *ASHRAE Transactions*, vol. 101, pp. 292–304, 1995.

[96] M. Andrade and C. Bullard, "Modulating blower and compressor capacities for efficient comfort control," *ASHRAE Transactions*, vol. 108, pp. 631–640, 2001.

[97] N. Li, L. Xia, S. Deng, X. Xu, and M. Chan, "Steady-state operating performance modelling and prediction for a direct expansion air conditioning system using artificial neural network," *Building Services Engineering Research and Technology*, vol. 33, no. 3, pp. 281–292, 2012.

[98] N. Li, L. Xia, S. Deng, X. Xu, and M. Chan, "Dynamic modeling and control of a direct expansion air conditioning system using artificial neural network," *Applied Energy*, vol. 91, no. 1, pp. 290–300, 2012.

[99] N. Li, L. Xia, S. Deng, X. Xu, and M. Chan, "On-line adaptive control of a direct expansion air conditioning system using artificial neural network," *Applied Thermal Engineering*, vol. 53, no. 1, pp. 96–107, 2013.

[100] X. Xu, L. Xia, M. Chan, and S. Deng, "Inherent correlation between the total output cooling capacity and equipment sensible heat ratio of a direct expansion air conditioning system under variable-speed operation (XXG SMD SHR DX AC unit)," *Applied Thermal Engineering*, vol. 30, no. 13, pp. 1601–1607, 2010.

[101] Z. Li, X. Xu, S. Deng, and D. Pan, "A novel neural network aided fuzzy logic controller for a variable speed (VS) direct expansion (DX) air conditioning (A/C) system," *Applied Thermal Engineering*, vol. 78, pp. 9–23, 2015.

[102] W. Chen and S. Deng, "Development of a dynamic model for a DX VAV air conditioning system," *Energy Conversion and Management*, vol. 47, no. 18, pp. 2900–2924, 2006.

[103] Q. Qi and S. Deng, "Multivariable control-oriented modeling of a direct expansion (DX) air conditioning (A/C) system," *International Journal of Refrigeration*, vol. 31, no. 5, pp. 841–849, 2008.

[104] S. Deng, "A dynamic mathematical model of a direct expansion (DX) water-cooled air-conditioning plant," *Building and Environment*, vol. 35, no. 7, pp. 603–613, 2000.

[105] L. Xia, M. Chan, and S. Deng, "Development of a method for calculating steady-state equipment sensible heat ratio of direct expansion air conditioning units," *Applied Energy*, vol. 85, no. 12, pp. 1198–1207, 2008.

[106] S. Deng, "The application of feedforward control in a direct expansion (DX) air conditioning plant," *Building and Environment*, vol. 37, no. 1, pp. 35–40, 2002.

[107] Z. Li and S. Deng, "A DDC-based capacity controller of a direct expansion (DX) air conditioning (A/C) unit for simultaneous indoor air temperature and humidity control-part I: Control algorithms and preliminary controllability tests," *International Journal of Refrigeration*, vol. 30, no. 1, pp. 113–123, 2007.

[108] Z. Li and S. Deng, "A DDC-based capacity controller of a direct expansion (DX) air conditioning (A/C) unit for simultaneous indoor air temperature and humidity control-part II:

REFERENCES

Further development of the controller to improve control sensitivity," *International Journal of Refrigeration*, vol. 30, no. 1, pp. 124–133, 2007.

[109] X. Xu, S. Deng, and M. Chan, "A new control algorithm for direct expansion air conditioning systems for improved indoor humidity control and energy efficiency," *Energy Conversion and Management*, vol. 49, no. 4, pp. 578–586, 2008.

[110] Q. Qi and S. Deng, "Multivariable control of indoor air temperature and humidity in a direct expansion (DX) air conditioning (A/C) system," *Building and Environment*, vol. 44, no. 8, pp. 1659–1667, 2009.

[111] Q. Qi, S. Deng, X. Xu, and M. Chan, "Improving degree of superheat control in a direct expansion (DX) air conditioning (A/C) system," *International Journal of Refrigeration*, vol. 33, no. 1, pp. 125–134, 2010.

[112] W. Chen and S. Deng, "Research on a novel DDC-based capacity controller for the direct-expansion variable-air-volume A/C system," *Energy Conversion and Management*, vol. 51, no. 1, pp. 1–8, 2010.

[113] X. Xu, Y. Pan, S. Deng, L. Xia, and M. Chan, "Experimental study of a novel capacity control algorithm for a multi-evaporator air conditioning system," *Applied Thermal Engineering*, vol. 50, no. 1, pp. 975–984, 2013.

[114] J. Cai and J. E. Braun, "A generalized control heuristic and simplified model predictive control strategy for direct-expansion air-conditioning systems," *Science and Technology for the Built Environment*, vol. 21, no. 6, pp. 773–788, 2015.

[115] J. Mei and X. Xia, "Energy-efficient predictive control of indoor thermal comfort and air quality in a direct expansion air conditioning system," *Applied Energy*, vol. 195, pp. 439–452, 2017.

[116] V. Vakiloroaya, B. Samali, and K. Pishghadam, "Investigation of energy-efficient strategy for direct expansion air-cooled air conditioning systems," *Applied Thermal Engineering*, vol. 66, no. 1, pp. 84–93, 2014.

[117] A. S. 540, *Performance Rating of Positive Displacement Refrigerant Compressors and Compressor Units*.   Air Conditioning and Refrigeration Institute, 2015.

[118] ASHRAE, *2001 ASHRAE Handbook: Fundamentals*.   American Society of Heating, Refrigeration and Air-conditioning Engineers, Atlanta, GA, USA, 2001.

[119] M. Maasoumy, *Modeling and Optimal Control Algorithm Design for HVAC Systems in Energy Efficient Buildings*.   EECS Department, University California, Berkeley, 2011.

[120] P. Fanger, *Thermal Comfort: Analysis and Applications in Environmental Engineering*.   Denmark: Danish Technical Press, 1981.

[121] M. Owen, *2009 ASHRAE Handbook: Fundamentals*.   ASHRAE, SI Edition, 2009.

[122] J. C. K. Cena, *Bioengineering, Thermal Physiology and Comfort*.   Elsevier Scientific Publishing Company, 1981.

[123] N. Djongyang, R. Tchinda, and D. Njomo, "Thermal comfort: A review paper," *Renewable and Sustainable Energy Reviews*, vol. 14, no. 9, pp. 2626–2640, 2010.

[124] S. R. West, J. K. Ward, and J. Wall, "Trial results from a model predictive control and optimisation system for commercial building HVAC," *Energy and Buildings*, vol. 72, pp. 271–279, 2014.

[125] X. Xia, J. Zhang, and A. Elaiw, "An application of model predictive control to the dynamic economic dispatch of power generation," *Control Engineering Practice*, vol. 19, no. 6, pp. 638–648, 2011.

[126] J. Zhang and X. Xia, "A model predictive control approach to the periodic implementation of the solutions of the optimal dynamic resource allocation problem," *Automatica*, vol. 47, no. 2, pp. 358–362, 2011.

[127] ASHRAE, *Handbook of HVAC Applications*. American Society of Heating, Refrigeration and Air-conditioning Engineers, Atlanta, GA, USA, 2003.

[128] V. Vakiloroaya, Q. Ha, and M. Skibniewski, "Modeling and experimental validation of a solar-assisted direct expansion air conditioning system," *Energy and Buildings*, vol. 66, pp. 524–536, 2013.

[129] M. Jiménez, H. Madsen, and K. Andersen, "Identification of the main thermal characteristics of building components using MATLAB," *Building and Environment*, vol. 43, no. 2, pp. 170–180, 2008.

[130] P. Bacher and H. Madsen, "Identifying suitable models for the heat dynamics of buildings," *Energy and Buildings*, vol. 43, no. 7, pp. 1511–1522, 2011.

[131] H. Yu and X. Xia, "Adaptive leaderless consensus of agents in jointly connected networks," *Neurocomputing*, vol. 241, pp. 64–70, 2017.

ADDENDUM A   SYSTEM MATRICES

A.1   SYSTEM MATRICES

The system matrices for the DX A/C system are listed as follows:

$$
A_c = \begin{bmatrix}
-2.8372 & 0 & -1.2297 & 4.0669 & -1959.2805 & 1469.4603 & 0 \\
0.0039 & -0.0039 & 0 & 0 & 0 & 0 & 11.3071 \\
0 & 4.3962 & -11.5218 & 8.1436 & 0 & 0 & 0 \\
0.0314 & 0.0051 & 0.0381 & -0.0763 & 0 & 0 & 0 \\
-0.0015 & 0 & -0.0007 & 0.0022 & -1.0588 & 0.7941 & 0 \\
0 & 0 & 0 & 0 & 0.0039 & -0.0039 & 0.0054 \\
0 & 0 & 0 & 0 & 0 & 0 & -0.0013
\end{bmatrix},
$$

$$
B_c = \begin{bmatrix}
30.6267 & 0 & 0 \\
-0.1621 & 0 & 0 \\
225 & 0 & 0 \\
0 & -4.2254 & 0 \\
0.0166 & 0 & 0 \\
-0.00003 & 0 & 0 \\
0 & 0 & -0.000006
\end{bmatrix}.
$$